NASA CR-92122

FINAL REPORT

IMPACT FLASH FOR MICROMETEOROID DETECTION

9659/FR1

SUBMITTED TO

NATIONAL AERONAUTICS AND SPACE ADMINISTRATION
MANNED SPACECRAFT CENTER
HOUSTON, TEXAS

CONTRACT NO. NAS 9-6790

7 MAY 1968

PREPARED BY:
T.L. ROLLING
B. JEAN

Computing Devices of Canada Limited

Bendix

NASA CR. 92128

FINAL REPORT

IMPACT FLASH FOR MICROMETEOROID DETECTION

9899/FR1

SUBMITTED TO

NATIONAL AERONAUTICS AND SPACE ADMINISTRATION
MANNED SPACECRAFT CENTER
HOUSTON, TEXAS

CONTRACT NO. NAS 9-5790

7 MAY 1968

PREPARED BY:
T.L. ROLLINS
B. JEAN

Computing
Devices of
Canada Limited

Bendix

CONTENTS

LIST OF ILLUSTRATIONS

LIST OF ILLUSTRATIONS (CONT'D)

LIST OF ILLUSTRATIONS (CONT'D)

LIST OF ILLUSTRATIONS (CONT'D)

ABSTRACT

The radiation emitted during hypervelocity impact consists of emission lines of the target and projectile material and continuum radiation associated with the broadening of these lines. Spectroscopic observation of the radiation emitted yields information about the composition, velocity, and size of the impacting particle. When the composition is known, the velocity and diameter can be obtained from simple measurements involving only one photomultiplier. A possible application is the detection of micrometeoroids and measurement of their velocity and size.

SECTION 1

INTRODUCTION

When a high velocity projectile strikes a target, part of the kinetic energy of the projectile is transformed into electromagnetic radiation. The intensity, spectral distribution, and time history of the impact radiation can yield information about the projectile and target. When the target properties are known, radiation in the wavelength region 3000Å - 9000Å (which for our purposes we define as the impact "flash") yields information about the velocity, size, and composition of the projectile. The possible application of impact flash for the detection and analysis of micrometeoroids is the subject of this report.

Relatively little research has been conducted on the nature and origin of the impact flash. In 1959, Clark [1] studied flashes produced by the impact of copper on copper at velocities below 2 km/sec, and concluded that the flash is due to the interaction of a high velocity spray from the impact region with the ambient atmosphere. He did not propose a mechanism which could generate such a high velocity spray. In 1963, R.W. MacCormack[2] observed that the rise time of the luminosity is an increasing function of the ambient range pressure for aluminum impacting aluminum. His spectrographic studies also revealed the existence of a line structure characteristic of the material involved. The above mentioned authors, however, were in apparent disagreement with the work conducted by Gehring and Warnica[3] who failed to measure any peak intensity variation of the flash with pressure when the ambient pressure in the range was lower than one millimeter of Hg. R.A. Koehler[4] impacted

different material on lead targets. From his spectrographic analysis of the flash, he concluded that the spectrum is characterized by excitation of the atoms of the projectile material rather than the target material. He also detected continuum radiation emanating from the impact point and superimposed line emission coming from the ejecta. Our work shows that continuum radiation is present at the impact point, and that line emission characteristic of both target and projectile material is present in the spray. We have proposed a mechanism which accounts for the observed properties of both the continuum and the line emission. We have concluded that the continuum radiation emitted by a micrometeoroid when it impacts a target whose characteristics are known can be used to deduce the velocity and size of the micrometeoroid. This report presents the reasoning and experimental evidence which support the conclusion.

Section 2 describes the experimental facilities: the launchers, the range, and the instrumentation. A description of the impact flash and a proposed mechanism for its generation follows in Section 3. The principal method of experimental investigation was spectroscopy, and a discussion of spectroscopic methods and results is found in Section 4. Section 5 describes the effect of such parameters as velocity, range pressure, and projectile shape on the impact flash. A complete listing of all experimental firings is found in Section 6.

SECTION 2

EXPERIMENTAL SET UP

2.1 LAUNCHER

Two types of launchers have been used during the course of the program. For impacts at 2.5 - 8 km/sec, a 0.5 inch light gas gun was used. A photograph of the gun is shown in Figure 1. For shots 1 - 61, smooth bore barrels were used and air separation type sabots were employed. For shots 62-150, rifled barrels were used and the sabots were spin separated. The rifled barrel resulted in better sabot separation, and also resulted in in-flight stability for non-spherical projectiles such as spheroids.

For impacts at velocities of 1 - 2.5 km/sec, a .22 calibre conventional rifle was installed in the dump tank of the light gas gun. Four low velocity shots were fired with the .22 calibre rifle.

2.2 RANGE

Figure 2 shows the range associated with the 0.5 inch light gas gun. It is divided into three sections: the dump tank, the travelling section, and the impact section.

The dump tank consists of a tank three feet in diameter and 15 feet in length. Baffles in the dump tank prevent sabot segments and other debris from entering the travelling section. The dump tank supports two pulsed x-ray heads which can be used to obtain x-ray photographs of the

projectile and sabot at various stages of separation. The x-rays are triggered by a broken light beam at the muzzle of the gun.

The travelling section is connected to the dump tank by a pipe two inches in diameter. Isolation of the dump tank is accomplished by a 25 μm thick mylar diaphragm at the end of the pipe. Broken beam light detectors placed at five foot intervals along the travelling section are used to measure the velocity of the projectile as it travels down the range. The broken beam detectors also trigger shadowgraph cameras which are mounted at right angles to the line of flight of the projectile.

The experimental section consists of a reservoir 3 feet in diameter and 5 feet long, with 9 viewing ports placed around the target area. Pressures as low as 4×10^{-6} Torr are maintained by a 6 inch oil diffusion pump and a large area cold trap.

2.3 INSTRUMENTATION

Instrumentation includes a spectrograph, a broadband photomultiplier, open shutter cameras, and image converter cameras. Each of these will be discussed below.

The spectrograph used was a 0.75 meter f/6.8 Czerney Turner instrument. It was generally used as a polychromator, with 4 photomultipliers at the exit slits. When spectra were recorded, u.v. sensitive plates were used, usually Kodak Type 103-0. Quartz windows were used in the spectrograph port in the range. For a few shots at the end of the program a medium quartz Hilger spectrograph was used in conjunction with the Czerney Turner.

Radiation produced by the impact was also monitored by a photomultiplier sensitive from 3500-6500Å (S-5 sensitivity). Neutral density filters were used to prevent saturation. The signal from the photomultiplier was displayed on a scope externally triggered by another unfiltered photomultiplier. A fixed delay of approximately one microsecond was externally established between the triggering signal and the displayed pulse. Figure 3 shows a block diagram of the electronic logic used to record the impact signature. The gated delayed trigger was used in order to avoid any spurious signals which could have triggered the scope prior to the impact signal.

Time integrated photographs of the impact flash were taken for each shot. Two cameras, loaded with panchromatic and red sensitive film, were mounted at right angles to the line of flight in the plane of the target, and their shutters were left open for the entire duration of the impact flash.

Time resolved photographs were also obtained for each shot by means of four image converter cameras. Three of the cameras were mounted to observe the impact flash from the side, and a fourth was mounted to observe the flash head-on through a front surface mirror. The exposure time of each photograph could be set at .01, .1, or 1.0 usec. The time at which each picture was taken was recorded on a scope triggered by the P.M. trigger. From the sequence of photographs obtained, the velocity of the luminous ring could be measured.

SECTION 3

THE IMPACT FLASH

3.1 DESCRIPTION OF THE IMPACT FLASH

The pact flash consists of two parts: a narrow, fast rise-time pulse of light followed by a much wider pulse which decays slowly to zero intensity. An example of an impact signature is shown in Figure 4. The initial pulse, which we refer to as the "spike", is typically less than 1 μsec wide. Spike widths as short as 0.1 μsec have been observed for .318 cm projectiles. Following the decay of the spike, the light intensity again rises and then slowly decays. We refer to this second pulse as the "tail".

In some cases, the spike and tail merge together. This makes it difficult or impossible to make measurements on the spike. Two examples of impact signatures in which the spike and the tail have partially merged are shown in Figure 5. In such cases as these, it is often possible to make some measurements on the spike, for example the initial rate of change of intensity, but impossible to make other measurements such as peak intensity. Figure 6 shows an example of impact signature in which the spike and the tail have merged completely. In such cases, it may still be possible to measure the initial rate of change of intensity of the spike, but not the spike intensity or time to reach maximum.

There are also cases in which the tail is very small and the spike is predominant. An example of an impact signature in which the spike is predominant is shown in Figure 7.

Before we can understand the reasons for such a variety of impact signatures, we must consider the origin of the tail and of the spike. This will be done in the next two subsections.

3.2 ORIGIN OF THE TAIL

Image converter photographs show that the tail is associated with a luminous ring which expands along the target plane at a velocity higher than the impact velocity. A head-on photograph of the luminous ring is shown in Figure 8. The time at which the photograph was taken is indicated on the scope trace.

The velocity of the luminous ring is a slowly increasing function of the impact velocity, as shown in Figure 9. The number inside each circle is the shot number.

Many of the properties of the luminous ring are most easily demonstrated by firing cone shaped projectiles. The reason for this is that many of the properties are a function of the angle between the target surface and the projectile surface. For the case of a spherical projectile, this angle varies from 0^{o} at the instant of impact to 90^{o} when the projectile has penetrated a distance equal to its radius. The angle is a constant for a conical projectile. In order to explain the origin of the luminous ring, and thus of the tail, we list here for reference a summary of results obtained from cone firings which were conducted previous to this program.

1. The luminous ring disappears when the angle between the target surface and the cone surface is less than

a certain critical angle α_c. The angle α_c depends on the target material, the cone material, and the cone velocity. Little or no light is emitted by an impacting cone whose impact angle is smaller than α_c.

2. For a given impact velocity, the luminous ring velocity decreases as the cone angle increases. The maximum ring velocity is observed at the critical angle.

3. The luminous ring produced by a cone at the critical angle travels faster than the luminous ring produced by a sphere at the same velocity.

These observations suggest that the luminous ring is related to the jet predicted by shaped-charge theory. In Birkhoff's[5] treatment of the collision of two plates, a jet of material is predicted and the velocity of the jet decreases as the angle between the plates increases. The geometry of the two-plate collision is shown in Figure 10.

In the co-ordinate system moving with the collision region, the two plates move towards the collision point with a speed $|V|$ and both the slug and the jet move away from the collision point with the same speed $|V|$. The similarity of a cone or sphere impact to the impact of two plates is evident from Figure 11.

Birkhoff's theory[5] predicts that the jet produced by a spherical projectile will have an infinite velocity. There is no concept of a critical angle in his theory. Walsh[6] considered the effect of shock waves on the collision and found that below a certain critical angle jetless collisions were possible. He found that if the point of contact between the target and projectile moved at a velocity greater than that or the shock waves in the target and projectile, the shocked material was effectively

held between the two shock surfaces and no jetting resulted. If, however, one of the shocks moved faster than the point of contact, shocked material could escape in the form of a jet. Three possible cases are illustrated in Figure 12. In case (a), the velocity of the point of contact is greater than the horizontal velocity of either the target shock or the projectile shock. The shocked material is trapped between the two shock surfaces, and no jetting results. The critical angle has not yet been reached. In (b), the horizontal velocity of the target shock is greater than the velocity of the contact point. Shocked material can escape in the form of a jet. A similar situation is shown in (c). In (b) and (c) the angle between the projectile surface and the target surface exceeds the critical angle. The critical angle, according to this picture, is the angle at which the velocity of the contact point is just equal to the horizontal velocity of the faster of the two shock waves.

In jetless collisions, very high pressures exist in the region between the two shock surfaces. A jetless configuration for an asymmetric collision (unlike materials, unequal velocities), is shown in Figure 13. The co-ordinate system is moving with the collision region, such that the point of contact between the target and projectile appears to be stationary. $\rho 1$ and $\rho 2$ are the densities of the projectile material and the target material. U_{o1} is the velocity of the projectile material, measured in the plane of the projectile surface, and U_{o2} is the velocity of the target material measured in the plane of the target surface. In the laboratory system of co-ordinates the target is stationary, so U_{o2} is also the velocity of the co-ordinate system which is moving with the contact point. The pressure P must be constant across the contact surface (slipstream) which separates the two dissimilar streams. A breakdown of the jetless

configuration must occur when either $\emptyset(P)$ or $\emptyset(P)$ reaches the critical angle associated with that stream. The critical angle is then given by

$$\alpha_c(P_c) = \phi_1(P_c) + \phi_2(P_c)$$

where Pc is the smaller of Pc_1 and Pc_2. Pc_1 is the pressure associated with the maximum possible deflection of the projectile stream, and Pc_2 is the pressure associated with the maximum possible deflection of the target stream. The equation for Pc_1 is given by Walsh[6] as

$$\frac{dP}{d\mu_1} = \frac{P(P-\rho_{o1}\mu_1)}{(\mu_1+1)\left[\mu_1\rho_{o1}U_{o1}^2 - P(\mu_1+2)\right]} \quad \text{at} \quad P = P_{c1},$$

where $\mu_1 = (\rho_1/\rho_{o1}) - 1$, ρ_1 is the density of the shocked projectile material, ρ_{o1} is the density of the unshocked projectile material, and U_{o1} is the velocity of the unshocked projectile material. A similar equation exists for Pc_2. The density of the shocked material can be calculated from the Rankine-Hugoniot equation

$$\rho_o W = \rho(W-U),$$

where W is the shock wave velocity and U is the particle velocity behind the shock.

Using the above equations, the critical pressure for copper-cadmium, titanium-cadmium, and aluminum-cadmium impact has been calculated. Results are shown in Figure 14.

After the jetting begins, the pressure falls to a low value. As viewed by an observer at the collision point the collision process appears to remain unchanged in time or in other words appears as steady

motion. It follows that we can use the Bernoulli equation to describe the flow. For compressible flow,

$$\int \frac{dP}{\rho} + \frac{V^2}{2} = \text{constant}$$

where P is the pressure, ρ is the density, and V is the velocity of the stream of material. The assumption made by Birkhoff[5] is "that the liner moves away from the exploded gases so fast that the pressure of its surface is very low and hence pressures are constant on all surfaces of the collapsing liner". From this it follows that the projectile, the projectile jet, and the shocked material all appear to approach or recede from an observer stationary at the point of contact at equal speed. Since the collision is asymmetric, the projectile material approaches at a speed different from the target material speed.

In the laboratory co-ordinate system the jet velocity is the vector sum of the jet velocity as seen by an observer at the collision point and the velocity of the collision point in the laboratory co-ordinate system. Figure 15 shows the projectile and target vectors and their components.

The projectile jet velocity in the laboratory co-ordinate system is the sum of $Vo/\sin\alpha$ and $Vo/\tan\alpha$, where Vo is the projectile velocity. We obtain for the projectile jet velocity and the target jet velocity.

$$U_{PJ} = \frac{V_o}{\sin\alpha} \left[\cos^2\alpha + 2\cos\alpha\cos\beta + 1 \right]^{1/2}$$

$$U_{TJ} = \frac{V_o}{\tan\alpha} \left[2\left(1 + \cos\beta\right) \right]^{1/2} .$$

Both U_{PJ} and U_{TJ} decrease as α increases. The maximum jet velocity occurs at the critical angle.

The jet predicted by shaped-charge theory has two of the properties exhibited by the luminous ring, i.e. it disappears below a certain critical angle and the jet velocity decreases as the cone angle increases. The agreement between the jet theory and the first two properties of the luminous ring has been shown to be quantitative as well as qualitative in another program which has just been completed.(7)

The third property of the luminous ring is more difficult to understand. Jet theory predicts that the maximum jet velocity depends only on the projectile velocity and the critical angle. The shape and size of the projectile do not affect the maximum jet velocity. Why then should a cone at the critical angle produce a faster luminous ring than a sphere at the same velocity? A reasonable explanation is suggested by the dependence of luminous ring velocity on sphere size. A plot of luminous ring velocity vs projectile velocity for copper-cadmium impacts is shown in Figure 16.

The .635 cm spheres consistently produce a faster luminous ring than the .159 cm spheres. The smaller spheres sweep through the critical angle much faster than the larger spheres. The angle at any time t is given by

$$\alpha = \cos^{-1}\left[1 - V_o t/r\right] ,$$

where Vo is the projectile velocity and r is the projectile radius. A small projectile spends less time with $\alpha_c < \alpha < \alpha_c + \delta$, where δ is some small angle, than a larger projectile. Therefore, less material will be emitted at the velocity corresponding to the critical angle. As the sphere continues to penetra the target, the angle α becomes continuously larger and the jet velocity becomes continuously smaller. It may be that the

amount of material emitted at the critical angle produces insufficient luminosity to be detected by our image converter cameras. In the case of a cone, α is not a function of r or t, and the jet material is all emitted at the same velocity.

An example of the luminous ring produced by a non-spherical projectile is shown in Figure 17. The time at which the photograph was taken is shown on the scope traces. The projectile was a polyhedron. In the directions for which the face angle was slightly above the critical angle, large luminous ring velocities were observed. In the directions for which the face angle was smaller than or much larger than the critical angle, no luminous ring was observed.

The dependence of jet velocity on projectile material is not large. Results for projectiles of magnesium, aluminum, titanium, iron, copper and garnet are shown in Figure 18.

In conclusion, it appears likely that the luminous ring is produced by the jet of material predicted by shaped-charge theory, and that the tail of the impact signature is the light emitted by the luminous ring.

3.3 ORIGIN OF THE SPIKE

The impact signature consists of two parts - a spike and a tail. Jet theory gives a satisfactory explanation of the origin of the tail. The origin of the spike will be discussed below in terms of the same jet theory.

In the region around the point of contact, the pressure produced by an initially jetless collision falls to a low value after jetting begins.

A luminous ring is associated with the low pressure jetting. However, the pressure cannot fall to a low value instantaneously, and so there is a time, immediately after jetting begins, during which the pressure decays to the low value associated with the luminous ring. There is a fast jet, i.e. a jet faster than the luminous ring, caused by the transition pressures. The fast jet is emitted at successively lower velocities as the pressure decays, and ultimately becomes the jet associated with the luminous ring. It must be stressed that the fast jet and the luminous ring are produced by the same process, but at different pressures. The fast jet is not luminous, except very near to the impact point as will be discussed below. This is probably because very little material is emitted in the form of a fast jet, while much more material is emitted in the luminous ring. The initial luminosity of the fast jet, near the impact point, is apparently responsible for the spike.

The fast jet was detected by secondary targets at right angles to the main target. The targets were mounted at 5, 10 or 20 cm from the impact point. Two basic types of secondary targets were used:

(1) Penetration type. The fast jet was detected when the particles in the jet penetrated an aluminized mylar film 10 microns thick mounted on a grounded metallic support. The particles caused a short circuit between the aluminum layer and the support.

(2) Ionization type. A short circuit between two overlapping aluminized mylar strips indicated the presence of an ionized gas. The circuit used in this case was such that a single pulse was given out at the instant of impact on the mylar.

A fast jet was detected by both types of targets. The velocity of the fast jet was more than twice the velocity of the luminous ring

produced by a spherical projectile, and about 1-1/2 times faster than the luminous ring produced by a cone at the critical angle. A plot of fast jet velocity vs projectile velocity for aluminum-aluminum impacts is shown in Figure 19. Luminous ring velocities are included for comparison.

Evidence that the spike is produced in a region of high pressure is provided by space resolved spectra of the impact flash. We set up our spectrograph such that a line on the target face was imaged on the slit of the spectrograph. The optical arrangement will be presented in Section 4.4. An example of the spectrum obtained is shown in Figure 20. Considerable line broadening exists at the impact point. Away from the impact points, along the path of the luminous ring, little or no broadening is observed. A space resolved spectrum is in some respects also time resolved, since points on the film which are successively farther from the impact point are exposed at successively later instants of time. The broadened central portion of the spectrum corresponds to the spike, and the relatively sharp emission lines which extend on either side of the impact point correspond to the tail.

Polychromator results provide further evidence that the spike consists mainly of continuum radiation and the tail consists mainly of line emission. The polychromator records for the 5085Å line of cadmium and for background radiation at 4922Å are presented in Figure 21. Both the spike and the tail are present at 5085Å.

In conclusion, the spike consists mainly of continuum radiation which is associated with line broadening. The line broadening may be caused by the high pressure which exists at the moment jetting begins.

SECTION 4

SPECTROSCOPIC STUDIES

4.1 INTRODUCTION

Three types of spectroscopic studies were undertaken - space-integrated time-resolved, space-integrated time integrated, and space-resolved time-integrated. The first type of study, space-integrated time-resolved, was conducted by putting photomultipliers at the exit slit of the spectrograph, and looking at selected cadmium emission lines. For the second type of study, space-integrated time integrated, light from the impact flash was allowed to fall uniformly on the entrance slit and the resulting spectrum was recorded on a photographic plate. For the space-resolved time-integrated studies, light from the impact flash was focussed on the entrance slit such that there was a one to one correspondence between points on the target and points on the entrance slit, and the resulting spectrum was recorded on a photographic plate. Results of each of the three types of studies will be discussed in the following subsections.

4.2 SPACE-INTEGRATED TIME-RESOLVED SPECTRA

For this type of study, the spectrograph was used as a polychromator with four photomultipliers at the exit slits looking at four different wavelengths. Three of the photomultipliers looked at cadmium emission lines at 3261Å, 3610Å, and 5085Å. Cadmium was chosen as a target material because it has a relatively simple spectrum, it is easy to vaporize,

and it is not expected to be present in micrometeoroid materials. The fourth photomultiplier looked at background radiation at about 4900Å.

The origin of some of the emission lines of cadmium is shown on the energy level diagram in Figure 22. In the notation $N^{2S+1}L_J$, N is the principal quantum number, S is the spin, L is the orbital angular momentum quantum number, and J is the vector sum of S and L. A detailed account of the meaning of each quantum number can be found in any good text on atomic physics.

The signal from each of the four photomultiplier tubes was displayed on an oscilloscope and photographed. The photographs display the time history of the impact flash.

The time histories at 3610Å and 5085Å resemble each other and differ from the time history at 3261Å. Since the 3261Å line arises from a transition into the ground state, while the other two lines originate from transitions between excited levels, it is not surprising that the 3261Å line is unique. It is the most easily excited of the three lines. In general, the 3261Å line has a spike with a faster rise time than the other two lines, and a more predominant tail than the other two lines. Two examples are shown in Figure 23.

The polychromator can also be used to study line broadening. For shots 899 and 903 the photomultiplier which normally looked at 5085Å was moved to 5060Å. The exit slit was 5Å wide. In each of the two shots the intensity was down by a factor of 20 from what it would have been at 5085Å. The shape of the pulse was also different from that expected at 5085Å. The spike peaked at 0.2 usec instead of 1.0 usec, and the intensity

of the tail was so small that it was not detected. These observations lend support to the theory that the spike is associated with continuum radiation, and the tail is associated with line emission.

The background radiation was also measured at various wavelengths between 4824Å and 4942Å. The intensity observed was unexpectedly high, almost as high as the intensity at 5085Å. In the 118Å wide region, the intensity of the continuum radiation appears to be uniform.

While the width of the spike is very dependent on target and projectile surface finish at 3610Å and 5085Å, around 4900Å it is not. Figure 24 shows the spikes for a rough target (Shot No. 109), for a rough projectile (Shot No. 118), and for a normal target and projectile (Shot No. 92). The spike in the background region of the spectrum is not stongly affected by target or projectile surface effects. The effect of target and projectile surface finish on the spike will be discussed more fully in Section 5.3

4.3 SPACE-INTEGRATED TIME-INTEGRATED SPECTRA

For this type of study, light from the impact was allowed to fall directly on the entrance slit of the polychromator, and a photographic plate was used in place of the exit slits and photomultipliers. Only a few spectra of this type were recorded, since the space-resolved time-integrated type yields more information.

A spectrum for aluminum impacting cadmium is shown in Figure 25. Some of the more predominant cadmium and aluminum lines are identified. The 4800Å line of cadmium appears to be more intense than the 5085Å line. In addition, the 4800Å line seems to be broadened more than the 5085Å line.

Possibly the 5085Å line should be replaced by the 4800Å line as a source of observables.

Lines identified in the spectrum produced by aluminum impacting cadmium at 5 km/sec (Shot No. 8) are shown in Table I. The spectrograph was an f/6.3 instrument with a 100 μ wide entrance slit and a 600 line/mm grating. The chemical composition of the aluminum projectile is shown in Table 2.

4.4 SPACE-RESOLVED TIME-INTEGRATED SPECTRA

Space-resolved spectra were obtained by focussing an image of the impact region on the entrance slit by means of quartz optics. A diagram of the optical system used is shown below.

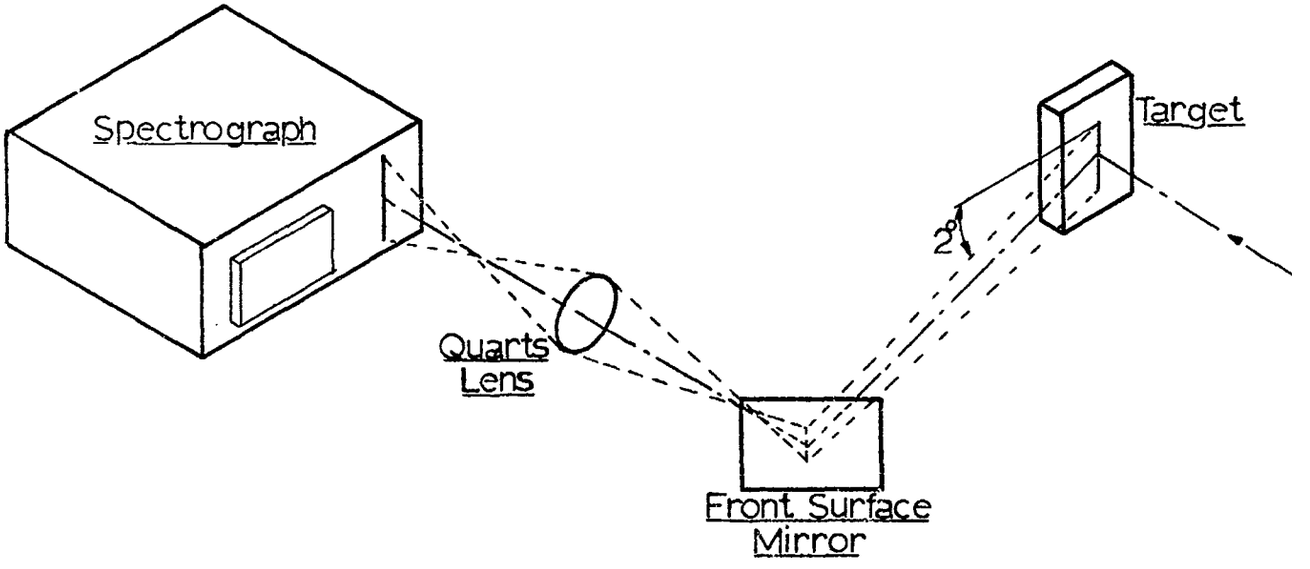

2265 Cd II	2707 Mg II	3934 Ca II
2312 Cd II	2802 Mg II	3944 Al I
2367 Al I	2816 Al II	3961 Al I
2373 Al I	2863 Si I	4033.1 Mn I
2506 Si I	2881 Si I	4226.7 Ca I
2516 Si I	3082.2 Al I	4254 Cr I
2529 Si I	3092.7 Al I	4274 Cr I
2573 Cd II	3247 Cd I	4289 Cr I
2575 Al I	3261.1 Cd I	4415 Cd II
2593 Mn II	3274 Cd I	4678.2 Cd I
2605 Mn II	3404 Cd I	4799.9 Cd I
2631.6 Al II	3466 Cd I	5085.8 Cd I
2652.5 Al I	3610 Cd I	
2660.4 Al I	3832 Mg I	
2748.6 Cd II	3838 Mg I	

TABLE 1. LINES IDENTIFIED, SHOT NO. 8

Copper	0.15 -- 0.40%
Iron	0.70
Magnesium	0.15
Silicon	0.40 -- 0.80
Titanium	0.15
Zinc	0.20
Chromium	0.15 -- 0.35

TABLE 2. COMPOSITION OF THE PROJECTILE

A space-resolved spectrum is also in some respects time-resolved, since points on the photographic plate which are successively farther from the image of the impact point are illuminated at successively later instants of time. The duration of the spike can be related to the width of the zone on the plate which shows strong line broadening. A long duration spike will show line broadening for some distance on either side of the impact point, while a short duration spike will show line broadening for a much smaller distance. The spectrum obtained from Shot No. 8, aluminum impacting cadmium, is shown in Figure 26. A record of the impact signature is also shown. The continuum which surrounds the impact point corresponds to the spike.

Figure 27 shows the spectrum obtained from Shot No. 120, titanium impacting cadmium. The line broadening extends for a large distance around the impact point. The record of the impact signature shows a very wide spike which peaks at about 1.5 usec. By way of contrast, the spike in Shot No. 8 peaks at about .4 usec.

An example of a very narrow spike and its associated spectrum is shown in Figure 28. The spectrum is from Shot No. 127, magnesium impacting cadmium. In this case the spike peaks at .05 usec and the region of line broadening on the plate is extremely narrow. The two narrow regions of line broadening which are visible on either side of the impact point correspond to two particles which came down range behind the main projectile. Their impact flash is indicated by "A" and "B" on the broadband record.

SECTION 5

PARAMETRIC STUDIES

5.1 INTRODUCTION

The purpose of the parametric studies was to find observables (measurable quantities) of the impact signature from which the velocity, size, and density of the impacting particle could be deduced. The observables chosen must satisfy several requirements. They must be functions of the projectile's velocity and size, but they must not depend very much on the projectile's shape or surface finish. They must not depend on an ambient atmosphere for their existence, i.e. they must continue to be good observables in the high vacuum conditions encountered in space. Several observables were investigated to see if they satisfied the necessary requirements. The peak intensity of the spike and of the tail, the time to reach maximum of the spike and the tail, and the rate of change of intensity of the spike were investigated. Of these observables, the only ones which satisfied the necessary requirements were the peak intensity of the spike and the rate of change of intensity of the spike.

The lines chosen for study were three lines of neutral cadmium. Cadmium was chosen as target material because it is easily excited, it has a relatively simple spectrum, and it is not expected to be present in typical micrometeoroids. The lines chosen were 3261Å, 3610Å, and 5085Å. A diagram of the transitions responsible for these wavelengths was shown in Figure 22. Projectile materials used were magnesium, aluminum, titanium, iron, copper, tungsten, and garnet. The metals were chosen to provide a wide range of densities; garnet was chosen to compare the behaviour of metallic and non-metallic projectiles.

5.2 BEHAVIOUR OF THE TAIL

Two measurements were made on the tail - peak intensity and time to reach maximum. Neither measurement yielded a good observable. The time to reach maximum was found to vary unpredictably from shot to shot, and so was rejected as an observable. The peak intensity of the tail varied as the velocity to the fourth power. The data exhibited considerable scatter. Experimental data points for smooth .318 cm spherical projectiles impacting on smooth cadmium targets are shown in Figure 29. The ordinate of the graph gives the number of microwatts of light energy which are incident on an area of 1 cm^2 at a distance of 1 meter from the impact point. Above about 5 km/sec the spike, which increases as velocity to the eighth power, becomes predominant and the tail intensity is difficult or impossible to measure. For this reason, the peak intensity of the tail has also been rejected as an observable.

5.3 BEHAVIOUR OF THE SPIKE

Three measurements were made on the spike - peak intensity, initial rate of change of intensity, and time to reach maximum. As in the case of the tail, the time to reach maximum was rejected as an observable. The projectile shape and surface finish affected the time to reach maximum to such a large extent that consistent results were not obtainable. The peak intensity and initial rate of change of intensity were found to vary consistently with projectile size and velocity. In the following paragraphs, the effect of projectile and target properties on the peak intensity I and the initial rate of change of intensity dI/dt will be discussed.

5.3.1 Intensity of the Spike

The peak intensity varies as the eighth power of velocity for all three of the cadmium lines analyzed. Figure 30 shows the 5085Å data points for copper projectiles impacting cadmium targets. A line was fitted to the data points by the method of least squares, and then the line was adjusted to the nearest integer, which was 8. Data points for the .635 cm projectiles do not follow the same trend as data points for the two smaller projectile sizes. This makes it difficult to calculate the diameter dependence of the spike intensity, as will be discussed later. Results for the 5085Å data points for projectiles other than copper are shown in Figure 31. The line for .318 cm copper projectiles is repeated for comparison. Figures 32-39 show spike intensity at 3610Å, 3261Å, background wavelengths, and broadband wavelengths. Background wavelengths are around 4900Å, between the cadmium lines at 4800Å and at 5085Å. The background photomultiplier measures the time history of the continuum (line broadened) radiation. Broadband radiation is measured in the wavelength region 3500Å - 6500Å.

The peak intensity is also a function of projectile diameter. Figures 40-42 show the variation of I/V^8 with projectile diameter. The data points at d = .042 cm and d = .080 cm (log d = 2.62 and 2.9 respectively) were obtained from in-house firings conducted shortly after the conclusion of the present program. The intensity appears to vary as $d^{2.9-4.0}$, depending on the wavelength being observed.

The range pressure, i.e. the pressure in the neighborhood of the target, does not affect the peak intensity very much. Table 3

shows the broadband spike intensity for three shots. For two of the shots the pressure was relatively low. For the third shot, the pressure was 1000 times higher. The broadband spike intensity is reduced by a factor 2 at the higher pressure. Polychromator results are not available for the high pressure shot, but the spikes at 3261Å, 3610Å, and 5085Å are usually similar in shape to the broadband spike, so we can accept the behaviour of the broadband spike as being representative of all the spikes.

Shot No.	Projectile diameter, cm	Velocity km/sec	Pressure Torr	Spike Intensity (Broadband)
142	.318	5.20	1.2×10^{-5}	5100
150	.318	5.15	1.5×10^{-5}	4800
146	.318	5.25	1.0×10^{-2}	2250

TABLE 3. PRESSURE DEPENDENCE OF THE SPIKE

The target surface finish affects the shape of the spike but not its magnitude. For Shot No. 109, the target face was covered with concentric grooves 1 mm apart and .3 mm deep. For Shot 116 the target face was covered with random scratches. Both targets affected the spike in the same way. The time to reach maximum was increased by a factor of 3, while the peak intensity was not affected. Figure 43 shows the shape of the spike at 3610Å for a rough target and for a highly polished target.

The projectile shape and surface finish affect the spike in much the same manner as the target surface finish. Spherical projectiles whose surface was covered with scratches and grooves produced a spike whose magni-

tude was the same as that for a polished projectile, but whose time to reach maximum was increased by a factor of 2-4.

A series of projectiles of various shapes was fired with the polychromator situated as shown in Figure 44. Each projectile was equal in mass to a .318 cm sphere. The purpose of the series was two-fold:- to examine the effect of the projectile shape on the impact spike, and to examine the possibility of observing the impact flash by looking at the target head-on.

With the polychromator arranged as shown in Figure 44, the intensity of the spike produced by a sphere was reduced by a factor 10. The shape of the spike was the same as if the polychromator had been viewing the impact flash at right angles to the projectile line of flight, as it normally did. For this reason, it appears that results obtained with the polychromator in its normal position will still be valid when the polychromator views the impact from a more head-on direction.

Figures 45-48 show the spike intensity for the various projectile shapes. The scatter is quite small, especially considering the variation in the shape of the projectile. The spheroids were fired with their symmetry axis aligned parallel to the line of flight.

The projectile material affects the magnitude of the spike. A plot of the 3610Å spike intensity for spheres of magnesium, aluminum, titanium, iron, copper, tungsten, and garnet was shown in Figure 33. Insufficient data are available to identify the dependence of the spike intensity on projectile density. It appears that the spike intensity for different projectile materials is not a function of the projectile density alone, since the spike from an aluminum projectile is more intense than for a

tungsten, titanium, or iron projectile. However, as shown on the graphs in Figures 31, 33, 35 and 37, the spike intensity for each material appears to vary as V^8.

5.3.2 Rate of Change of Intensity of the Spike

The rate of change of spike intensity, dI/dt, also depends on the properties of the projectile, of the target, and of the ambient atmosphere. Figures 49-52 show the variation of dI/dt with projectile velocity. In each case, a line of slope 6 is drawn through the data points. The fit is quite good in all but a few cases. The scatter about the line of slope 6 is much the same as the scatter of the intensity data points about a line of slope 8.

dI/dt is also a function of projectile diameter. The quantity dI/dt divided by V^6 is plotted against log diameter in Figure 53. There is considerable scatter i the data for the .635 cm projectiles. The scatter seems to decrease as the projectile diameter decreases. A line of slope 2.1 has been drawn through the data points, but due to scatter the slope could vary considerably from 2.1.

The target surface finish affects the value of dI/dt. Polished targets tend to increase dI/dt, and rough targets tend to decrease it. Values of dI/dt for rough targets and for polished targets are shown in Table 4. Values are normalized to the same velocity by dividing by V^6.

Shot No.	Target Description	$dI/dt/V^6$ 3610Å
99	Normal, target, slight polish	.023
109	Rough, spiral grooves 1 mm apart, .3 mm deep.	.016
113	Highly polished	.0265
116	Rough, covered with random scratches and grooves.	.0225

TABLE 4. dI/dt FOR VARIOUS TARGET SURFACES

dI/dt is also affected by the shape and surface finish of the projectile. In general, the effect of a roughened projectile surface or of a non-spherical projectile was to increase dI/dt. The effect of projectile surface finish and shape is shown in Table 5. Values of dI/dt are again normalized to constant velocity by dividing by V^6. In each case, the target was polished.

Shot No.	Projectile	$dI/dt/V^6$ 3610Å
113	Normal, polished	.027
117	Polyhedron	.059
118	Scratched sphere	.059

TABLE 5. dI/dt FOR VARIOUS PROJECTILE SURFACES

For the series of head-on shots described on page 26, the variation of dI/dt with projectile shape is shown in Figures 54 and 55. The low value of dI/dt produced by the prolate spheroid is not surprising, since a prolate spheroid behaves like a sphere of smaller radius.

The dependence of dI/dt on projectile material is much the same as the dependence of I on projectile material. Complete plots of dI/dt for various projectile materials are found in Figures 50 and 52.

In conclusion, the peak intensity and rate of change of intensity of the spike vary consistently with projectile velocity and size, and are relatively unaffected by the projectile shape and surface finish. Time to reach maximum varies too much with projectile shape to be useful as an observable.

SECTION 6

EXPERIMENTAL RESULTS

6.1 TABULATED RESULTS

The tables on the following pages show the results of all shots which yielded measurable data. Most of the shots which are not included were failures either because the projectile missed the target or because small particles travelling ahead of the projectile caused the electronics to pretrigger. Eighty shots are listed in the tables.

Projectile materials used were magnesium, aluminum, titanium, iron, copper, tungsten, and garnet. Two alloys of aluminum were used, type 17ST4 for shots 1 and 2, and type 65ST6 for all other shots. Five projectile diameters were used, .158 cm (1/16"), .318 cm (1/8"), .478 cm (3/16"), .572 cm (.22 calibre), and .635 cm (1/4"). Only two shots were fired with a .478 cm projectile, and only four with a .572 cm projectile. In most cases, the projectile shape was spherical, although polyhedrons and spheroids were also fired. Projectile surface finish was smooth for all but a few shots. Velocity ranged from 1.04 km/sec to 7.72 km/sec.

Target materials used were mild steel, aluminum, and cadmium. Beginning with shot 27, all targets were cadmium. Up to shot 104, the targets were finished by turning them on a lathe. Although the targets felt smooth to the touch (hence the designation "smooth" in the tables) microscopic examination showed small concentric ridges on the target face. Data from shot 108 indicated that polishing the target results in better separation of the spike from the tail, so targets subsequent to 108 were

polished after they were turned on the lathe.

The pressure is given in Torr, i.e. in mm of Hg. Prior to shot 87, most range pressures were about 2×10^{-5} Torr. A new cold trap was added to the pumping system just prior to Shot 87, and as a result pressures for subsequent shots were around 5×10^{-6} Torr.

Luminous ring velocity is given in km/sec. The velocity of the luminous ring was obtained by time and distance measurements on the photographs of the luminous ring obtained from the image converter cameras. The fast jet velocity was obtained from the pulses from the secondary targets. Fast jet velocity was measured only on Shots 1-10. There were not enough scope channels to allow secondary targets and the polychromator to be used at the same time.

The broadband photomultiplier was sensitive from 3500Å to 6500Å. Intensity values given in the tables are relative, since absolute intensity measurements would require an accurate discription of the spectral distribution of the radiation in the impact flash. Such a description was not available.

Intensity values for the background wavelength and the for 3261Å, 3610Å, and 5085Å lines are given in microwatts per square centimeter of detector surface at a distance of one meter from the impact point. dI/dt is given in units of microwatt/cm^2/microsec at a distance of 1 m.

6.2 EXPERIMENTAL ERROR

Several sources of error which may affect the data are discussed below.

Error in the velocity measurement is less than 1%. For each shot, five time-and-distance measurements were obtained: muzzle detector to first velocity station, first velocity station to second velocity station, second velocity station to third velocity station, third velocity station to impact, and muzzle detector to impact. The velocities obtained from these measurements usually agreed with each other to within 1%. The reported velocity is the average of the five values obtained.

Errors in the polychromator data arise from several sources: calibration errors, electronic errors, and measurement errors. The photomultipliers were calibrated periodically with an Osram U.V. standard lamp, and they were also calibrated before each shot with a cadmium vapor lamp. Calibration error is probably less than 5%. Variations of 5-10% in photomultiplier response to the cadmium vapor lamp were observed from shot to shot. This variation could be caused by small changes in mirror, slit, grating, and photomultiplier positions due to vibration and temperature change. Small changes in the voltages applied to the photomultipliers could also contribute to the variation. The scopes used to record the signals from the polychromator were calibrated monthly, but errors in time and voltage measurements could still be present. Losses in the cables from the instrumentation area to the scopes in the control room was another source of error. Although the losses could be measured accurately at any given frequency, the losses were frequency dependent, and the actual attenuation suffered by any given polychromator signal was unknown. It is estimated that electronic errors, including cable losses, were about 10%. Measurement errors were highest on the dI/dt measurements. While it was easy to measure I from the scope photographs, assigning an initial slope to a line whose slope was often changing in time,

or obscured by noise, was sometimes difficult. It is estimated that the measurement error (from the scope traces) in I was less than 5% and in dI/dt was less than 25%. Including all sources of error, it is estimated that intensity measurements have an error of $\pm$ 25%, and dI/dt measurements have an error of $\pm$ 45%.

Shot No.	1	2	3	4	5	7	8	9	10
Projectile: Material	A117ST4	A117ST4	A165ST6	Al.	Al.	Al.	Al.	Al.	Al.
Diameter, cm.	.635	.635	.635	.635	.635	.635	.635	.635	.635
Shape	Sphere	Sphere	Sphere	Sphere	Sphere	Sphere	Sphere	Sphere	Sphere
Surface finish	Smooth	Smooth	Smooth	Smooth	Smooth	Smooth	Smooth	Smooth	Smooth
Velocity, km/sec	5.16	5.30	4.94	3.89	6.05	5.43	5.00	6.04	5.88
Target: Material	Mild steel	A165ST6	A165ST6	Al.	Al.	Cd.	Cd.	Al.	Al.
Surface finish	Smooth	Smooth	Smooth	Smooth	Smooth	Smooth	Smooth	Smooth	Smooth
Pressure, Torr x10^5	40.	4.0	2.5	3.2	2.0	3.2	2.0	1.5	2.0
Velocity-Luminous ring	14.0	15.6	17.0	14.6	18.6	-	14.4	16.8	16.0
Fast Jet (km/sec)	23.0	33.0	37.6	32.0	35.0	22.4	22.4	32.4	30.6
Broadband: Intensity	--	6000	4700	700	6000	--	--	15,000	330

Shot No.	11	13	15	17	18	20	27	29	30
Projectile: Material	Al.	Al.	Al.	Al.	Al.	Al.	Al.	Al.	Al.
Diameter, cm.	.318	.318	.318	.635	.318	.159	.478	.478	.318
Shape	Sphere	Sphere	Sphere	Sphere	Sphere	Sphere	Sphere	Sphere	Sphere
Surface finish	Smooth	Smooth	Smooth	Smooth	Smooth	Smooth	Smooth	Smooth	Smooth
Velocity km/sec	3.52	6.00	7.48	7.29	7.85	8.25	3.54	5.77	5.86
Target: Material	Al.	Al.	Al.	Al.	Al.	Al.	Cd.	Cd.	Cd.
Surface finish	Smooth	Smooth	Smooth	Smooth	Smooth	Smooth	Smooth	Smooth	Smooth
Pressure, Torr $x10^5$	2.4	2.0	2.2	4.0	1.7	2.0	6.0	2.0	2.4
Velocity-Luminous ring	16.3	17.0	16.2	21.6	14.8	--	10.9	12.2	11.2
Broadband: Intensity	18	210	1800	21,000	1500	80	1720	2880	16,500
Background: Wavelength Å	--	--	--	--	--	--	--	--	--
Intensity uw/cm^2@1m	--	--	--	--	--	--	--	--	--
3261Å: Intensity	--	--	--	--	--	--	--	--	200
3610Å: Intensity	--	--	--	--	--	--	132	650	475
dI/dt	--	--	--	--	--	--	150	965	770
5085Å: Intensity	--	--	--	--	--	--	70	1100	1750
dI/dt	--	--	--	--	--	--	77	1550	290

Shot No.	35	37	39	40	41	51	54	56	60
Projectile: Material	Cu	Cu	Cu	Cu	Mg	Cu	Al	Al	Ti
Diameter, cm.	.318	.318	.635	.635	.318	.318	.318	.318	.318
Shape	Sphere	Sphere	Sphere	Sphere	Sphere	Sphere	Sphere	Sphere	Sphere
Surface finish	Smooth	Smooth	Smooth	Smooth	Smooth	Smooth	Smooth	Smooth	Smooth
Velocity km/sec	5.97	3.82	4.60	6.00	3.77	5.87	4.14	7.00	4.25
Target: Material	Cd	Cd	Cd	Cd	Cd	Cd	Cd	Cd	Cd
Surface finish	Smooth	Smooth	Smooth	Smooth	Smooth	Smooth	Smooth	Smooth	Smooth
Pressure, Torr $x10^5$	2.6	1.6	3.0	3.3	2.0	2.8	2.3	2.4	1.0
Velocity-Luminous ring	-	-	-	14.6	9.6	-	-	-	-
Broadband: Intensity	3800	270	-	-	75	2400	730	62,500	-
Background:Wavelength Å	-	-	-	-	-	-	-	-	-
Intensity uw/cm^2@1m	-	-	-	-	-	-	-	-	-
3261Å: Intensity	29.	-	-	-	-	11.6	-	-	-
3610Å: Intensity	-	-	458	-	-	506	-	2400	-
dI/dt	-	-	720	-	-	960	-	1370	-
5085Å: Intensity	252	6.2	337	1200	-	522	26.5	1640	2.8
dI/dt	840	28	537	1590	-	542	33.6	940	84

Shot No.	62	63	64	65	67	69	72	75	77
Projectile: Material	Cu	Cu	Ti	Ti	Ti	Ti	Ti	Ti	Ti
Diameter: cm.	.572	.572	.572	.572	.318	.159	.635	.635	.635
Shape	Hemisphere	h'sphere	h'sphere	h'sphere	Sphere	Sphere	Sphere	Sphere	Sphere
Surface	Smooth	Smooth	Smooth	Smooth	Smooth	Smooth	Smooth	Smooth	Smooth
Velocity: km/sec	1.04	1.60	1.28	1.90	5.19	5.0	5.25	3.72	3.98
Target: Material	Cd	Cd	Cd	Cd	Cd	Cd	Cd	Cd	Cd
Surface finish	Smooth	Smooth	Smooth	Smooth	Smooth	Smooth	Smooth	Smooth	Smooth
Pressure, Torr x10^5	3.7	2.6	4.0	3.8	3.8	3.2	4.1	3.8	3.9
Velocity-Luminous ring	-	-	-	-	-	-	-	-	-
Broadband: Intensity	1.18	650	8	10	-	600	220,000	-	-
Intensity uw/cm^2@1m	-	-	-	-	-	-	-	-	-
3261Å: Intensity	-	4.8	.16	-	-	-	4250	-	-
3610Å: Intensity	-	.66	-	.26	-	.96	9000	-	-
dI/dt	-	5.7	-	-	650	11	8500	113	96
5085Å: Intensity	.31	.17	-	.78	-	-	5060	-	-
dI/dt	12.5	1.47	-	8.8	175	-	3800	480	182

Shot No.	78	81	82	84	85	87	88	89	90
Projectile: Material	Ti	Ti	Cu	Cu	Cu	Cu	Cu	Cu	Cu
Diameter, cm.	.318	.159	.635	.318	.318	.159	.159	.635	.635
Shape	Sphere	Sphere	Sphere	Sphere	Sphere	Sphere	Sphere	Sphere	Sphere
Surface finish	Smooth	Smooth	Smooth	Smooth	Smooth	Smooth	Smooth	Smooth	Smooth
Velocity km/sec	4.50	6.25	2.86	3.30	5.00	4.97	7.20	5.20	3.95
Target: Material	Cd	Cd	Cd	Cd	Cd	Cd	Cd	Cd	Cd
Surface finis: e	Smooth	Smooth	Smooth	Smooth	Smooth	Smooth	Smooth	Smooth	Smooth
Pressure, Torr x10^5	4.0	1.6	2.0	1.3	2.5	.68	1.0	1.0	.6
Velocity-Luminous ring	-	-	11.4	-	-	-	11.0	-	-
Broadband: Intensity	-	5500	1360	280	2000	230	-	9000	3000
Background:Wavelength Å	-	-	4824	4824	4824	4824	4824	4824	4824
Intensity uw/cm^2@1m	-	-	-	-	27.	-	26.	320	37.5
3261Å: Intensity	-	108.	4.8	0.9	25.	-	85.	-	-
3610Å: Intensity	-	47	23.4	5.7	-	4.0	120.	945	158
dI/dt	42	136	133	53	686	75.6	970	7000	1600
5085Å: Intensity	-	-	10.1	2.2	-	4.3	96.5	361	40.7
dI/dt	29	230	70.	23.8	345	20.	177	870	330

Shot No.	92	94	99	100	103	104	108	109
Projectile: Material	Cu	Cu	Cu	Cu	Cu	Cu	Cu	Cu
Diameter: cu.	.318	.159	.318	.318	.635	.635	.318	.318
Shape	Sphere	Sphere	Sphere	Sphere	Sphere	Sphere	Sphere	Sphere
Surface finish	Smooth	Smooth	Smooth	Smooth	Smooth	Smooth	Smooth	Smooth
Velocity km/sec	3.85	7.72	4.40	4.47	5.00	4.07	3.90	4.10
Target: Material	Cd	Cd	Cd	Cd	Cd	Cd	Cd	Cd
Surface finish	Smooth	Smooth	Smooth	Smooth	Smooth	Smooth	Highly Polished	Rough
Pressure, Torr $x10^5$	1.2	.84	.5	3.5	.45	.48	.70	.70
Velocity-Luminous ring	-	-	-	-	14.2	12.4	11.0	-
Broadband: Intensity	520	3900	1440	1330	-	-	3000	530
Background-Wavelength Å	4824	4824	4824	4824	4942	4925	4925	4905
Intensity: uw/cm^2@1m	11.3	83	9.65	14.2	75.	18.7	14.3	16.5
3261Å: Intensity	3.6	7.0	7.6	11.7	48.	-	16.	4.8
3610Å: Intensity	29.	132	18.2	46.3	-	-	84.	34.
dI/dt	177.	1000.	167.	143.	-	-	360.	78
5085Å: Intensity	7.85	145.	12.0	25.6	90.	33.6	54.	23.
dI/dt	72.4	350.	96.5	-	510.	-	164.	52.

Shot No.	110	113	115	116	117	118	120	122	123
Projectile: Material	Cu	Cu	Cu	Cu	Cu	Cu	Ti	Al	Fe
Diameter, cm.	.159	.318	.318	.318	.318	.318	.318	.318	.318
Shape	Sphere	Sphere	Sphere	Sphere	Poly-hedron	Sphere	Sphere	Sphere	Sphere
Surface finish	Smooth	Smooth	Smooth	Smooth	Smooth	Scratched	Smooth	Smooth	Smooth
Velocity, km/sec	5.44	6.80	6.65	5.86	6.10	6.10	5.95	3.70	3.80
Target: Material	Cd	Cd	Cd	Cd	Cd	Cd	Cd	Cd	Cd
Surface finish	Smooth	Polished	Polished	Rough	Polished	Polished	Polished	Polished	Polished
Pressure, Torr $x10^5$	.42	.78	.72	.78	.78	.55	.70	.75	.76
Velocity-Luminous ring	11.0	-	-	-	-	12.0	-	11.8	11.0
Broadband: Intensity	105	4500	5000	2700	9000	9000	33,000	600	26.
Background:Wavelength Å	-	5060	-	5060	4925	4905	-	4925	4925
Intensity: uw/cm^2@1m	-	90.5	-	20.	86.	110.	-	5.	0.1
3261Å: Intensity	3.0	-	-	49.	77.	79.	-	9.5	-
3610Å: Intensity	23.3	-	-	530.	720.	800.	-	27.	4.
dI/dt	99.	2600	-	900.	3000.	3000.	-	185.	-
5035Å: Intensity	12.6	-	-	-	245.	245.	-	7.	.65
dI/dt	70.	-	-	-	400.	-	-	60.	-

Shot No.	124	125	126	127	128	129	130	131	132
Projectile: Material	Fe	Ti	Ti	Mg	Mg	W	Cu	Cu	Cu
Diameter: cm,	.318	.318	.318	.318	.318	.318	.318	.159	.635
Shape	Sphere	Sphere	Sphere	Sphere	Sphere	Sphere	Sphere	Sphere	Sphere
Surface finish	Smooth	Smooth	Smooth	Smooth	Smooth	Smooth	Smooth	Smooth	Smooth
Velocity, km/sec	5.20	3.52	5.10	4.05	5.00	4.32	5.08	4.91	5.32
Target Material	Cd	Cd	Cd	Cd	Cd	Cd	Cd	Cd	Cd
Surface finish	Polished	Polished	Polished	Polished	Polished	Polished	Polished	Polished	Polished
Pressure, Torr $x10^{5}$	.52	.85	.48	.50	.10	.80	2.0	.58	.60
Velocity:Luminous ring	-	11.6	12.0	11.6	-	-	-	10.6	13.7
Broadband: Intensity	145.	-	1340	160	280	680	2770	525	23,000
Background:Wavelength Å	4922	4922	4922	4922	4922	4922	4922	4922	4922
Intensity uw/cm^{2}@1m	2.8	8.0	6.3	0.5	5.5	18.	29.	4.5	71.
3261Å; Intensity	2.95	8.8	11.5	0.22	2.45	5.3	29.	4.8	136.
3610Å: Intensity	-	28.	25.	.38	4.4	8.	-	8.65	880.
dI/dt	-	318	286.	6.5	75.	-	-	110	186
5085Å: Intensity	3.6	19.	10.8	.42	3.75	9.	51.	7.	145
dI/dt	-	170.	70.	8.25	42.	-	193.	26.	560.

Shot No.	138	140	141	142	143	144	146	149	150
Projectile: Material	Garnet	Cu	Cu	Cu	Cu	Cu	Cu	W	Cu
- ameter: cm.	.318	.318	.318	.318	.318	.318	.318	.318	.318
Shape	Poly-hedron	Poly-hedron	Sphere	Sphere	Oblate Spheroid	Prolate Spheroid	Sphere	Sphere	Sphere
Surface finish	Smooth	Smooth	Scratched	Smooth	Smooth	Smooth	Smooth	Smooth	Smooth
Velocity km/sec	4.16	5.05	5.28	5.20	5.10	5.30	5.25	5.10	5.15
Target: Material	Cd	Cd	Cd	Cd	Cd	Cd	Cd	Cd	Cd
Surface finish	Polished	Polished	Polished	Polished	Polished	Polished	Polished	Polished	Polished
Pressure, Torr $x10^5$	.75	1.0	.85	1.2	1.0	1.1	1000.	1.3	1.5
Velocity-Luminous ring	12.0	10.4	11.6	12.2	10.4	-	-	-	-
Broadband: Intensity	250.	2700	4600	5100	1200	590	2250	5300	4800
Background: Wavelength Å	4922	4922	4910	4922	4900	4890	-	-	-
Intensity uw/cm^2@1m	1.3	-	1.9	-	0.4	0.4	-	-	-
3261Å: Intensity	1.2	0.6	0.8	0.7	0.15	0.20	-	-	-
3610Å: Intensity	2.6	15.	18.	10.7	8.7	6.2	-	-	-
dI'dt	47.	137.	130.	110	-	41.	-	-	-
5085Å: Intensity	1.3	10.2	14.	12.5	-	5.2	-	-	-
dI/dt	16.7	68	98.	-	-	63.	-	-	-

SECTION 7

CONCLUSION AND DISCUSSION

A study of the radiation emitted when a hypervelocity projectile impacts a cadmium target can reveal the velocity and size of the impacting projectile, provided its composition is known. Since the emitted radiation contains line emission which is characteristic of the materials involved in the impact, the composition of the projectile can be measured spectroscopically. In the case of micrometeoroids where only a few types of composition are expected, measurement of a few emission lines of elements expected to be present in the micrometeoroid may be sufficient to yield the micrometeoroid type, and hence its composition. Once the composition of the impacting projectile is known, the velocity and size can be calculated from

$$I = K_1 V^8 d^{2.9-4.0}$$

$$\frac{dI}{dt} = K_2 V^6 d^{2.1}$$

where I is the intensity of the first pulse of radiation produced by the impact, $\frac{dI}{dt}$ is the initial rate of change of intensity of the pulse, V and d are the projectile velocity and diameter, and K_1 and K_2 are constants for a given projectile composition. Considerable confidence is placed on the values 8 and 6 for the velocity exponents. With the exception of a few titanium shots, all the data tend to support a V^8 and V^6 dependence. Less confidence is placed on the exponents showing the diameter dependence. The exponents are based entirely on copper projectiles, and only two projectiles smaller than .159 cm were fired. The diameter exponents also appear to depend on the wavelength of the radiation being observed.

The possibility that the two equations above are not independent has been considered. An example of diameter exponents which make the two equations dependent is

$$I = K_1 V^8 d^4$$

$$\frac{dI}{dt} = K_2 V^6 d^3$$

In this case V and d cannot be evaluated separately, and only the product $V^2 d$ can be evaluated. However, the implications of such a case do not seem reasonable. If the equations are dependent, dI/dt can be calculated from I. An example which shows that this is not reasonable is the example of a large slow projectile and a small fast projectile. The diameter can be adjusted such that a 1 km/sec projectile produces an impact flash of exactly the same intensity as one produced by a 100 km/sec projectile. If the equations are dependent, the dI/dt for the two impacts will also be identical. However, the critical angle associated with the large slow projectile is swept through much more slowly than the one associated with the small fast projectile, so identical dI/dt seems highly unlikely.

REFERENCES

1. J.S. Clark, R.R. Kadesch, R.W. Grow — Spectral Analysis of the Impact of Ultra Velocity Copper Spheres into Copper Targets. University of Utah, Technical Report No. OSR-13.

2. R.W. MacCormack — Investigation of Impact Flash at Low Ambient Pressure. Proceedings of the Sixth Symposium on Hypervelocity Impact, Vol. II, Part 2, p. 613.

3. J.W. Gehring, R.L. Warnica — An Investigation of the Phenomena of Impact Flash and Its Potential Use as a Hit Detection and Target Discrimination Technique. Proceedings of the Sixth Symposium in Hypervelocity Impact, Vol. II, Part 2, Page 627.

4. R.A. Koehler — Spectroscopic Studies of the Impact Flash. University of Western Ontario, 1965.

5. G. Birkhoff, D.P. MacDougall, E.M. Pugh, G. Taylor — Explosives with Lined Cavities. Journal of Applied Physics 19, 563 (1948).

6. J.M. Walsh, R.G. Shreffler, F.J. Willig — Limiting Conditions for Jet Formation in High Velocity Collisions. Journal of Applied Physics 24, 349 (1953).

7. B. Jean, T. Rollins — Hypervelocity Impact Flash for Hit Detection and Damage Assessment. Computing Devices Report No. 1188/FR1, March 1968. USAF Contract No. F08635-67-C-0044.

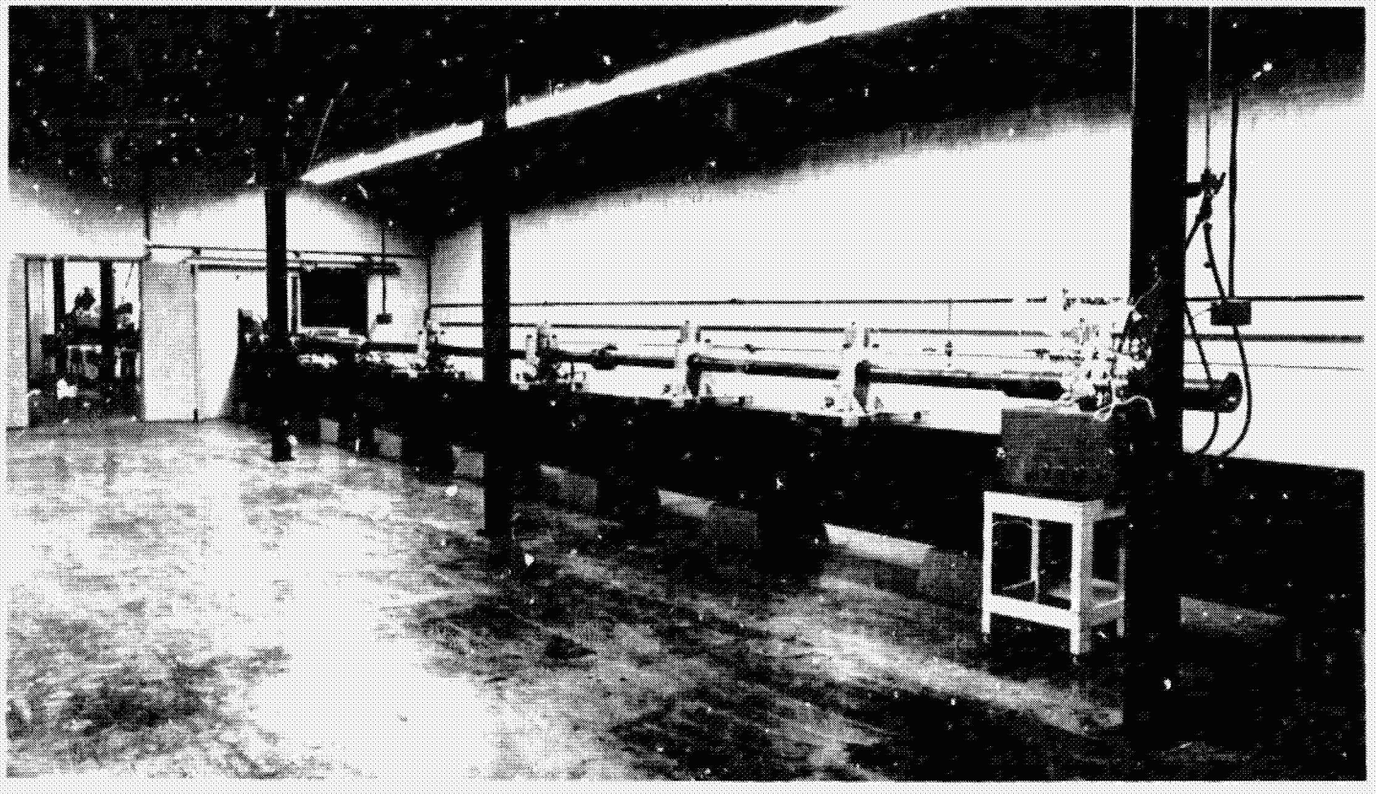

Figure 1. 1/2-inch Light Gas Gun

Figure 1.

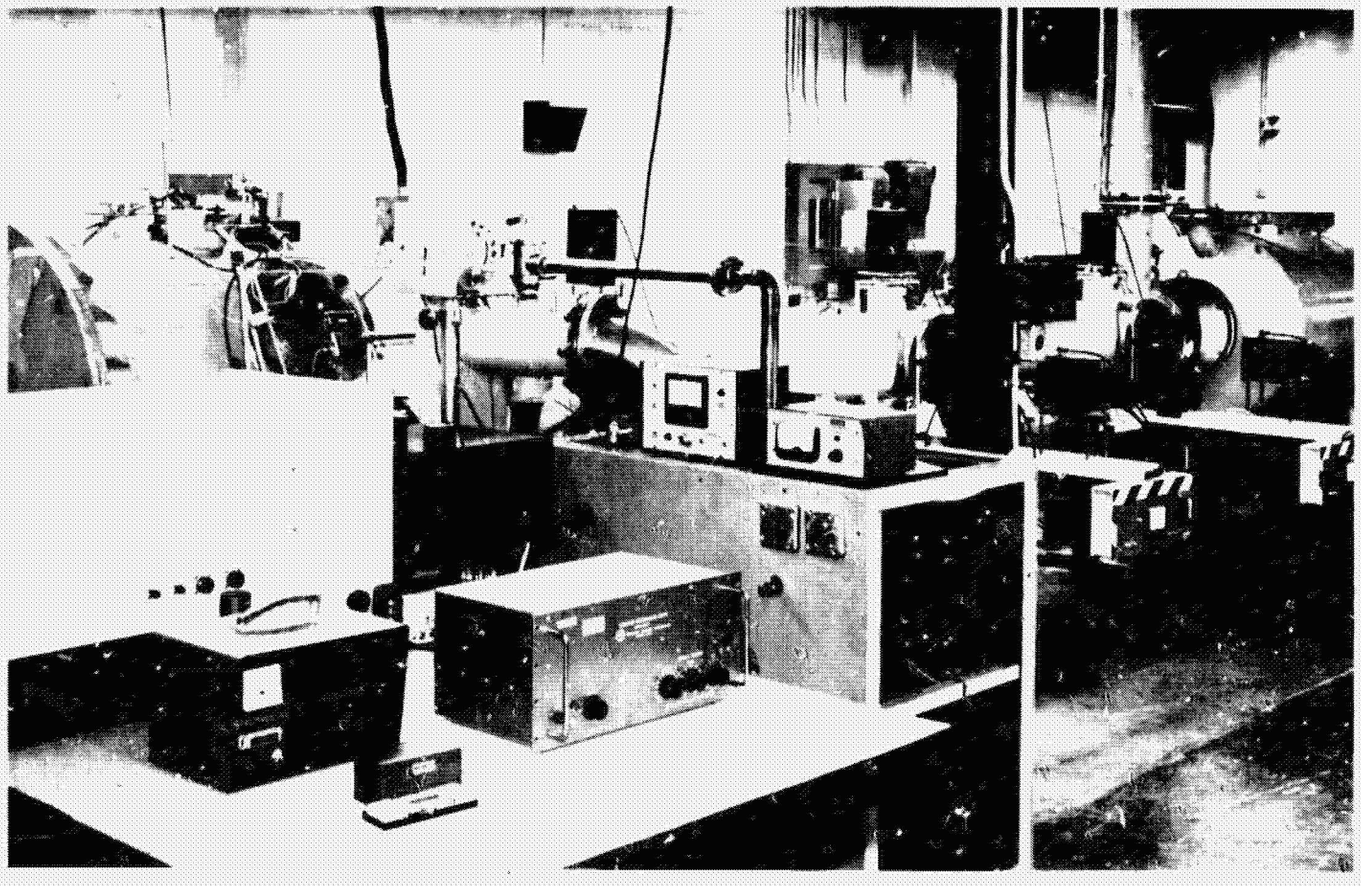

Figure 2(a). Hypervelocity Impact Range

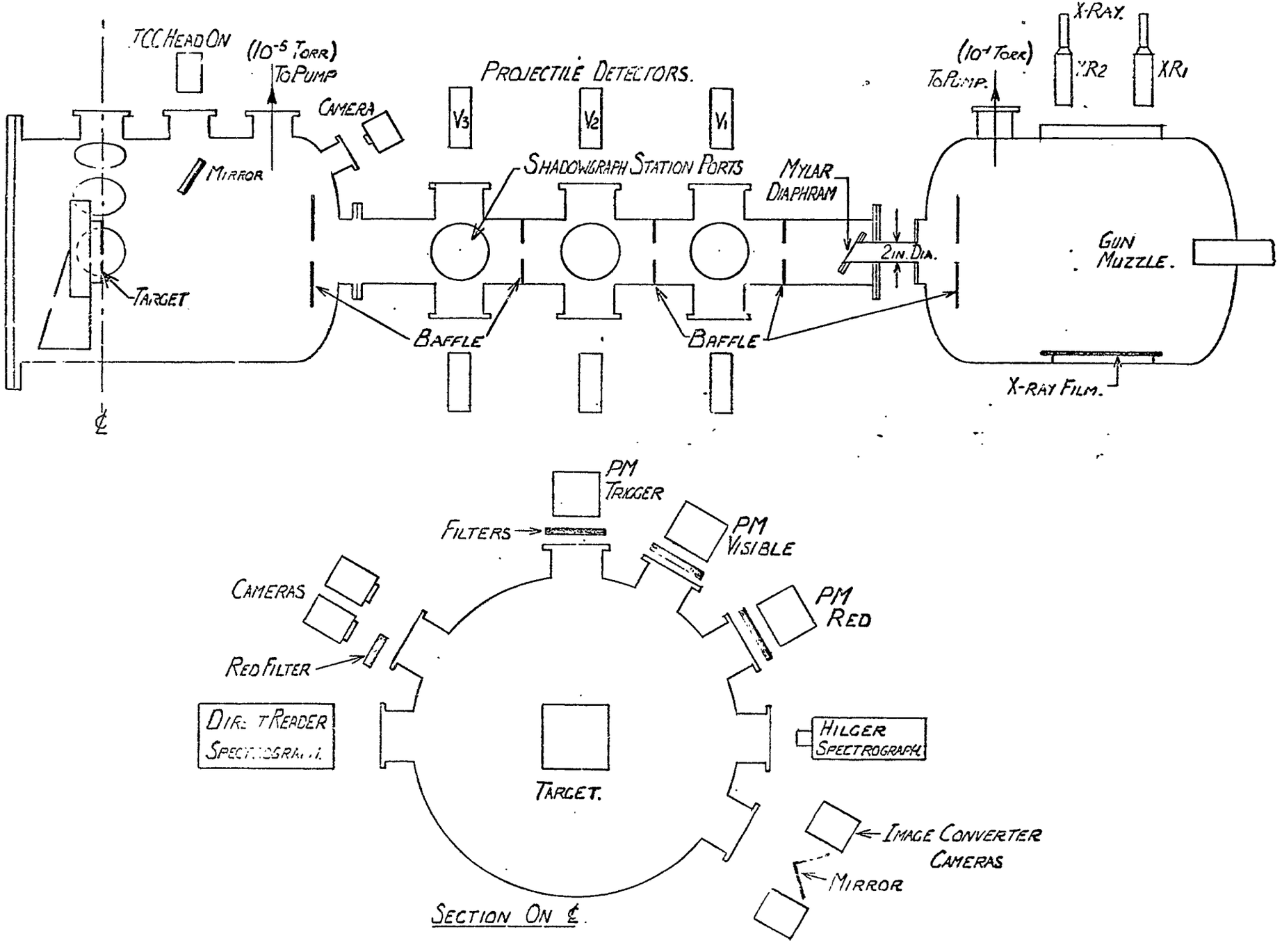

Figure 2(b) Hypervelocity Impact Range

Figure 2(b) Hypervelocity Impact Range

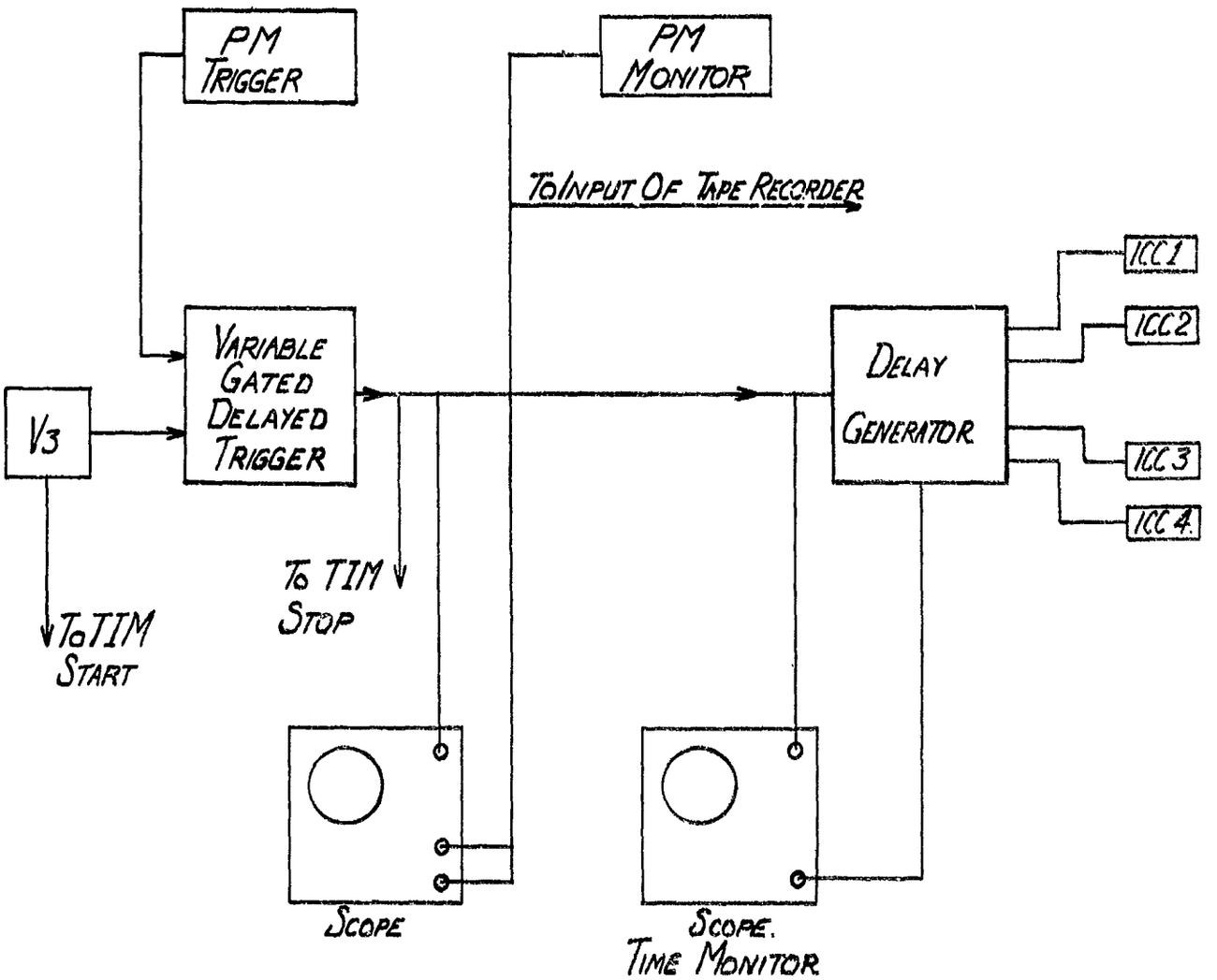

Figure 3. Block Diagram of Photomultiplier Radiation Monitors

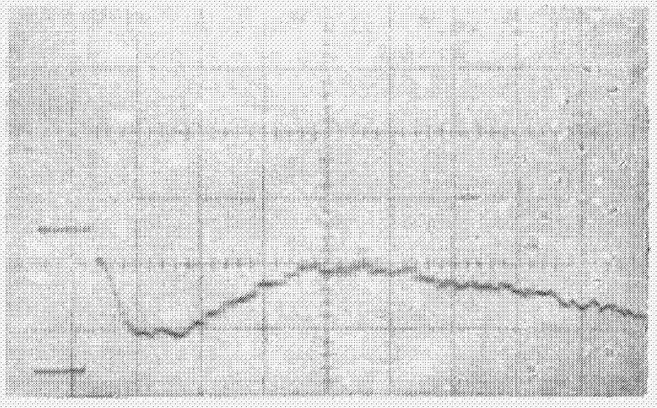

Shot No. - 125
Projectile - .318 cm Titanium
Target - Cadmium
Velocity - 3.5 km/sec
Wavelength - Broadband
Sweep - 1 usec/division

Figure 4. Example of Impact Signature

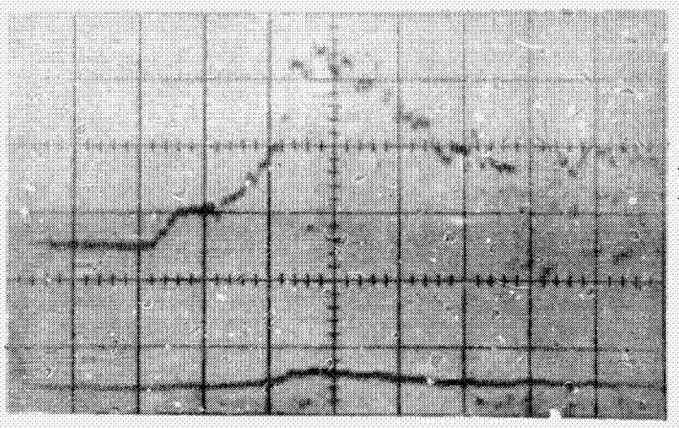

Shot No. - 103
Projectile - .635 cm Copper
Target - Cadmium
Velocity - 5.0 km/sec
Wavelength - 5085Å
Sweep - 0.5 usec/division

Figure 5(a). Spike and Tail Partially Merged

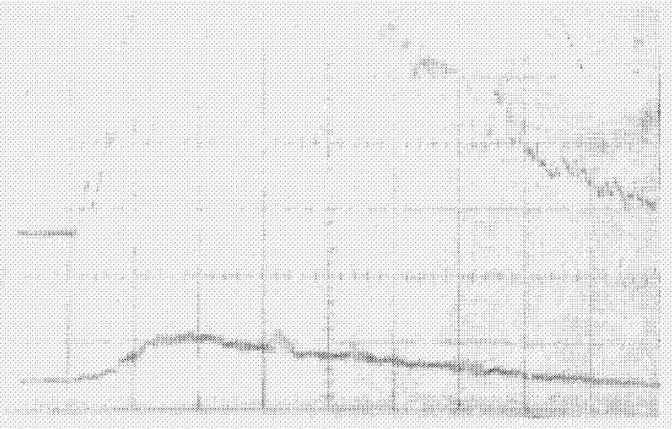

Shot No. - 126
Projectile - .318 cm Titanium
Target - Cadmium
Velocity - 5.1 km/sec
Wavelength - 5085Å
Sweep - 1 usec/division

Figure 5(b). Spike and Tail Partially Merged

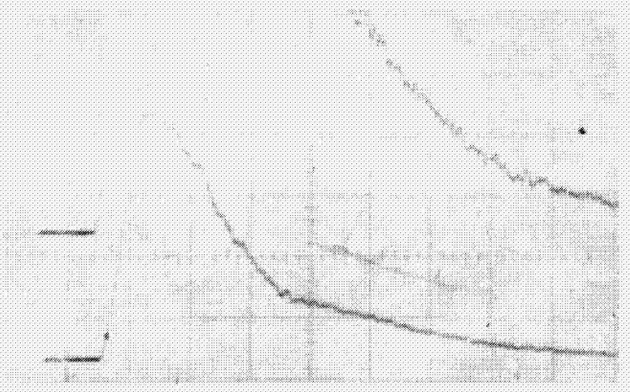

Shot No. - 81
Projectile - .159 cm Titanium
Target - Cadmium
Velocity - 6.25 km/sec
Wavelength - 3610Å
Sweep - 1 usec/division

Figure 6. Spike and Tail Completely Merged

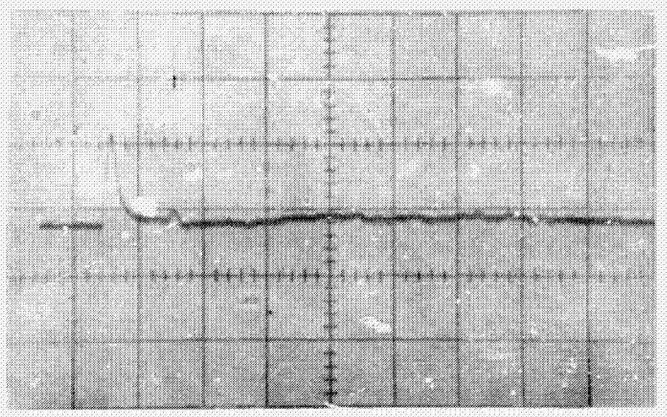

Shot No. - 82
Projectile - .635 cm Copper
Target - Cadmium
Velocity - 2.86 km/sec
Wavelength - Broadband
Sweep - 1 usec/division

Figure 7. Spike Predominant

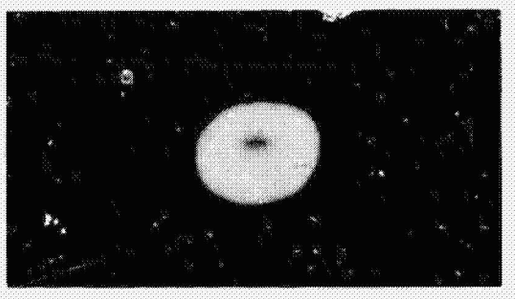

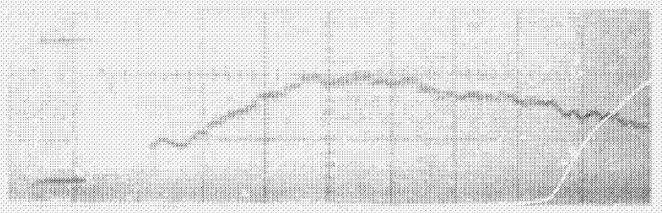

Shot No. - 125
Projectile - .318 cm Titanium
Target - Cadmium
Velocity - 3.5 km/sec
Pressure - 8.5×10^{-6} Torr
Ring Velocity 11.6 km/sec
Sweep - 1 usec/division

Figure 8. Luminous Ring

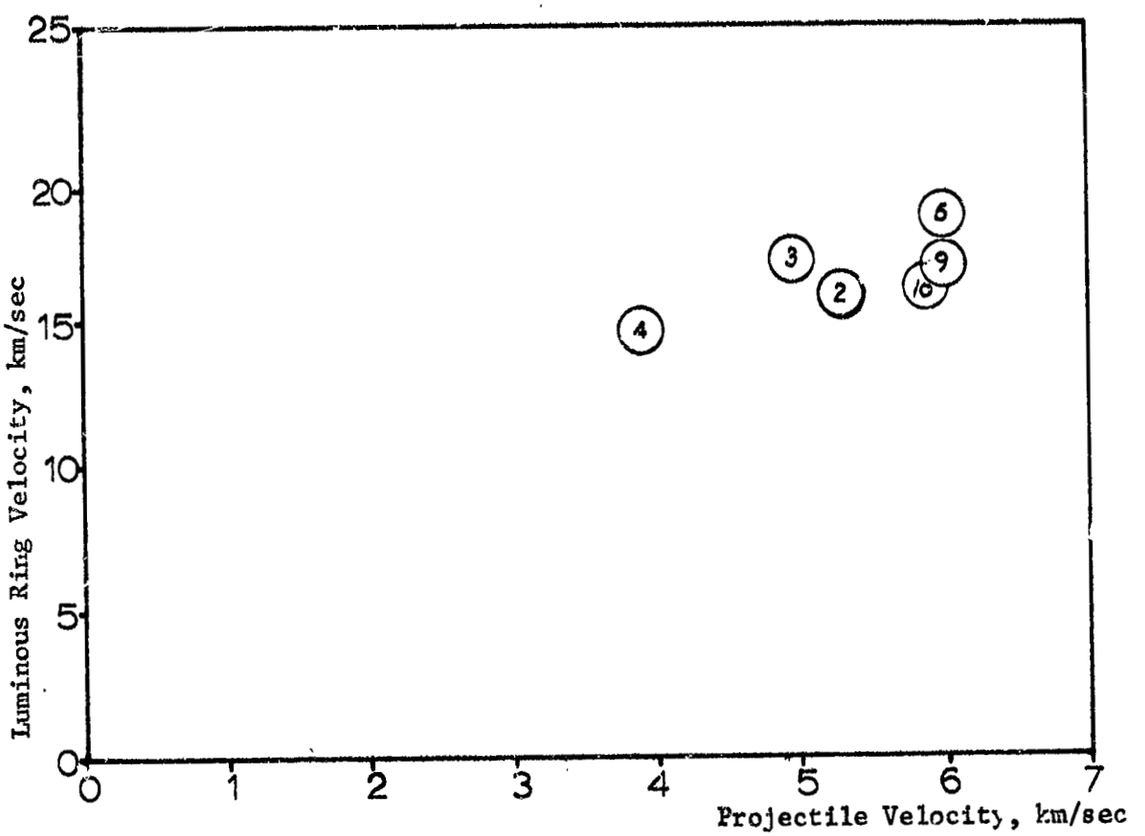

Figure 9. Luminous Ring Velocity, Al-Al Impacts

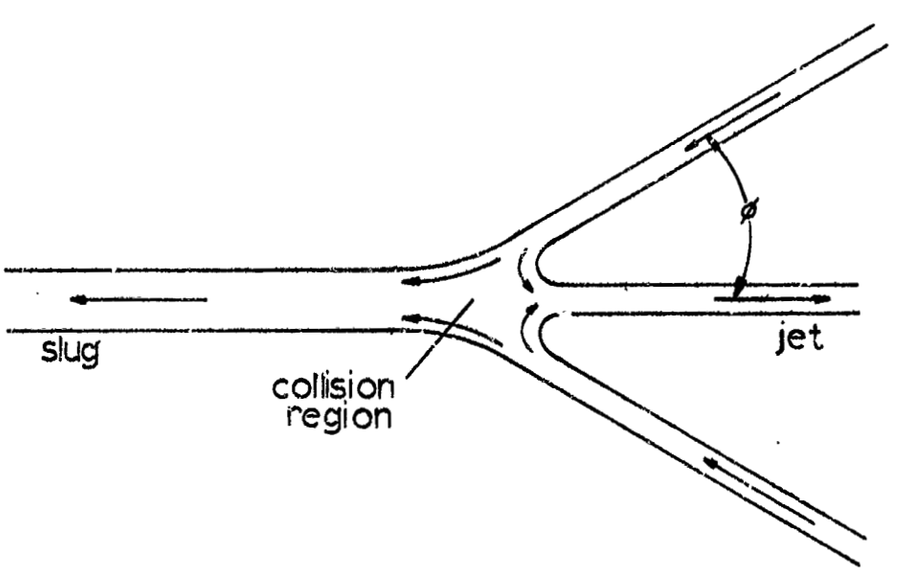

Figure 10. Geometry of Two Plate Collision

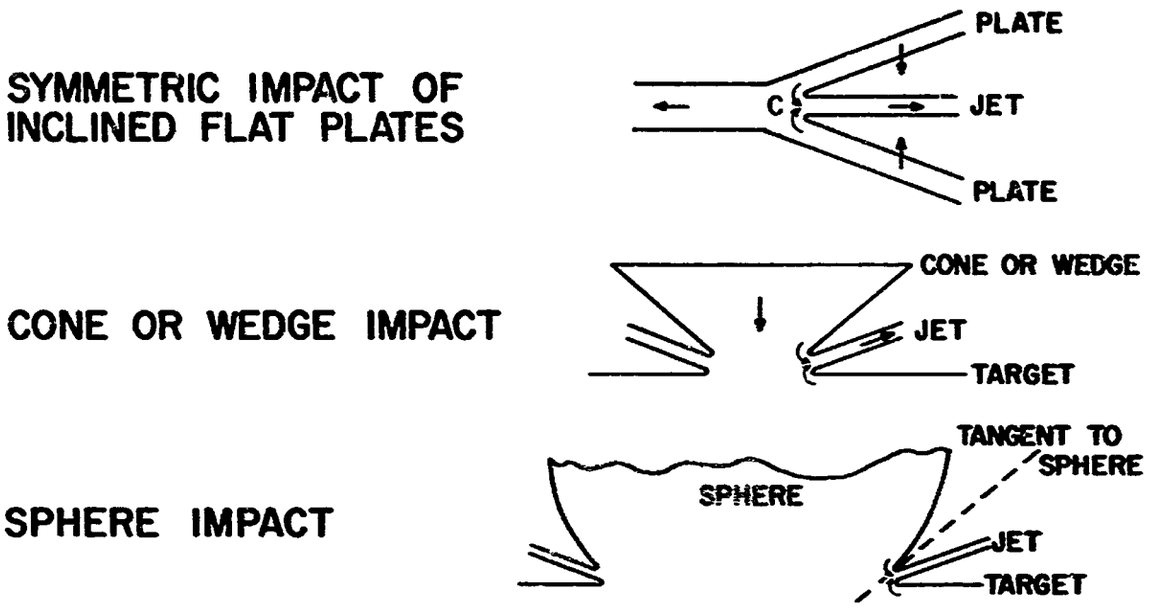

Figure 11 Similarity of Two Plate Collision to Sphere or Cone Impact

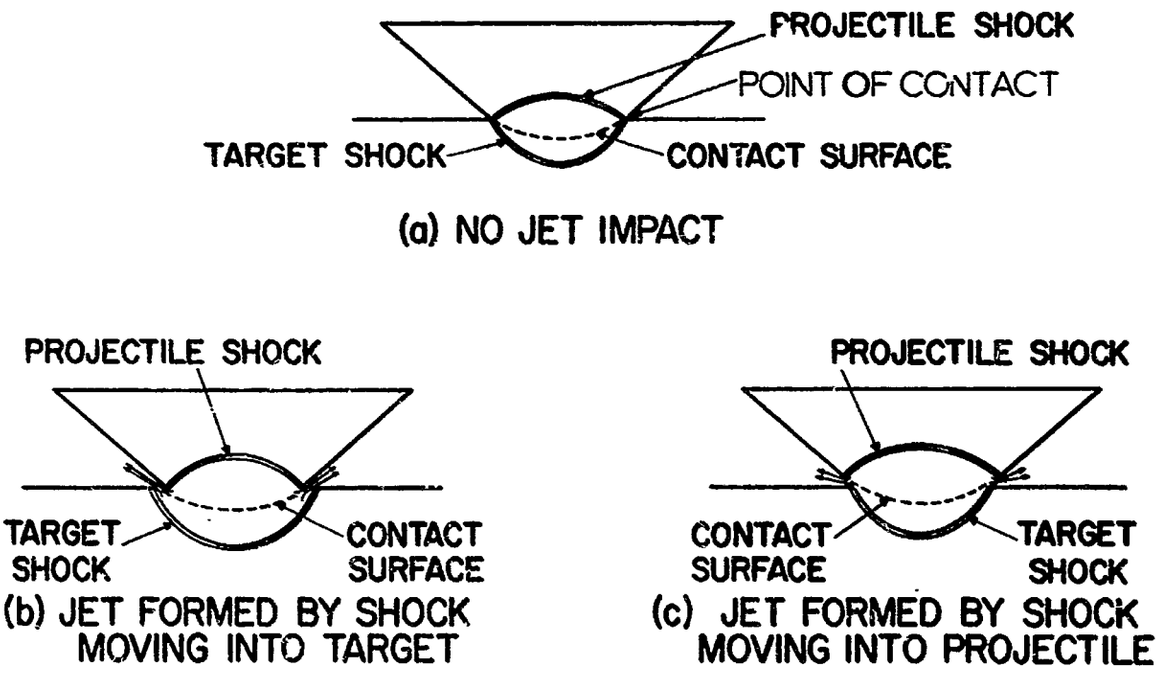

Figure 12 Jetless and Jet Producing Impacts

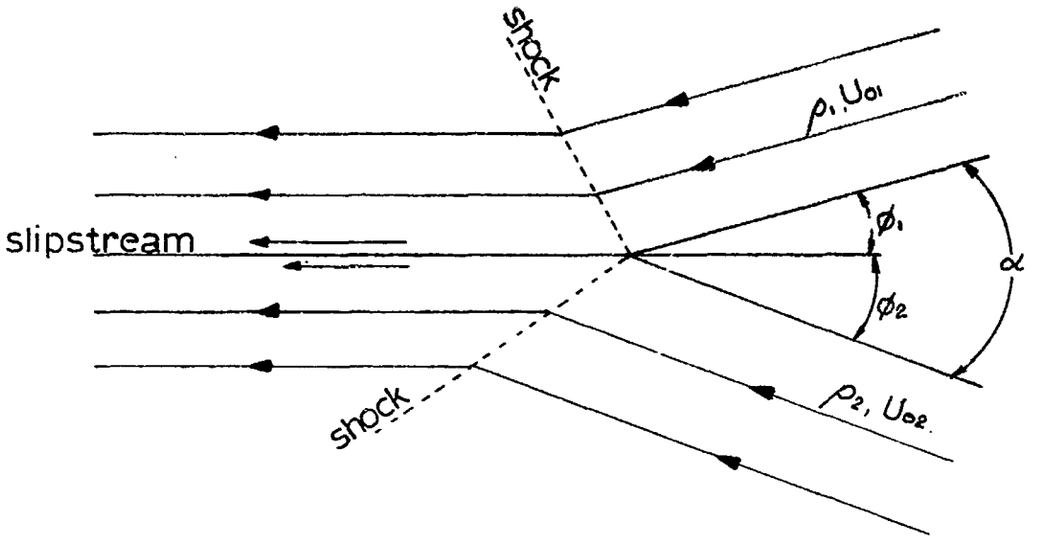

Figure 13. Jetless Configuration for Asymmetric Collision

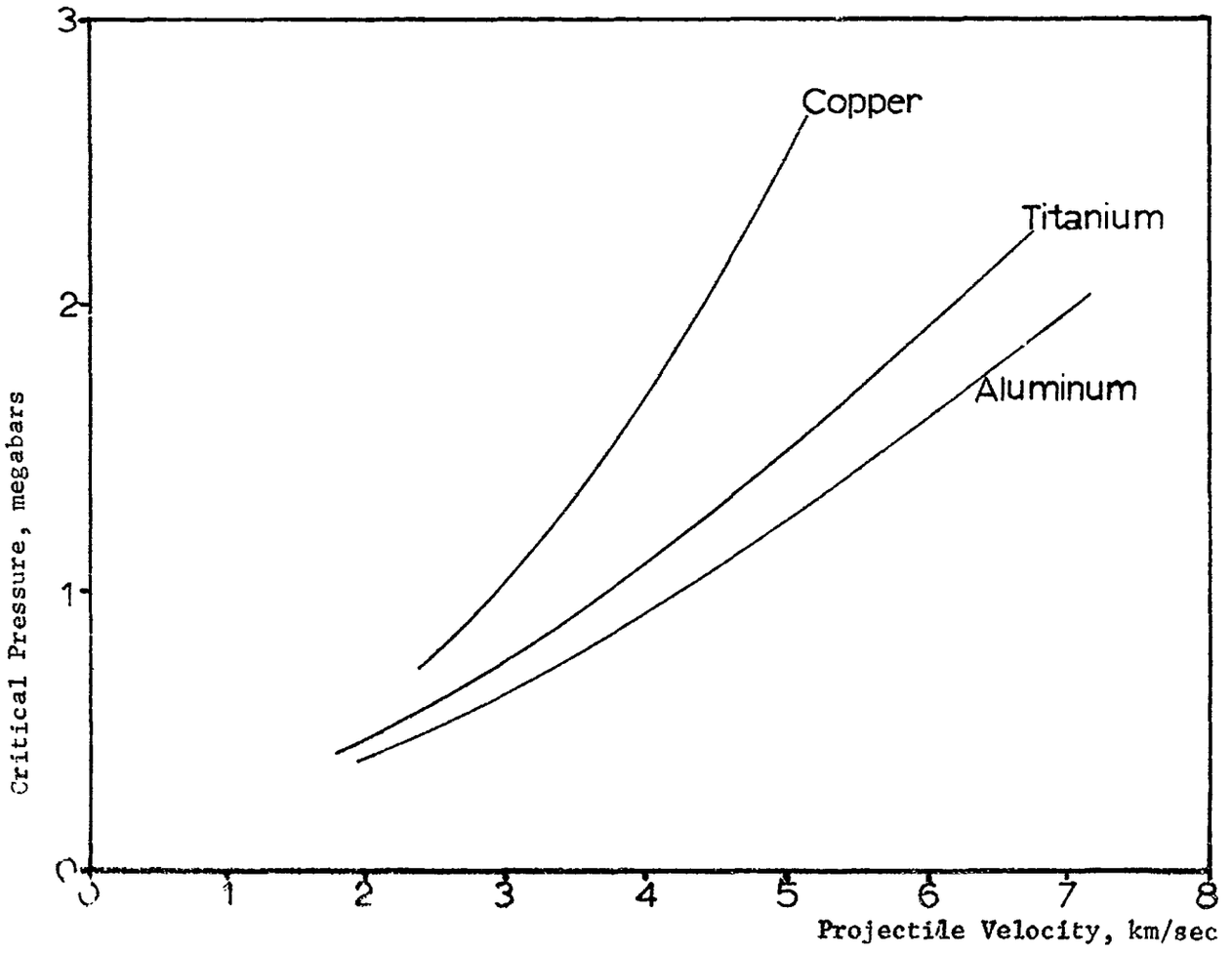

Figure 14. Critical Pressure vs Projectile Velocity

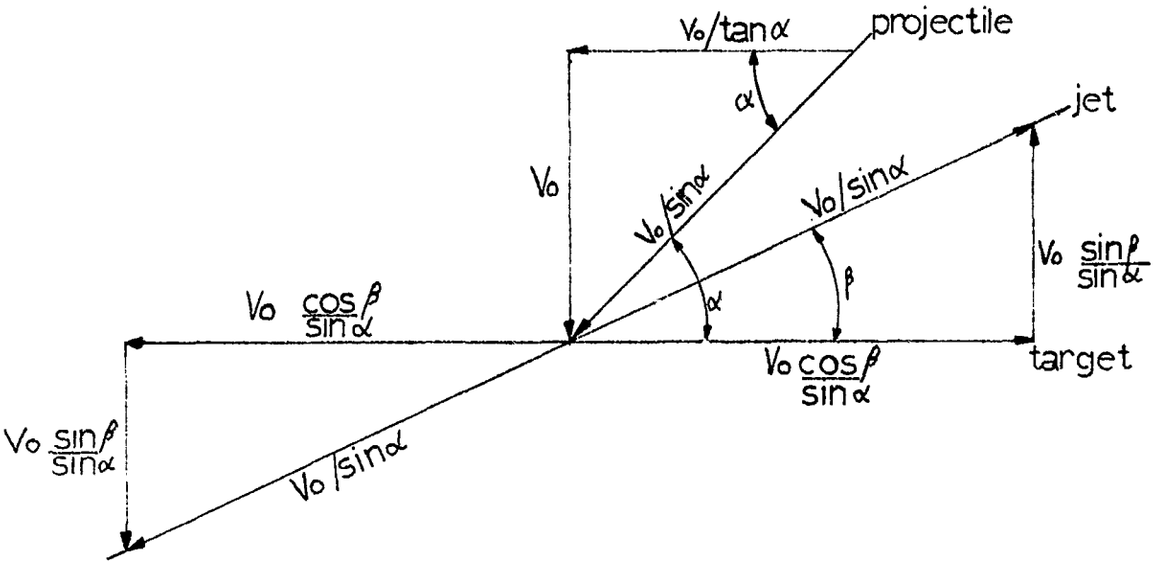

Figure 15(a) Projectile Velocity Vector and Components

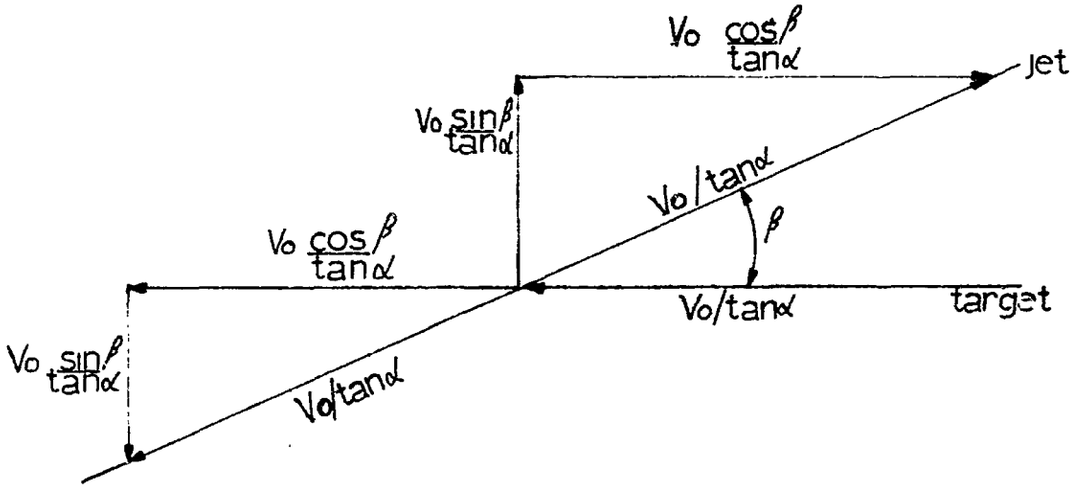

Figure 15(b) Target Velocity Vector and Components

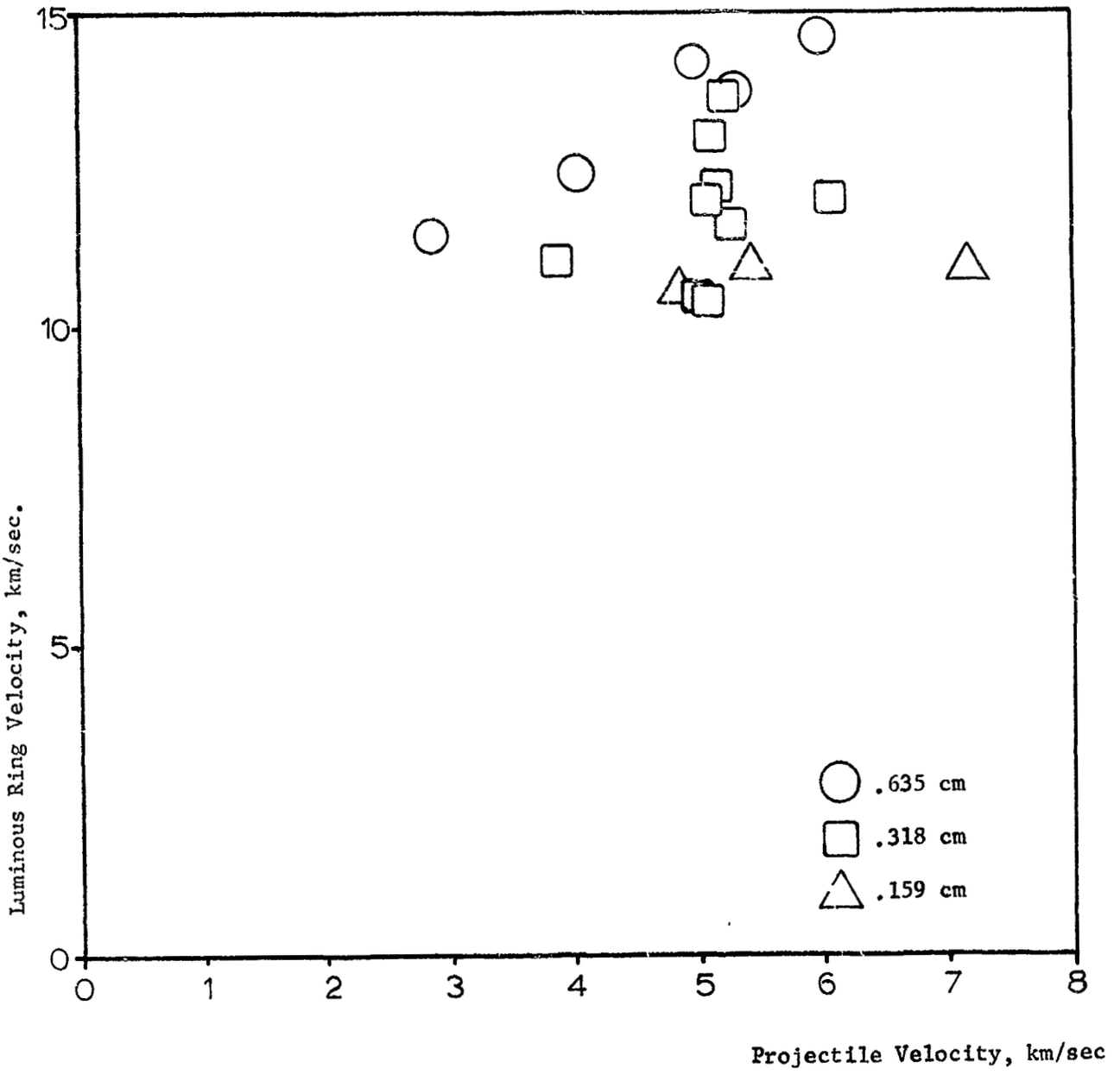

Figure 16. Luminous Ring Velocity vs Projectile Velocity, Cu-Cd Impacts

Shot No. - 117
Projectile - .635 cm Copper Polyhedron
Target - Cadmium
Velocity - 6.1 km/sec
Sweep - 0.5 usec/division

Figure 17. Luminous Ring Produced by Polyhedron (Head-on)

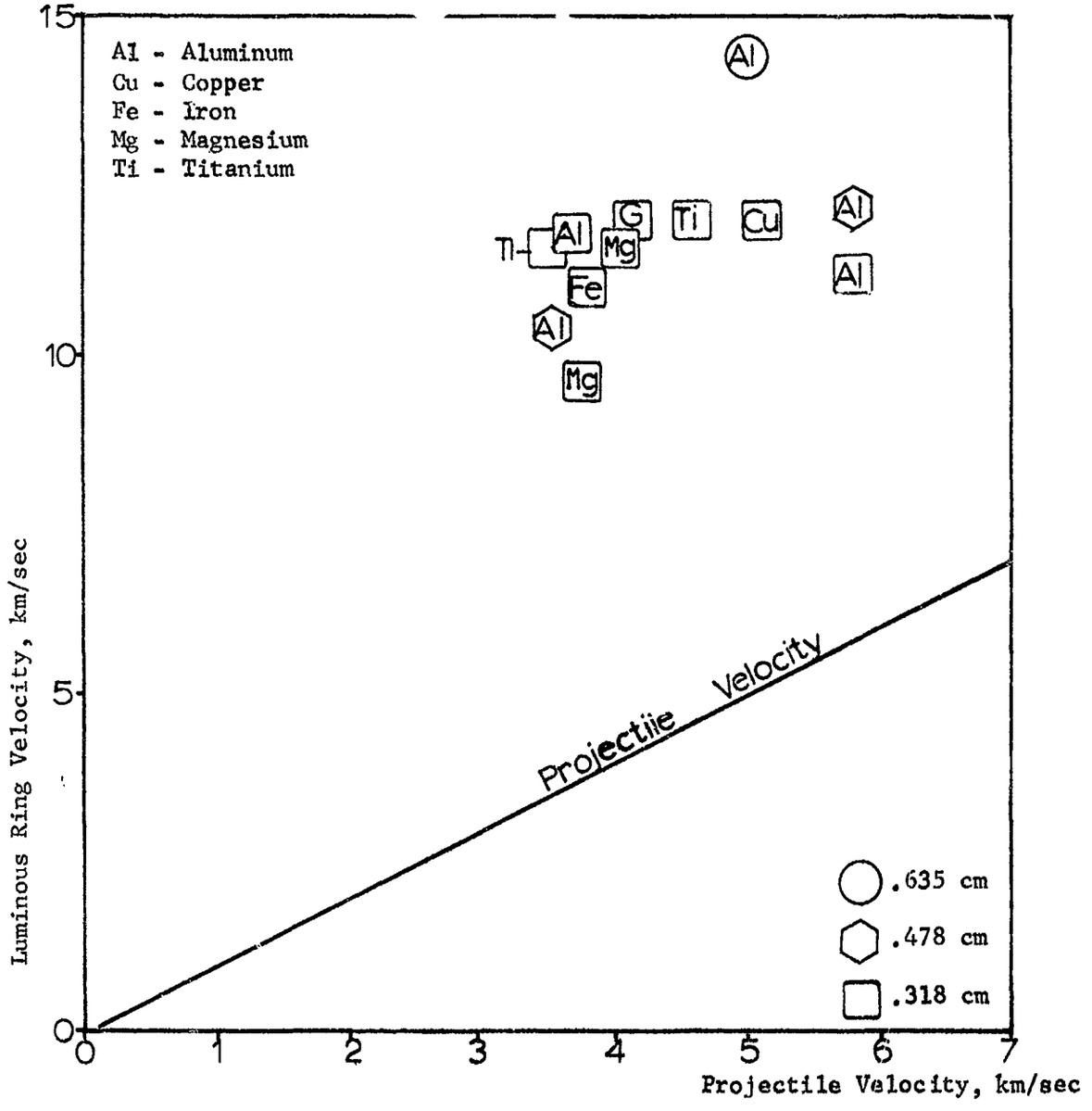

Figure 18. Dependence of Luminous Ring Velocity on Projectile Material

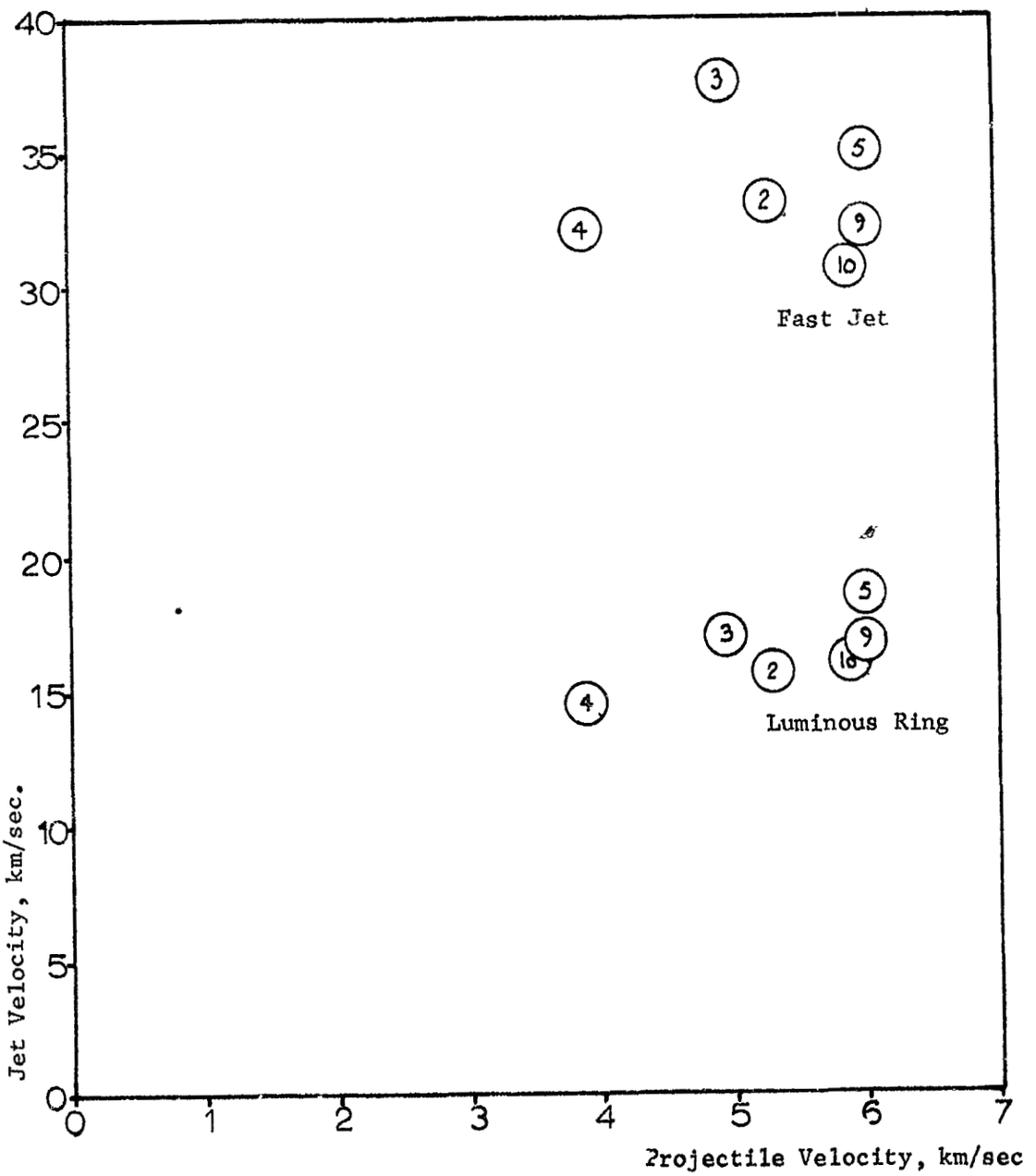

Figure 19. Fast Jet vs Projectile Velocity, Al-Al Impacts

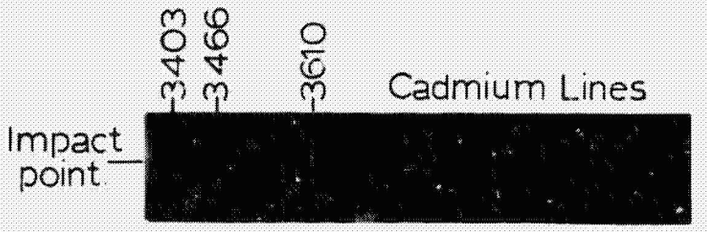

Figure 20. Space Resolved Spectrum Showing Line Broadening at the Impact Point

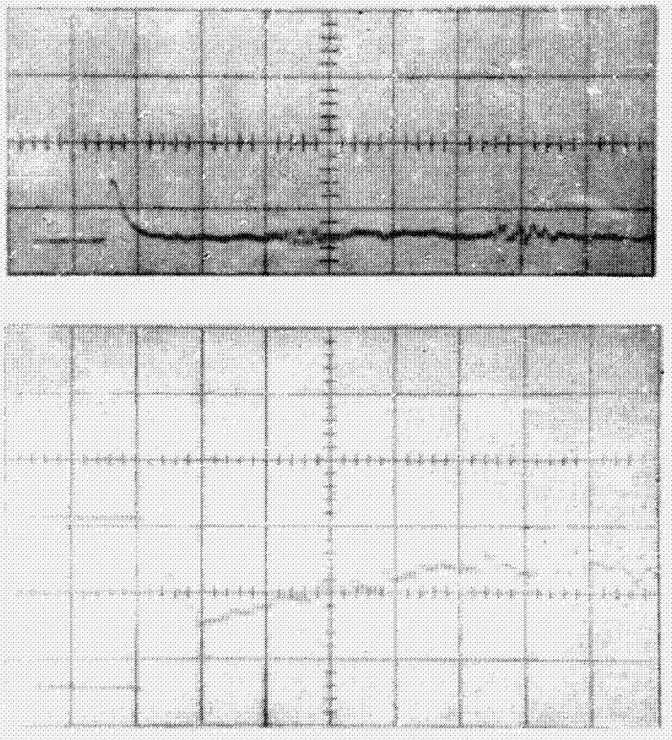

Shot No. - 131
Projectile - .159 cm Copper
Target - Cadmium
Velocity - 4.9 km/sec
Sweep - 0.5 usec/division

Figure 21. Polychromator Records for Background Radiation (4922Å) and Line Emission (5085Å)

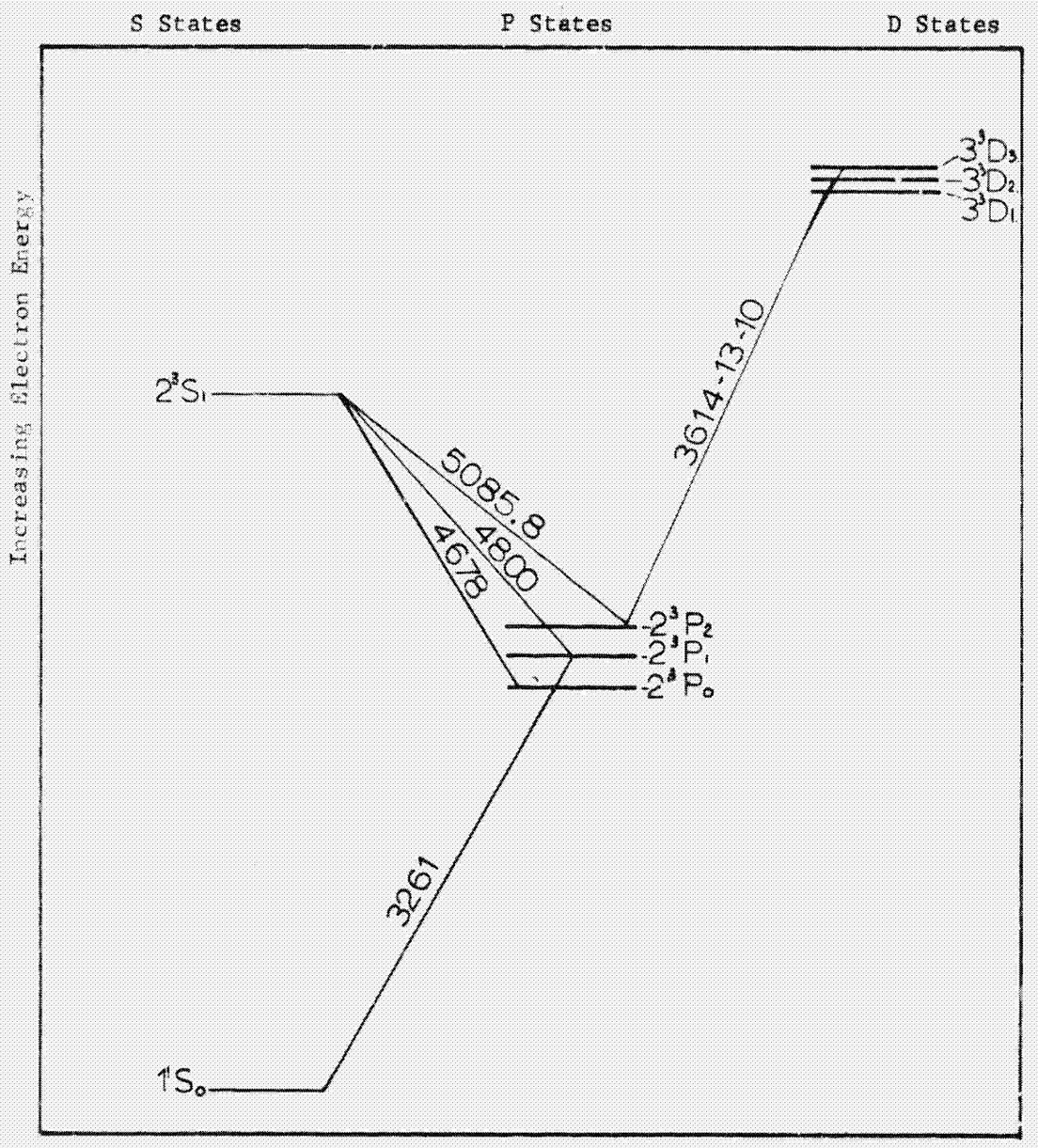

Figure 22. Energy Levels of Cadmium

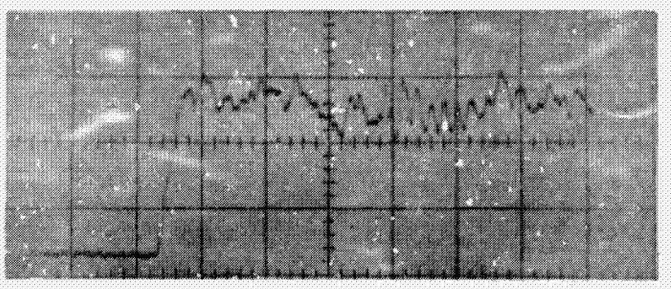

3261Å

Shot No. - 118
Projectile - .318 cm Copper
Velocity - 6.1 km/sec
Sweep - 0.5 usec/division

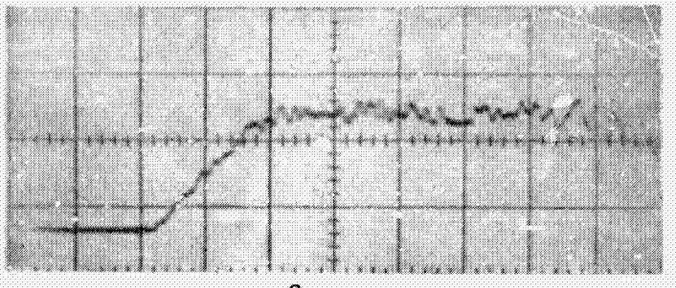

5085Å

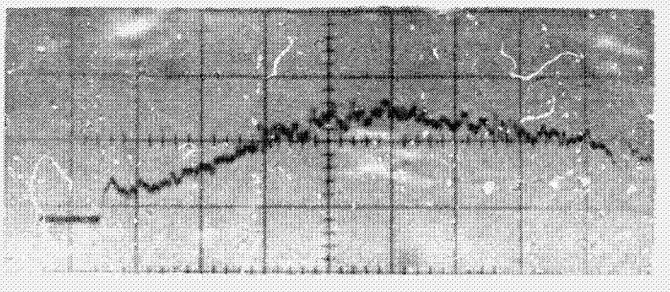

3261Å

Shot No. - 84
Projectile - .318 cm Copper
Velocity - 3.3 km/sec
Sweep - 1.0 usec/division

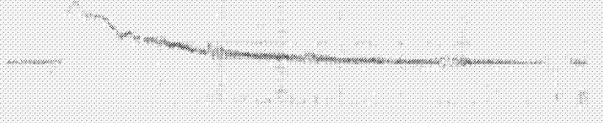

3610Å

Figure 23. Scope Traces Showing that the Shape of the 3261Å Line Differs from the Shape of the 3610Å or 5085Å Line

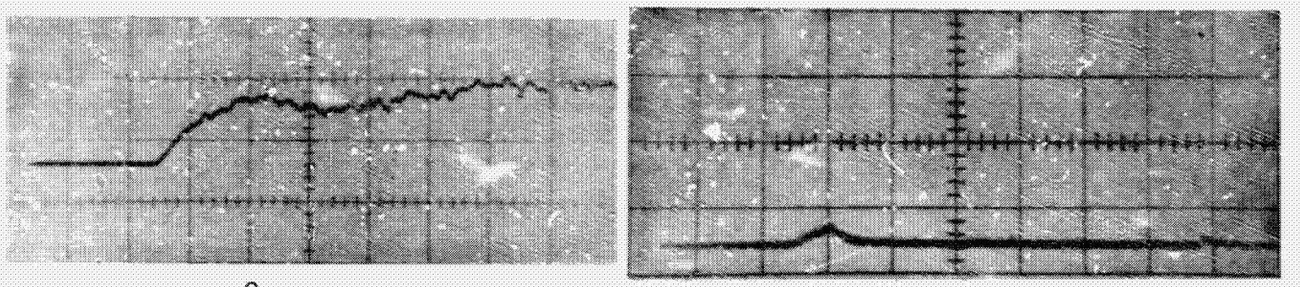

3610Å 4905Å

Rough Target (109)

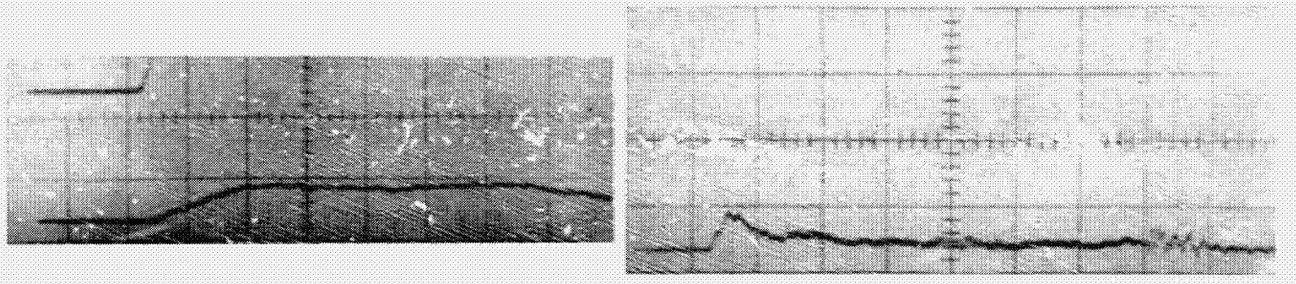

3610Å 4905Å

Rough Projectile (118)

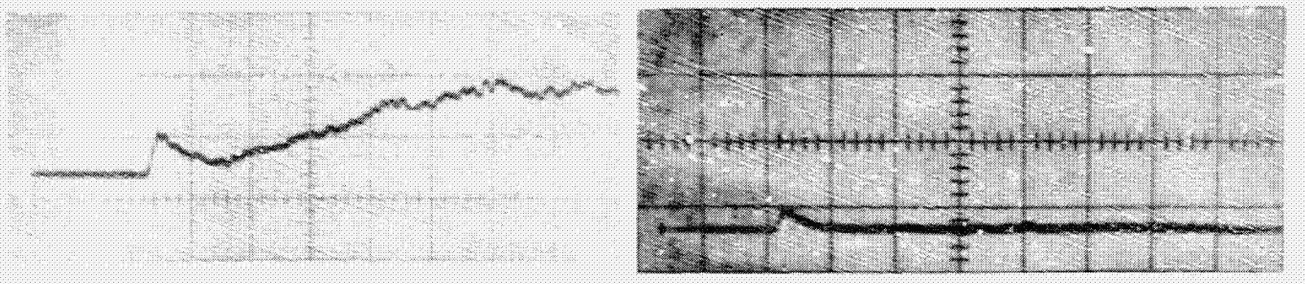

3610Å 4824Å

Normal Target and Projectile (92)

Figure 24. Dependence of Spike Shape on Projectile Surface Finish

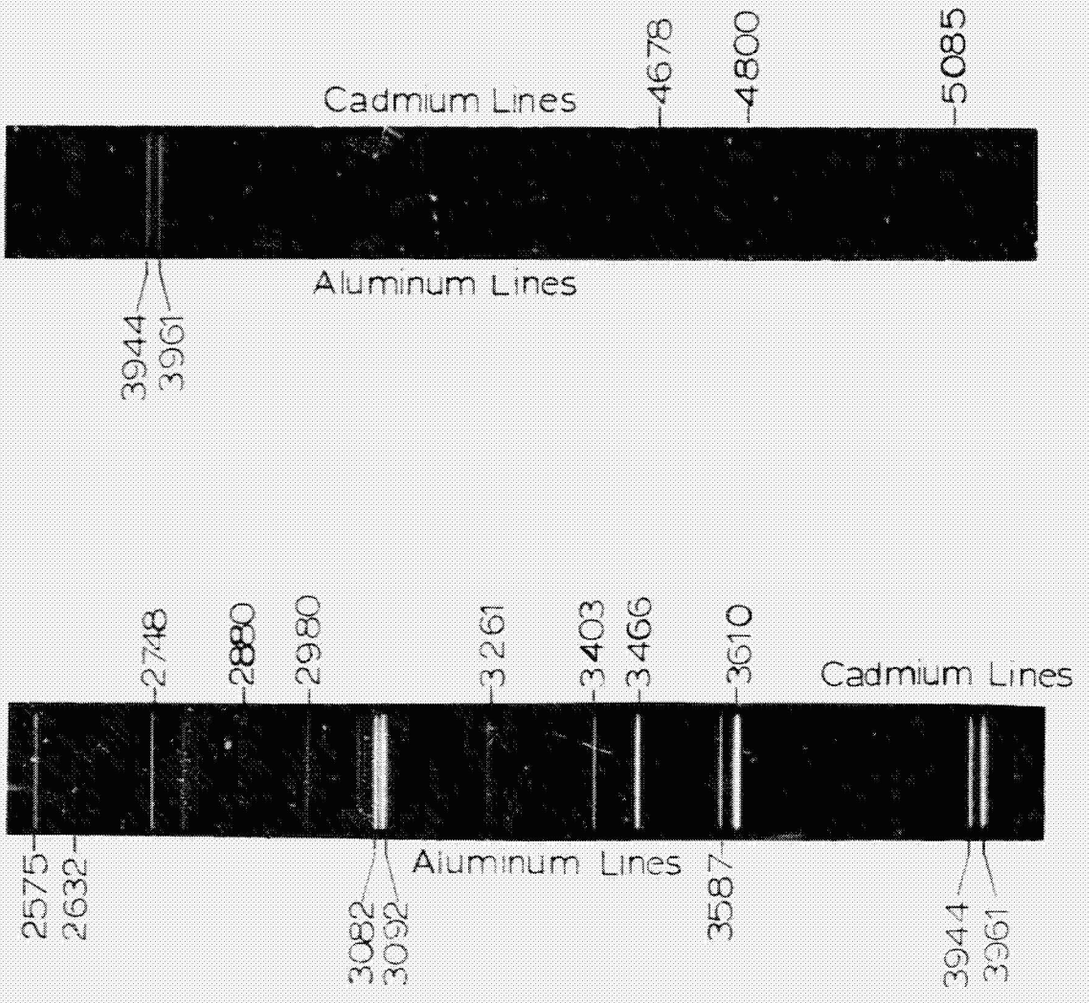

Figure 25. Integrated Spectrum, Al-Cd Impact

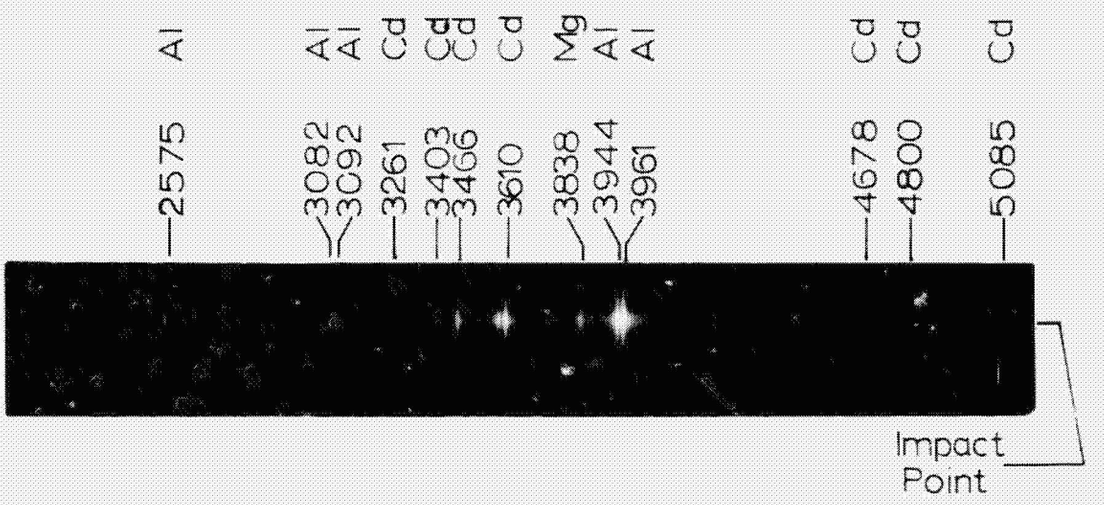

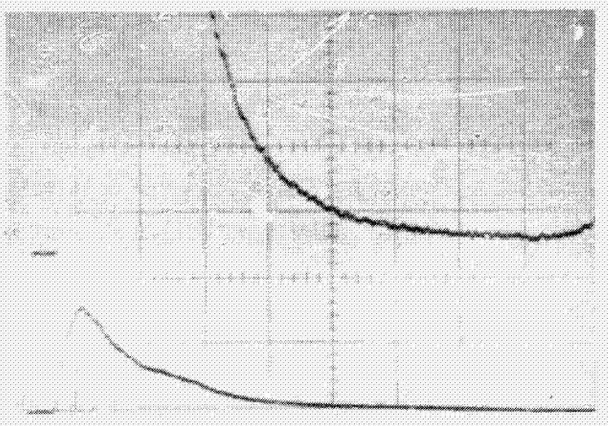

Shot No. - 8
Projectile - .635 cm Aluminum
Target - Cadmium
Velocity - 5.(km/sec
Wavelength - Broadband
Sweep - 2 usec/division

Figure 26. Impact Spike Associated with Line Broadening at the Impact Point

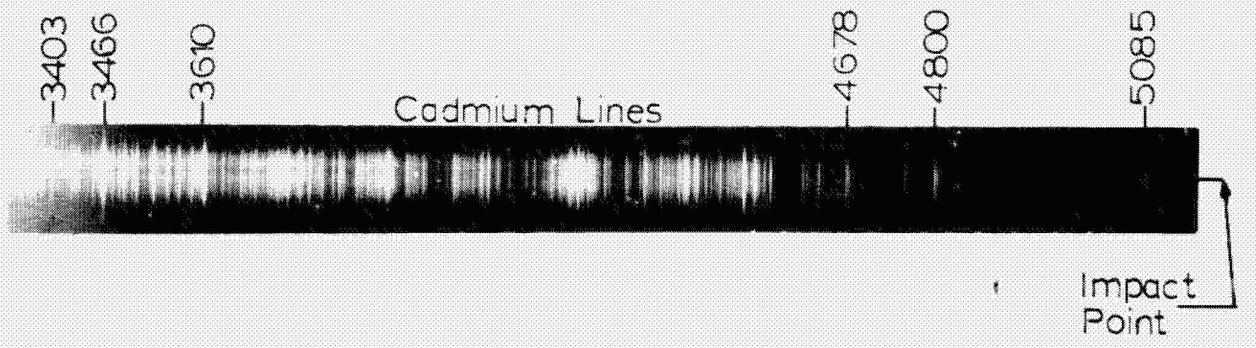

Shot No.	-	120
Projectile	-	.635 cm Titanium
Target	-	Cadmium
Velocity	-	5.95 km/sec
Wavelength	-	Broadband
Sweep	-	0.5 usec/division

Figure 27. Spectrum Showing Considerable Broadening at Impact Point

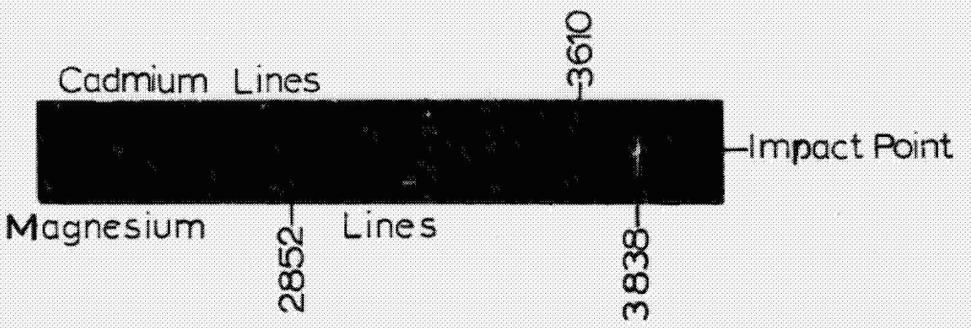

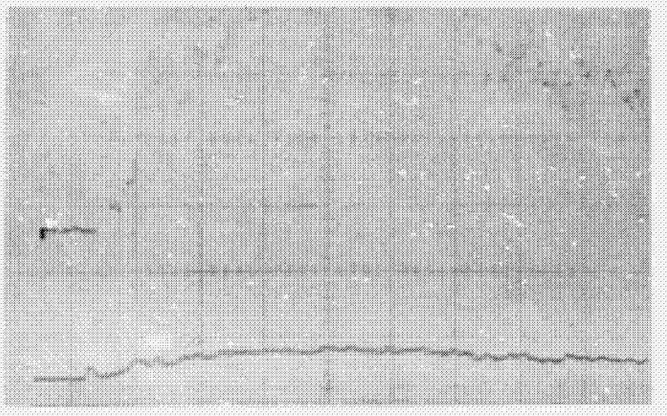

Shot No. - 127
Projectile - .318 cm Magnesium
Target - Cadmium
Velocity - 4.05 km/sec
Wavelength - Broadband
Sweep - 1 usec/division

Figure 28. Spectrum Showing Slight Broadening at Impact Point

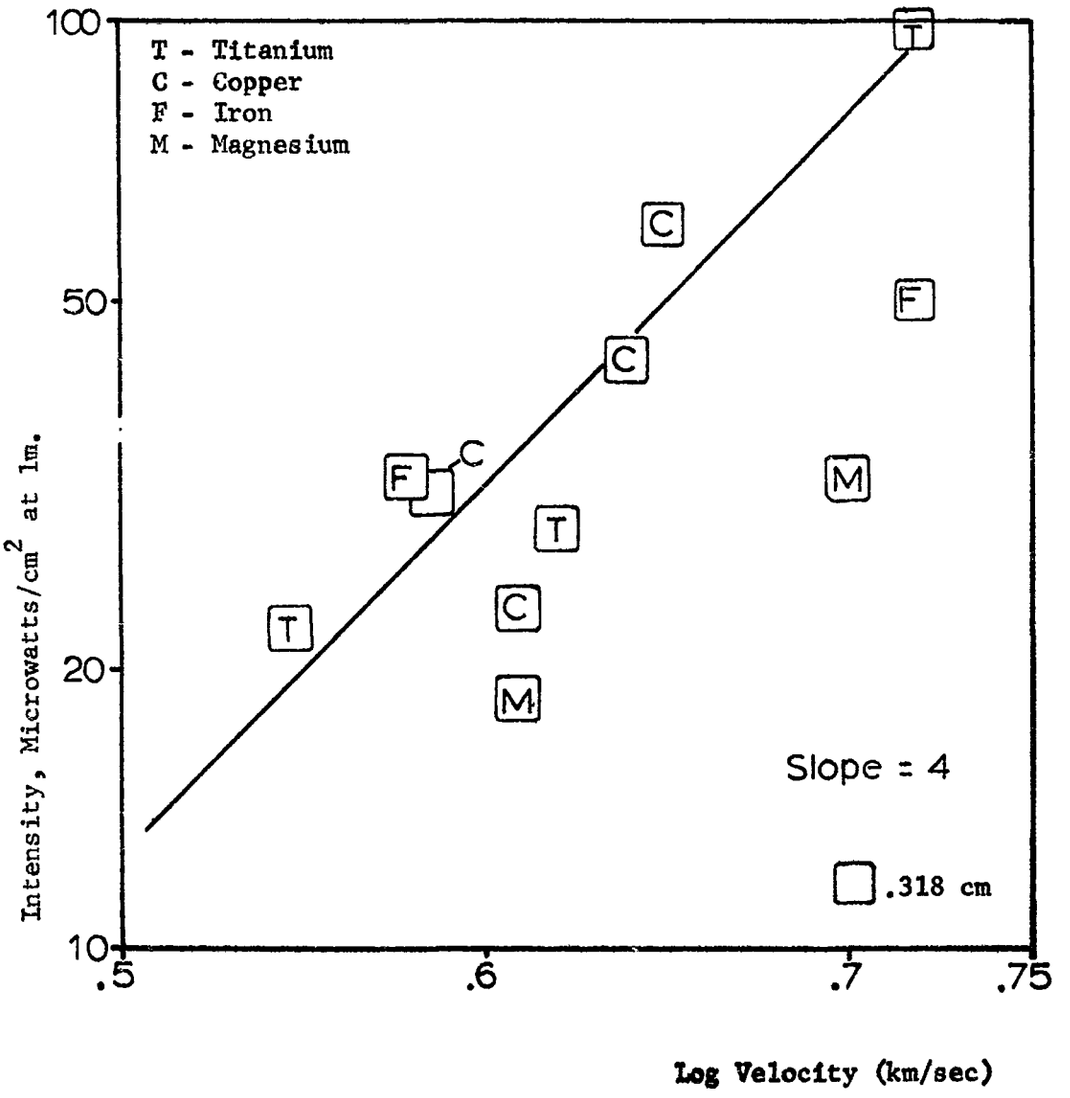

Figure 29. Intensity of the Tail vs Projectile Velocity

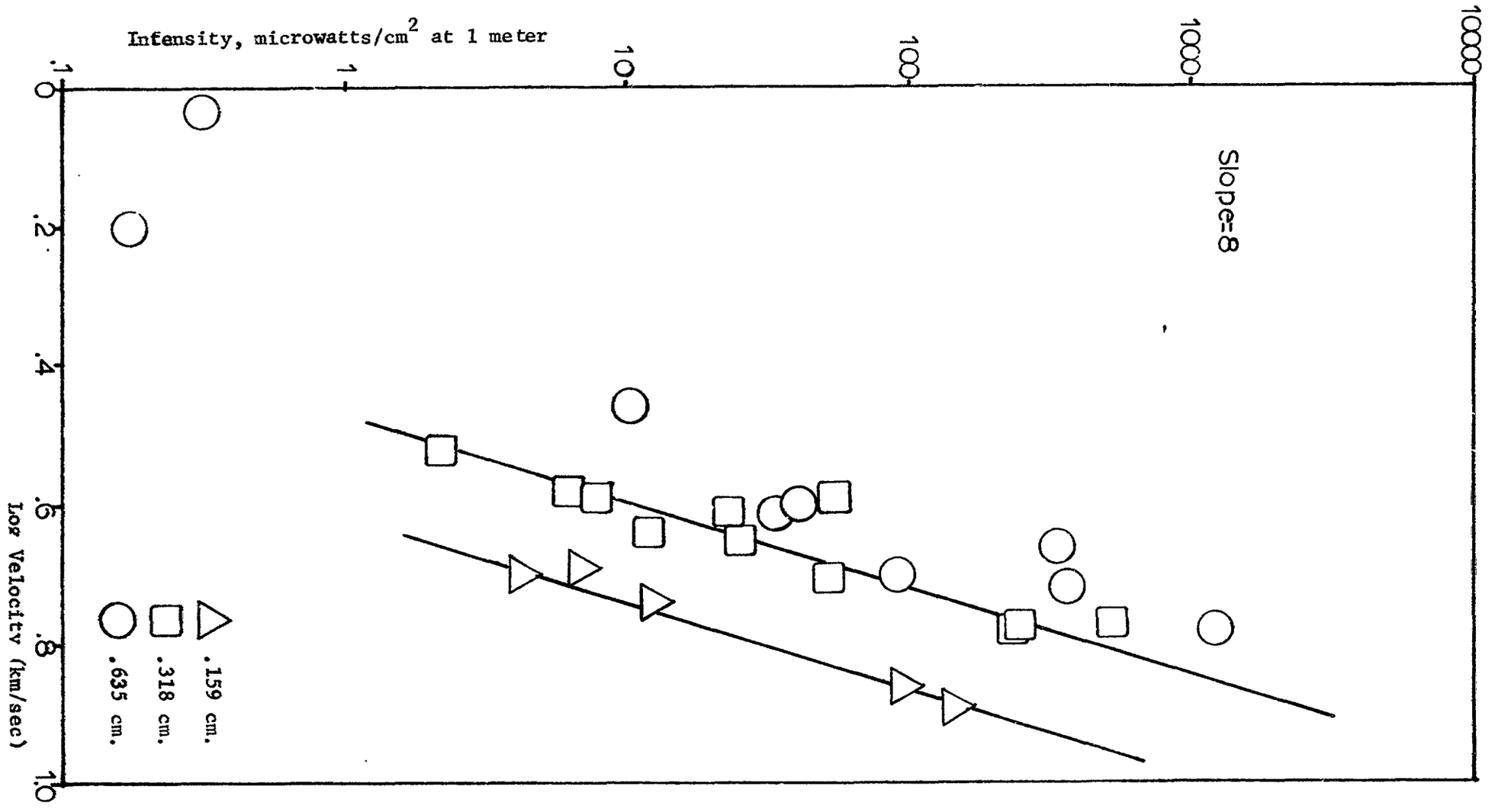

Figure 30. Spike Intensity for Cu-Cd Impacts, 5085Å

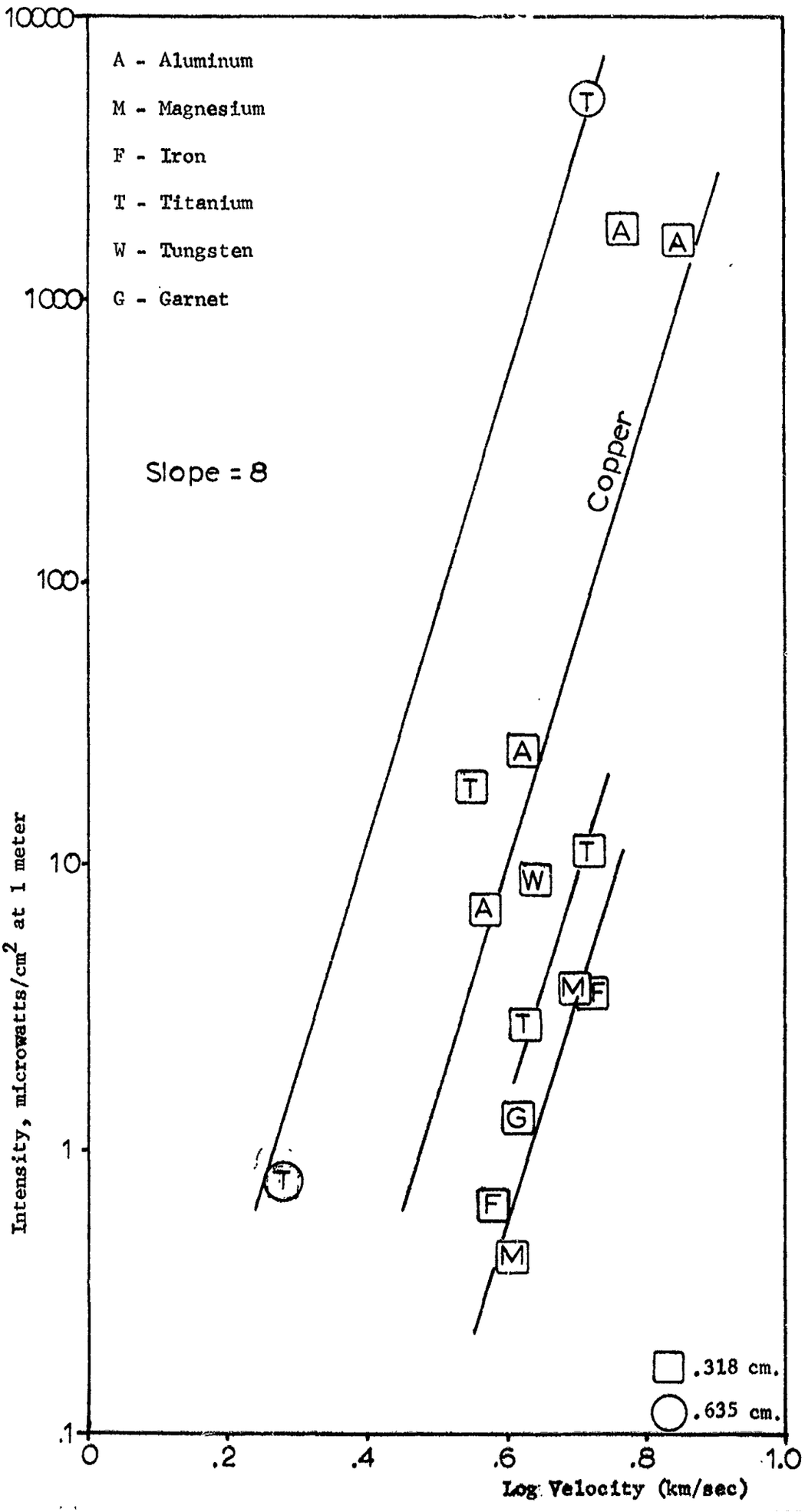

Figure 31. Spike Intensity for Various Projectile Materials Impacting Cadmium, Broadband (5085Å)

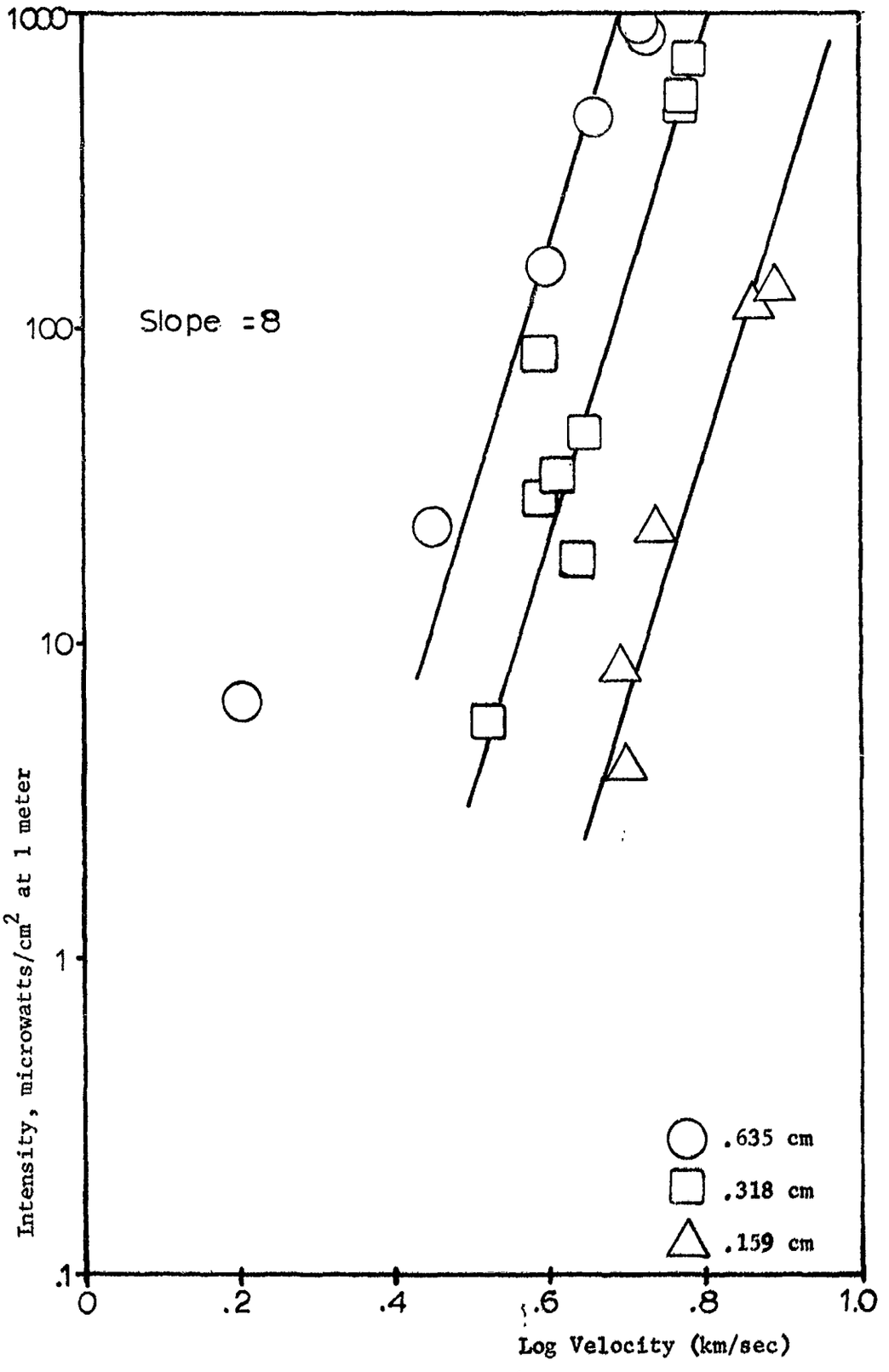

Figure 32. Spike Intensity for Cu-Cd Impacts, 3610Å.

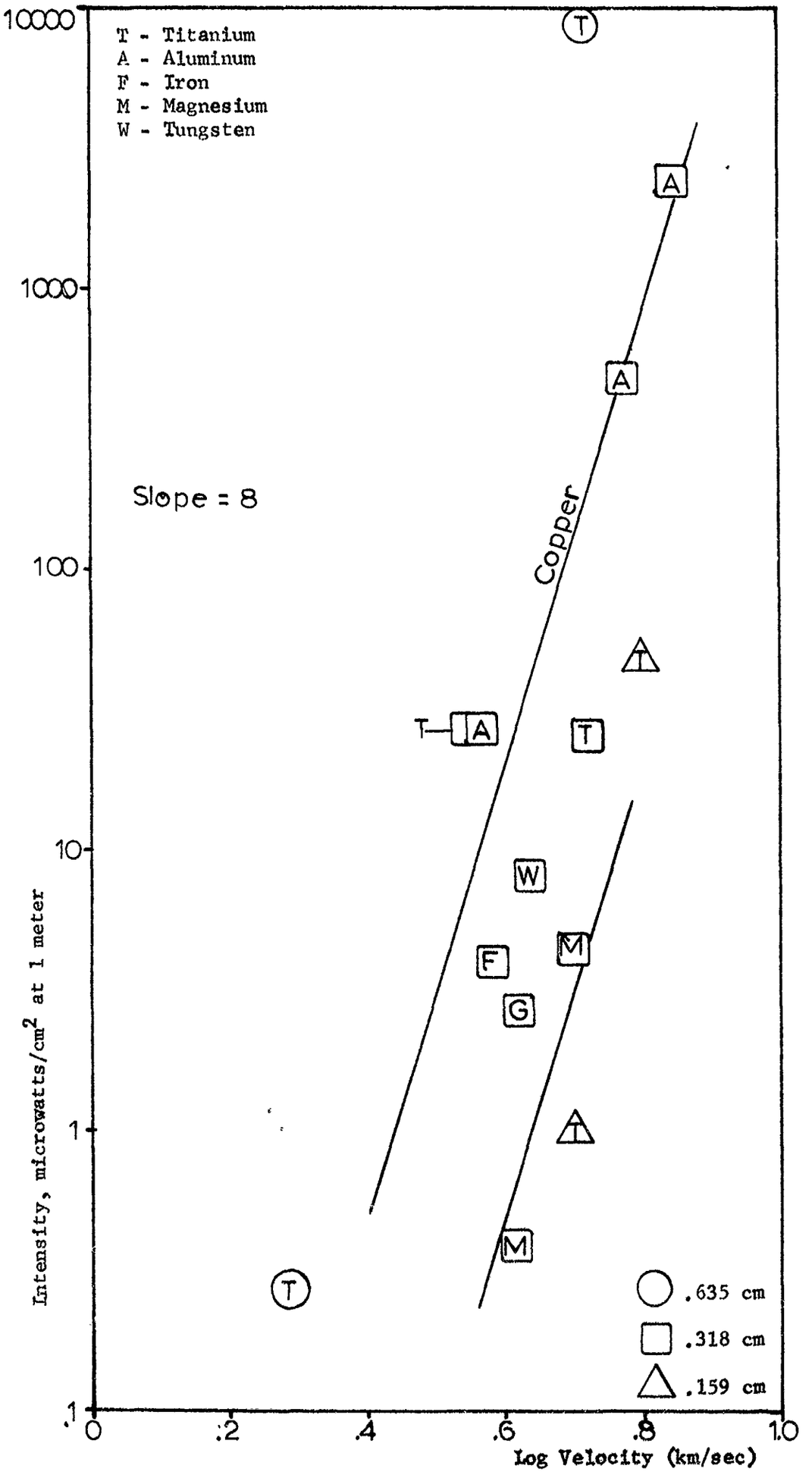

Figure 33. Spike Intensity for Various Projectile Materials Impacting Cadmium, (3610Å)

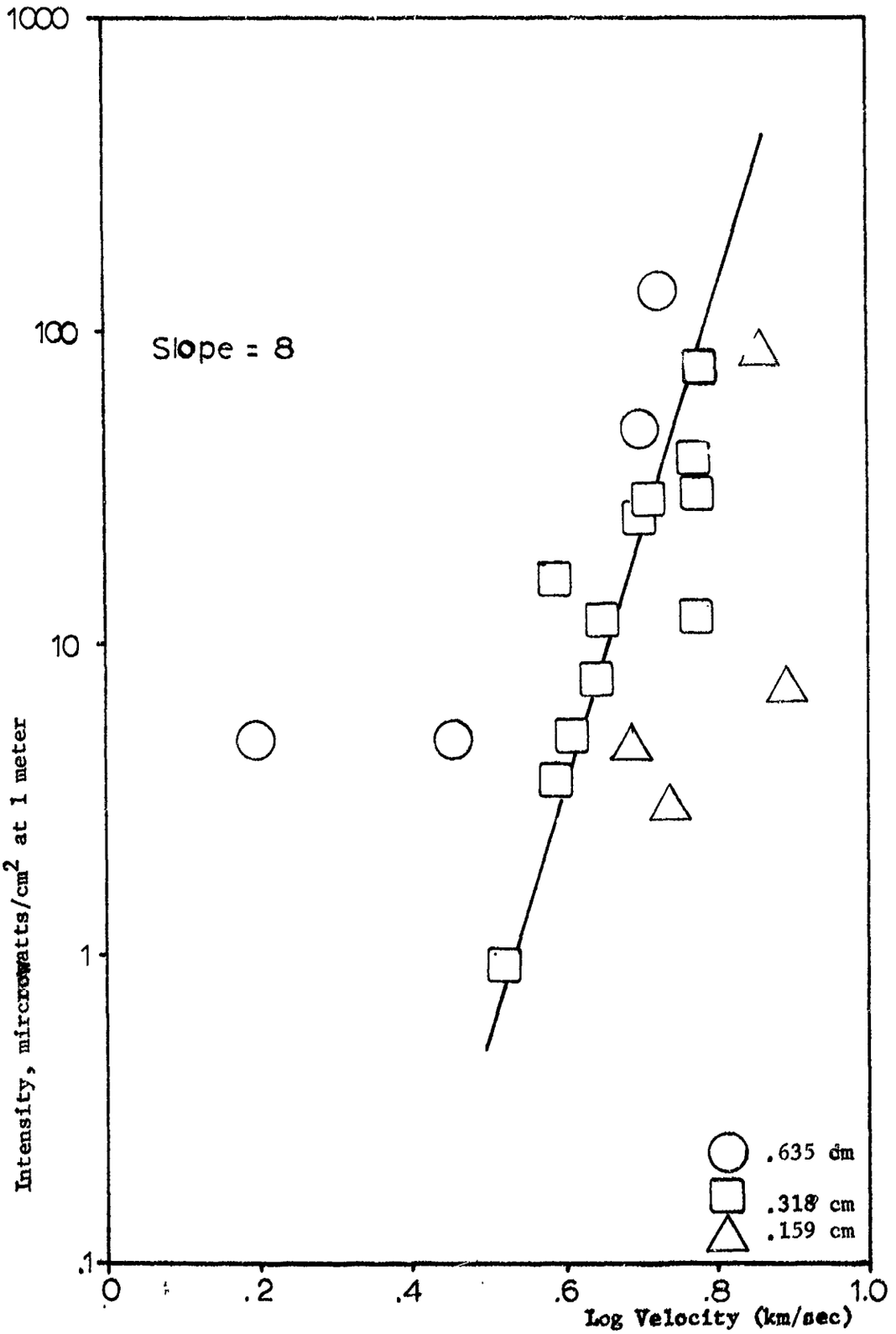

Figure 34. Spike Intensity for Cu-C$_6$ Impacts, 3261Å

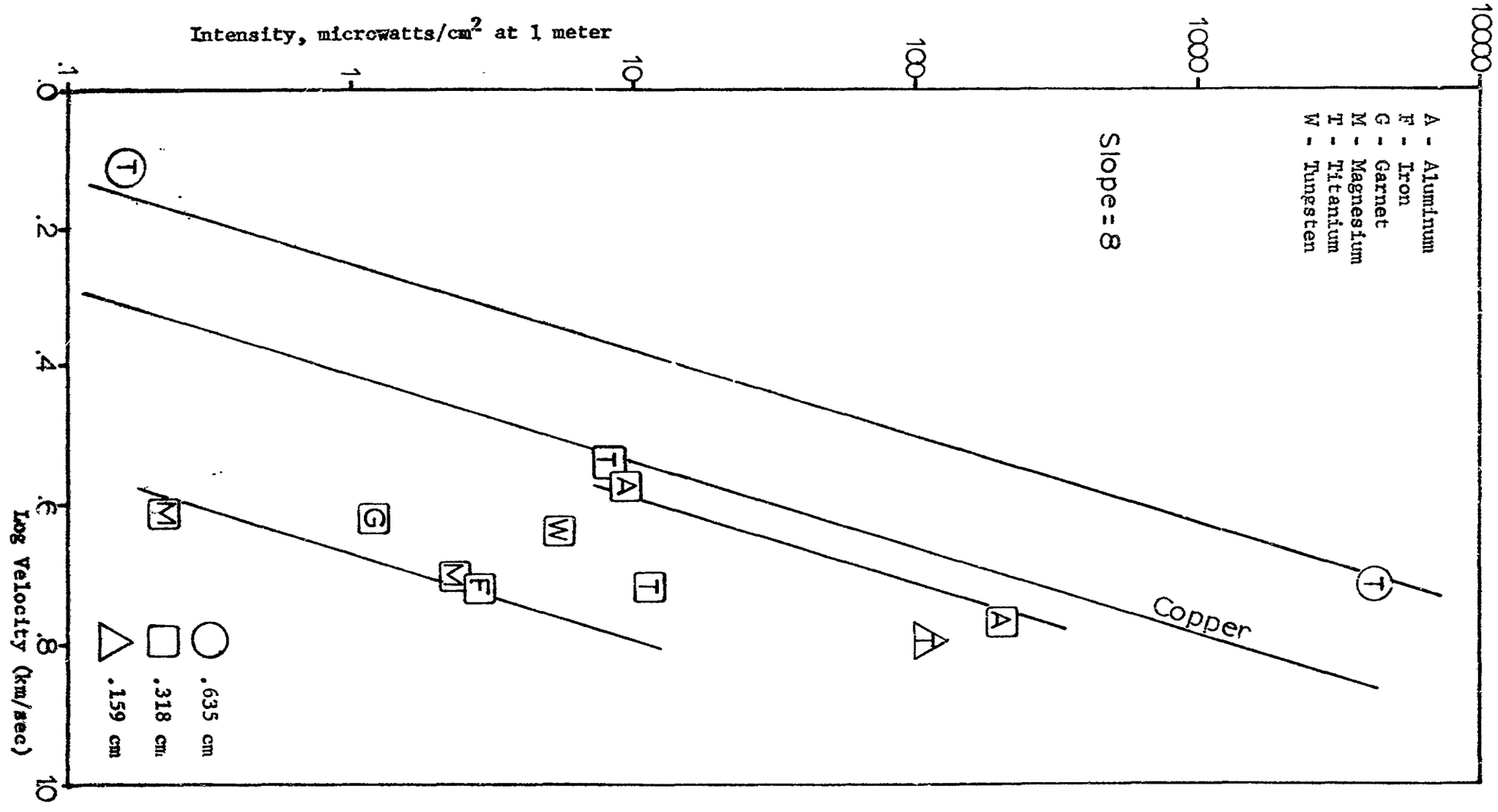

Figure 35. Spike Intensity for Various Projectile Materials Impacting Cadmium, (3261A)

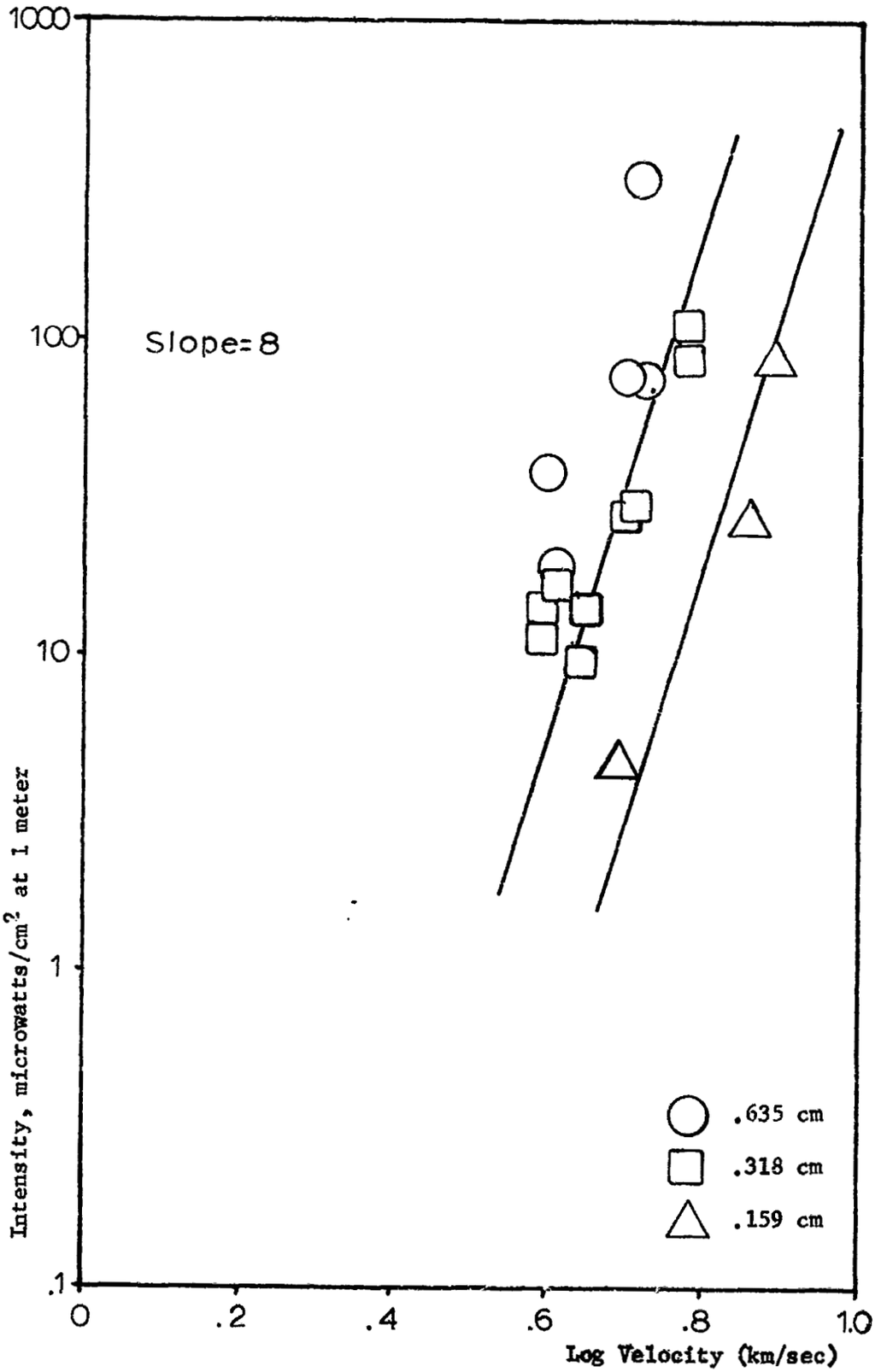

Figure 36. Spike Intensity f r Cu Jd Impacts, Background

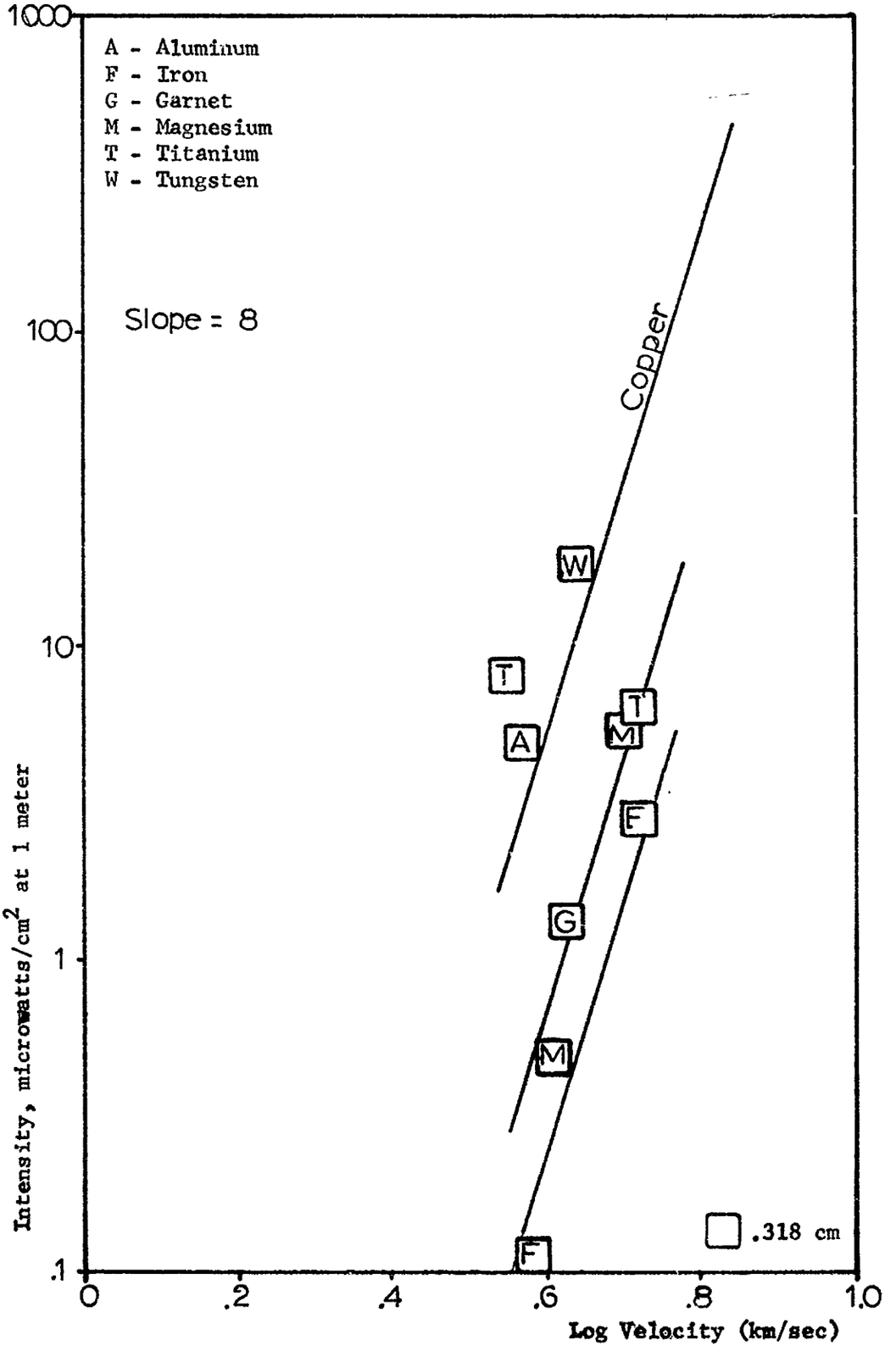

Figure 37. Spike Intensity for Various Projectile Materials Impacting Cadmium, Background.

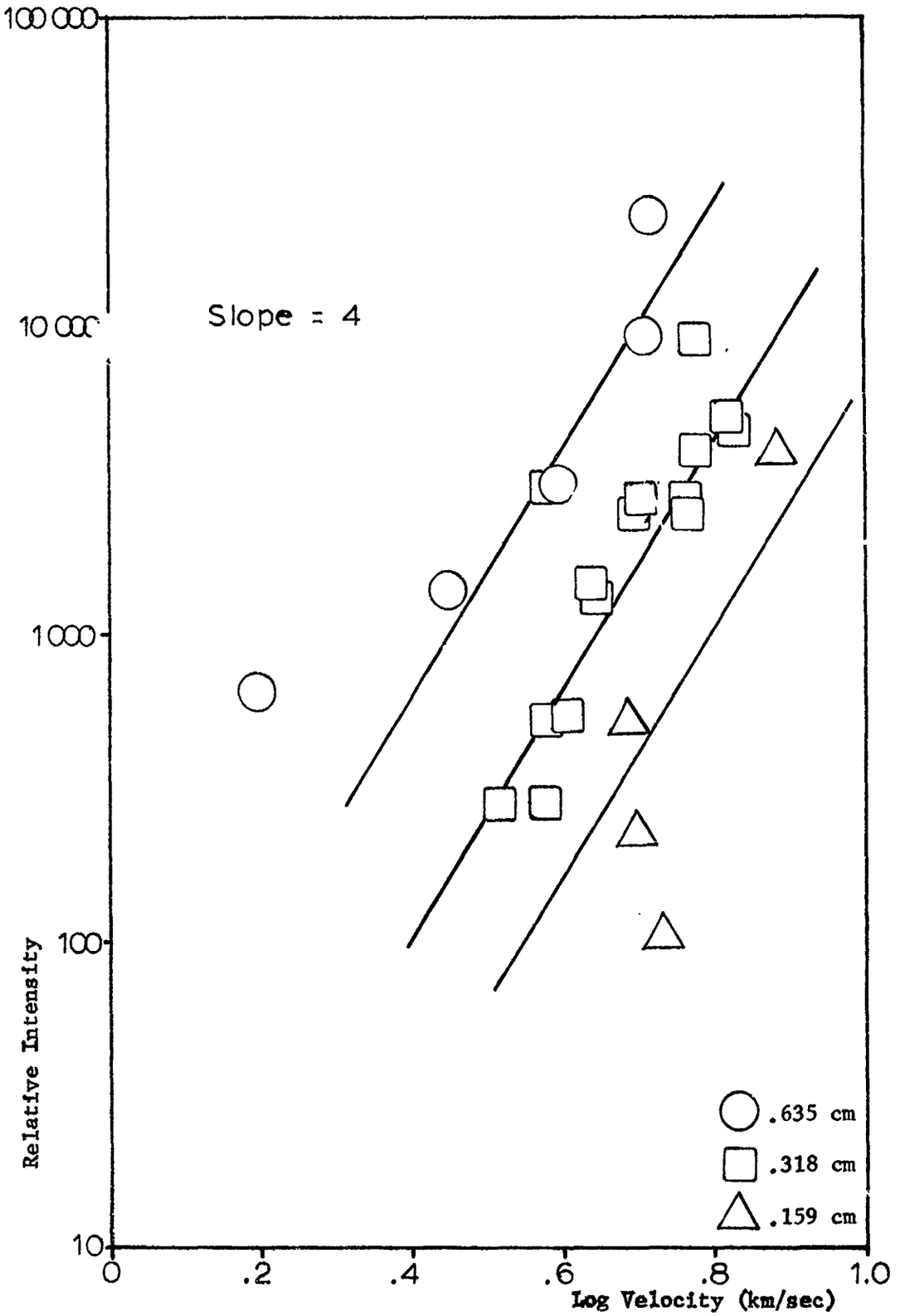

Figure 38. Spike Intensity for Cu-Cd Impacts, Broadband (3500-6500Å).

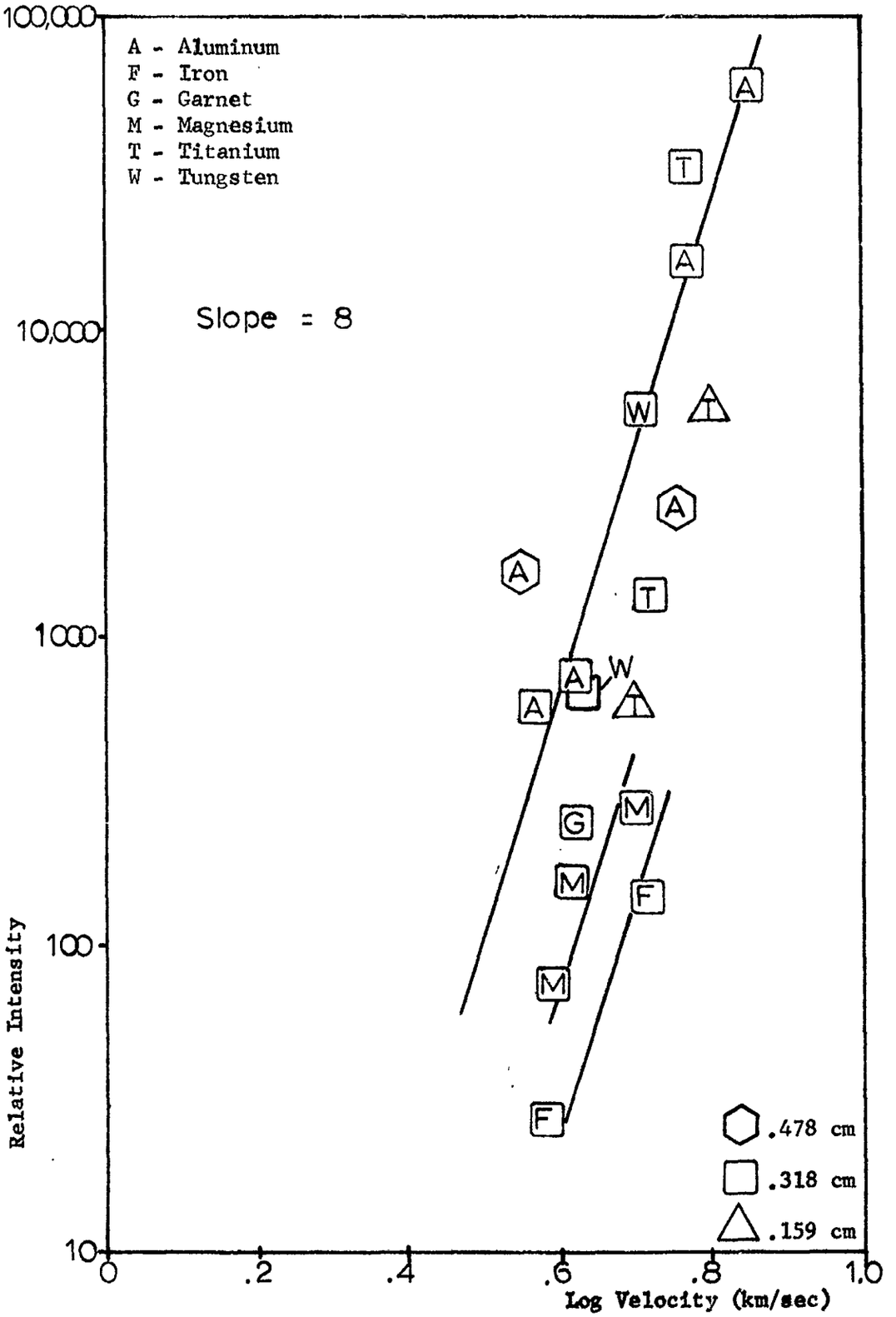

Figure 39. Spike Intensity for Various Projectile Materials Impacting Cadmium, Broadband (3500-6500Å).

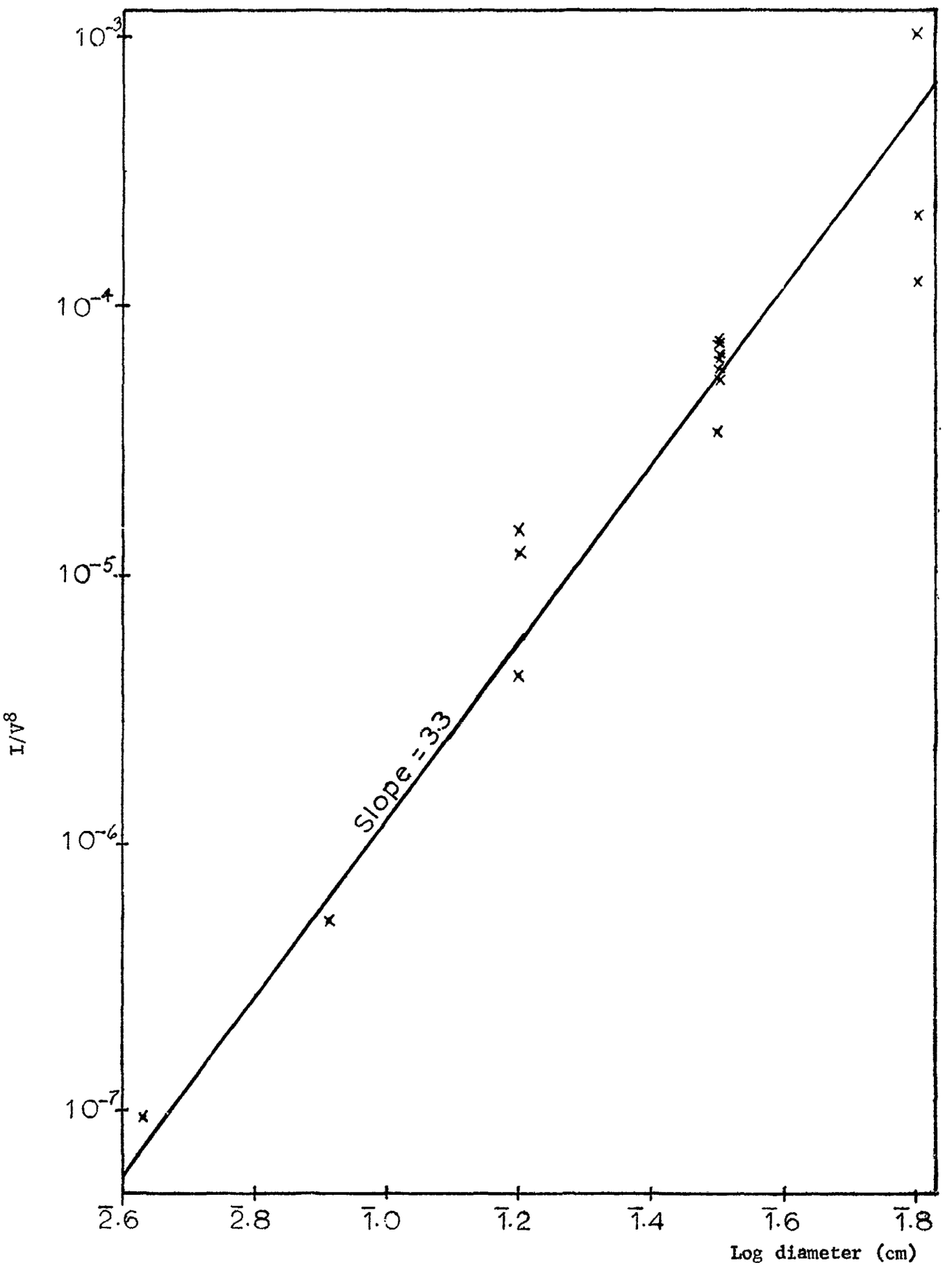

Figure 40. Dependence of Spike Intensity on Projectile Diameter, 3261Å.

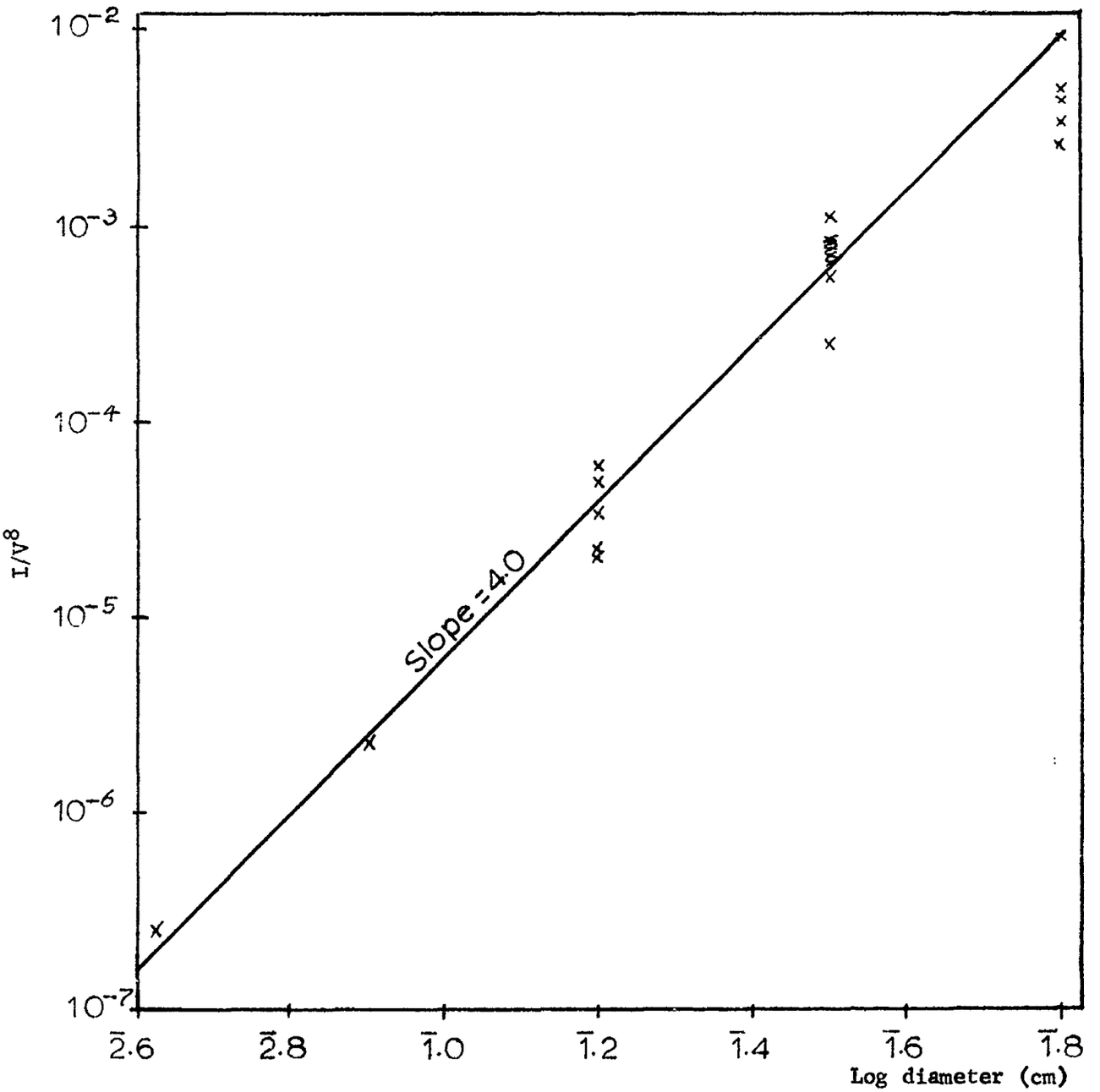

Figure 41. Dependence of Spike Intensity on Projectile Diameter, 3610Å.

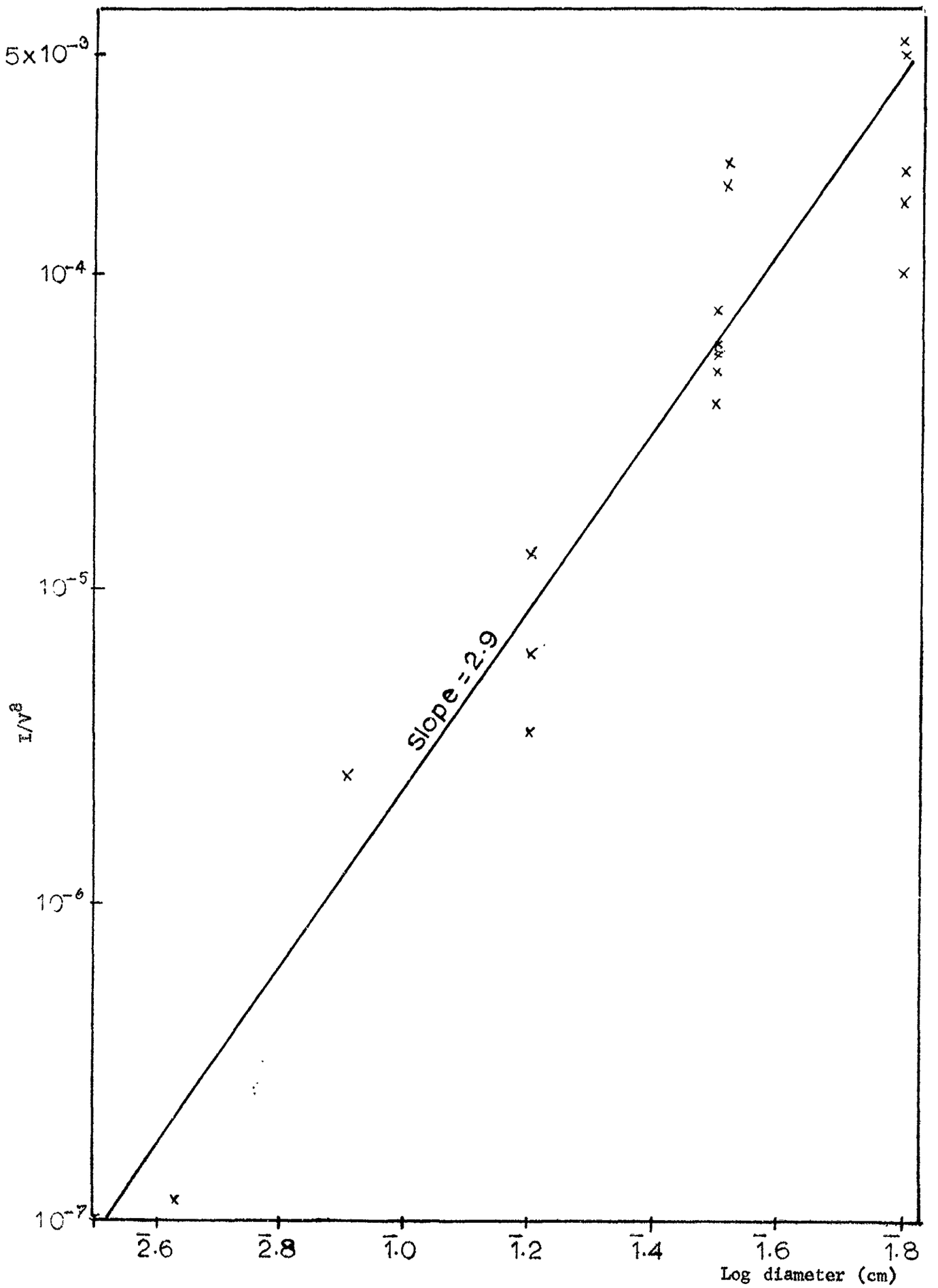

Figure 42. Dependence of Spike Intensity on Projectile Diameter, Background.

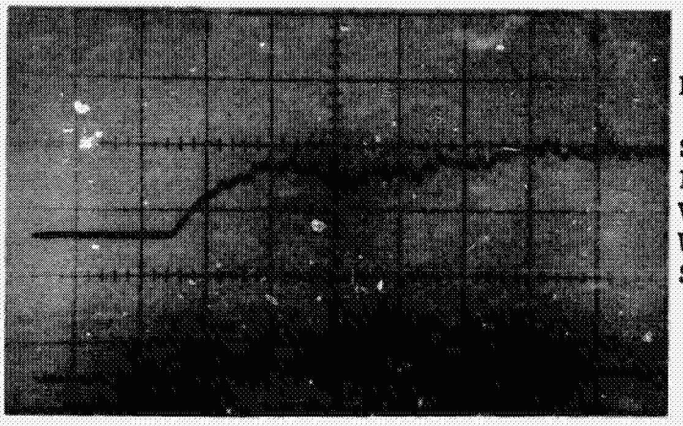

ROUGH TARGET

Shot No. - 109
Projectile - .318 cm Copper
Velocity - 4.1 km/sec
Wavelength - 3610Å
Sweep - 0.5 usec/division

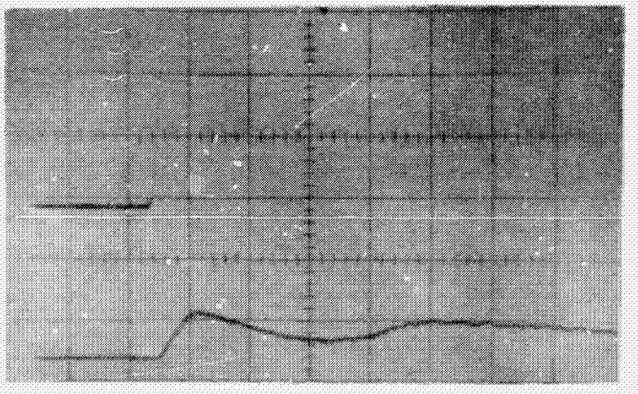

POLISHED TARGET

Shot No. - 108
Projectile - .318 cm Copper
Velocity - 3.9 km/sec
Wavelength - 3610Å
Sweep - 0.5 usec/division

Figure 43. Dependence of Spike Shape on Target Surface Finish

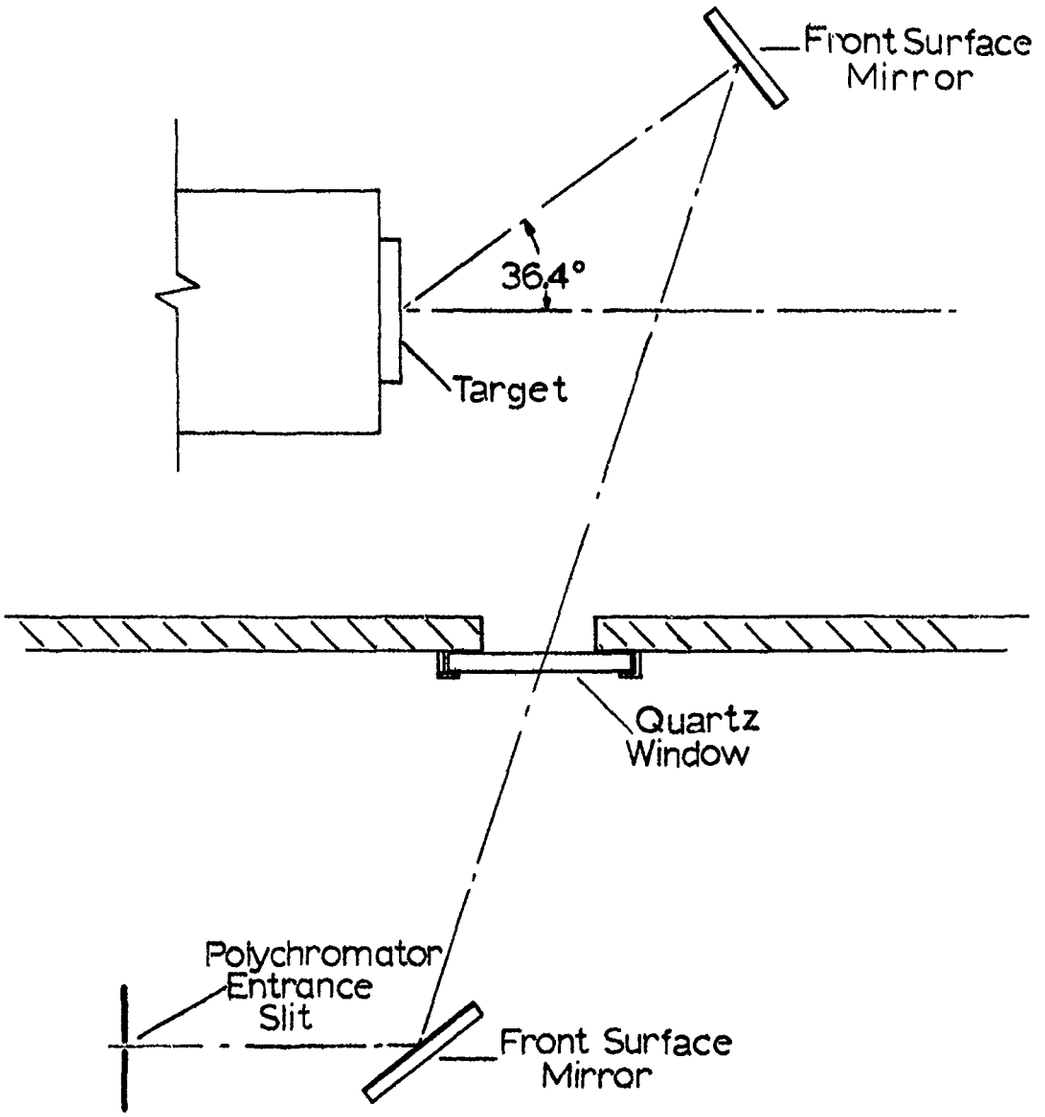

Figur 44. Polychromator Set Up for Shots 140-144.

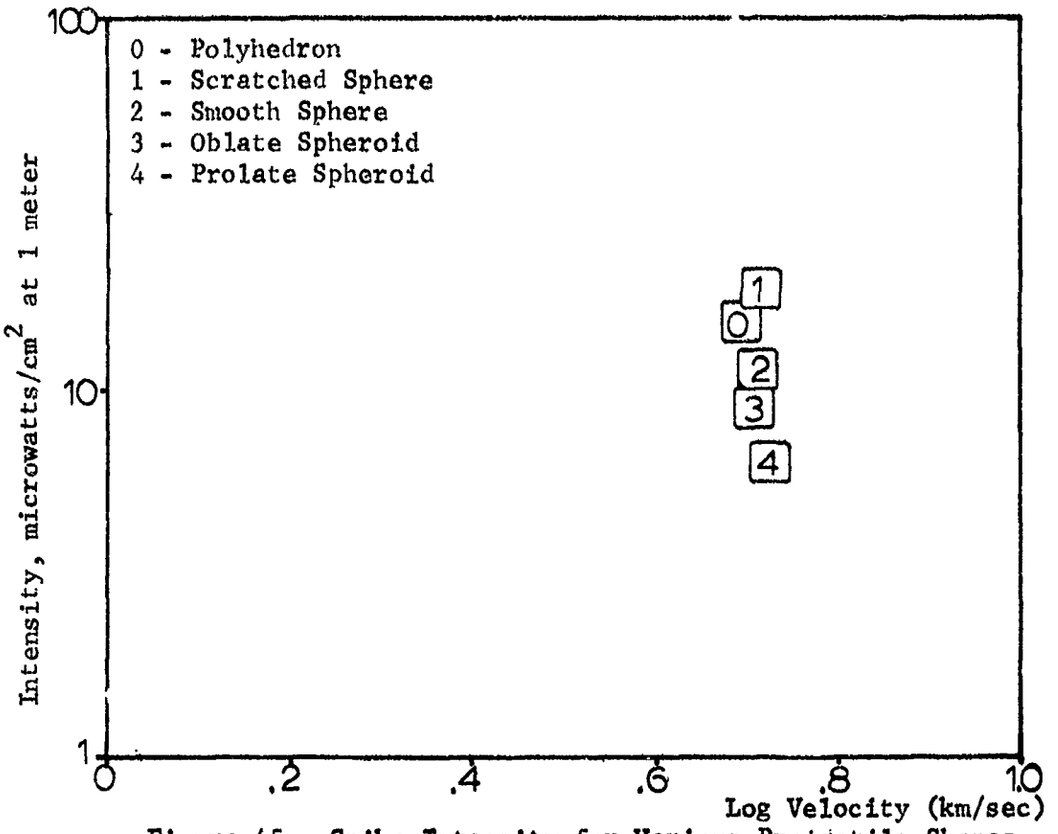

Figure 45. Spike Intensity for Various Projectile Shapes, Polychromator Head-on, 5085Å.

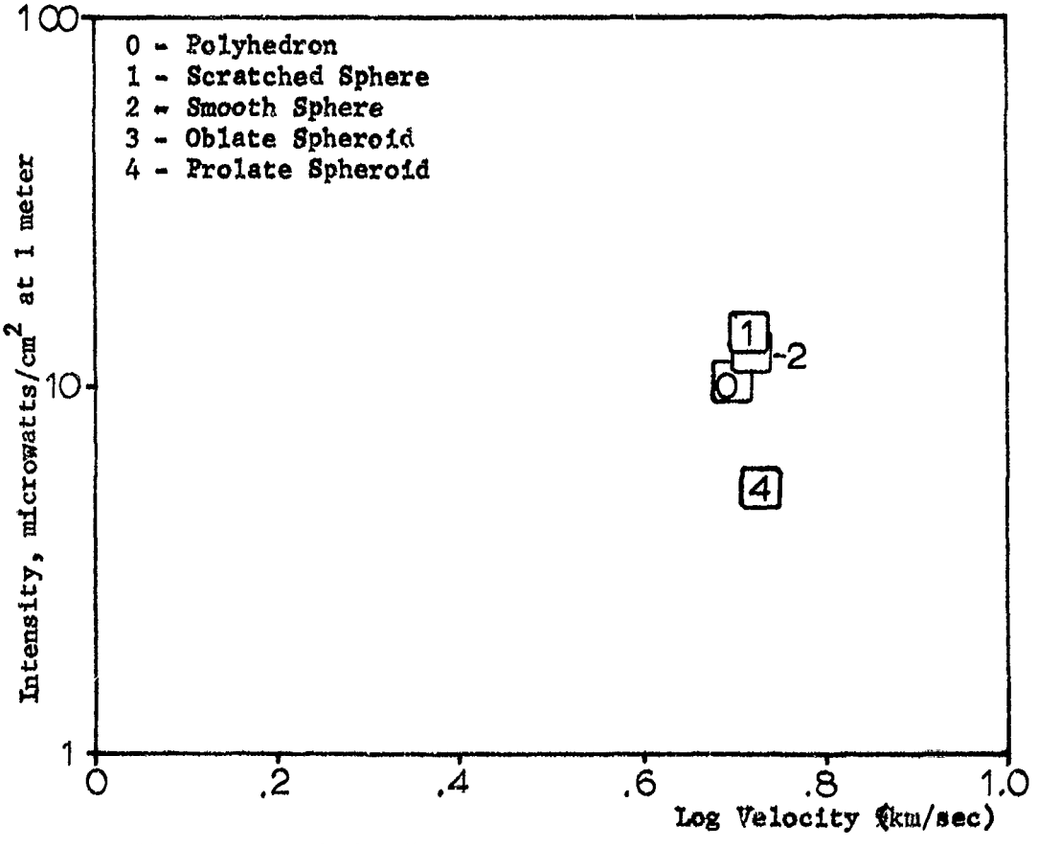

Figure 46. Spike Intensity for Various Projectile Shapes, Polychromator Head-on, 3610Å.

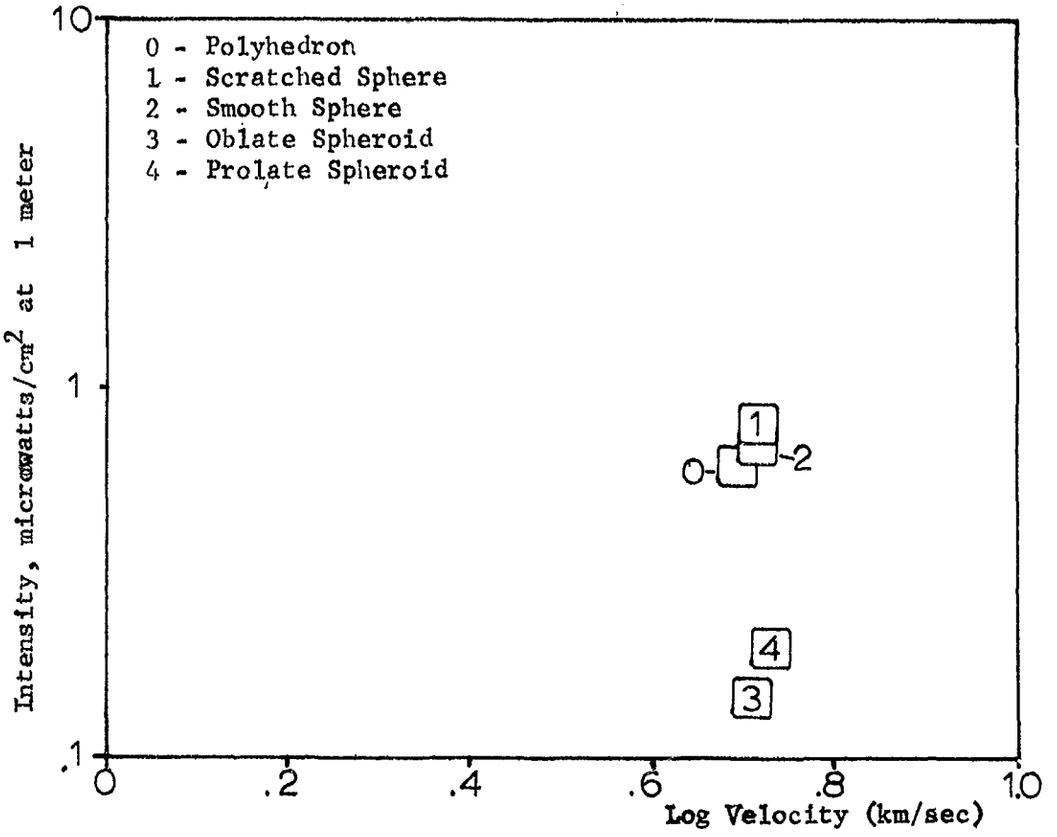

Figure 47. Spike Intensity for Various Projectile Shapes, Polychromator Head-on, 3261Å.

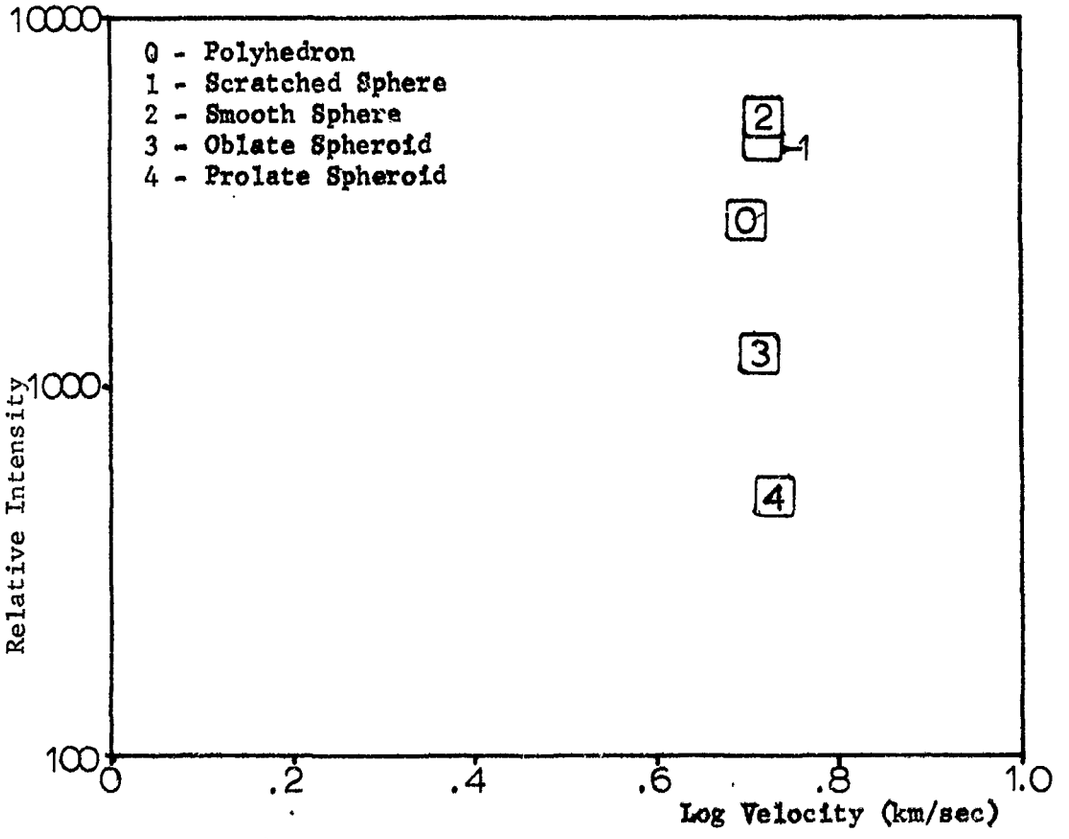

Figure 48. Spike Intensity for Various Projectile Shapes, Broadband (3500-6500Å).

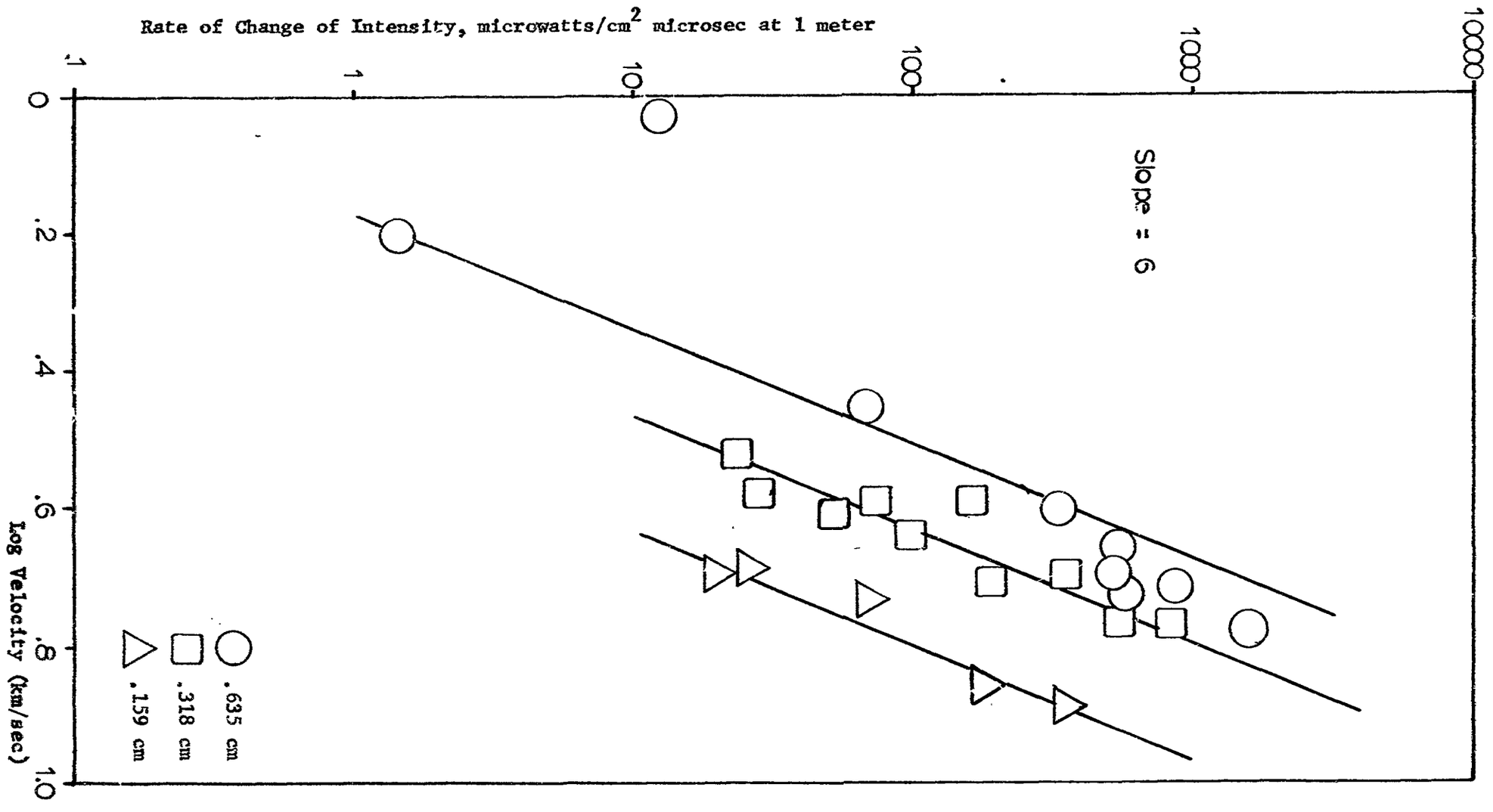

Figure 49. Spike Rate of Change of Intensity for Cu-Cd Impacts, 5085Å

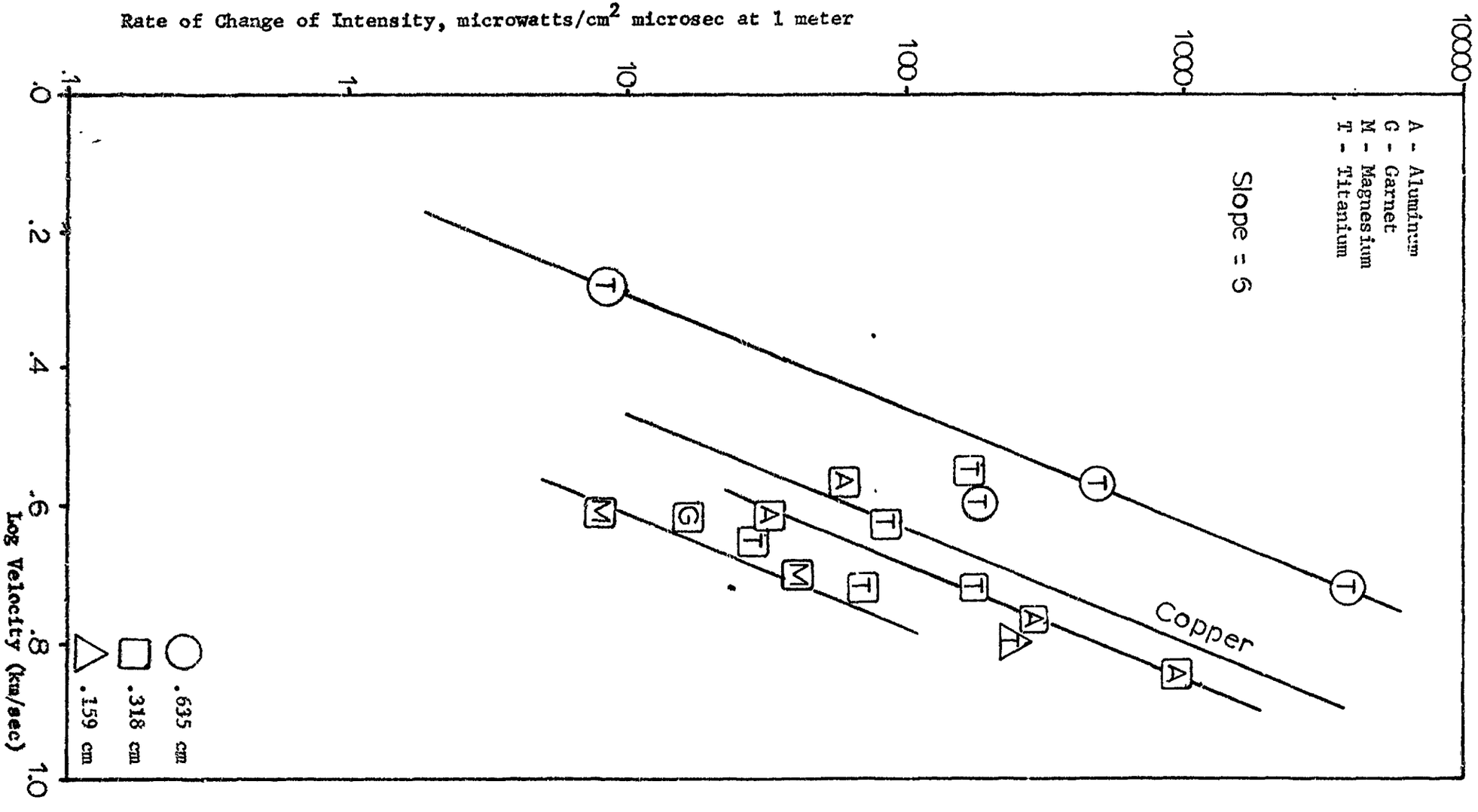

Figure 50. Spike Rate of Change of Intensity for Various Projectile Materials Impacting Cadmium, 5085Å

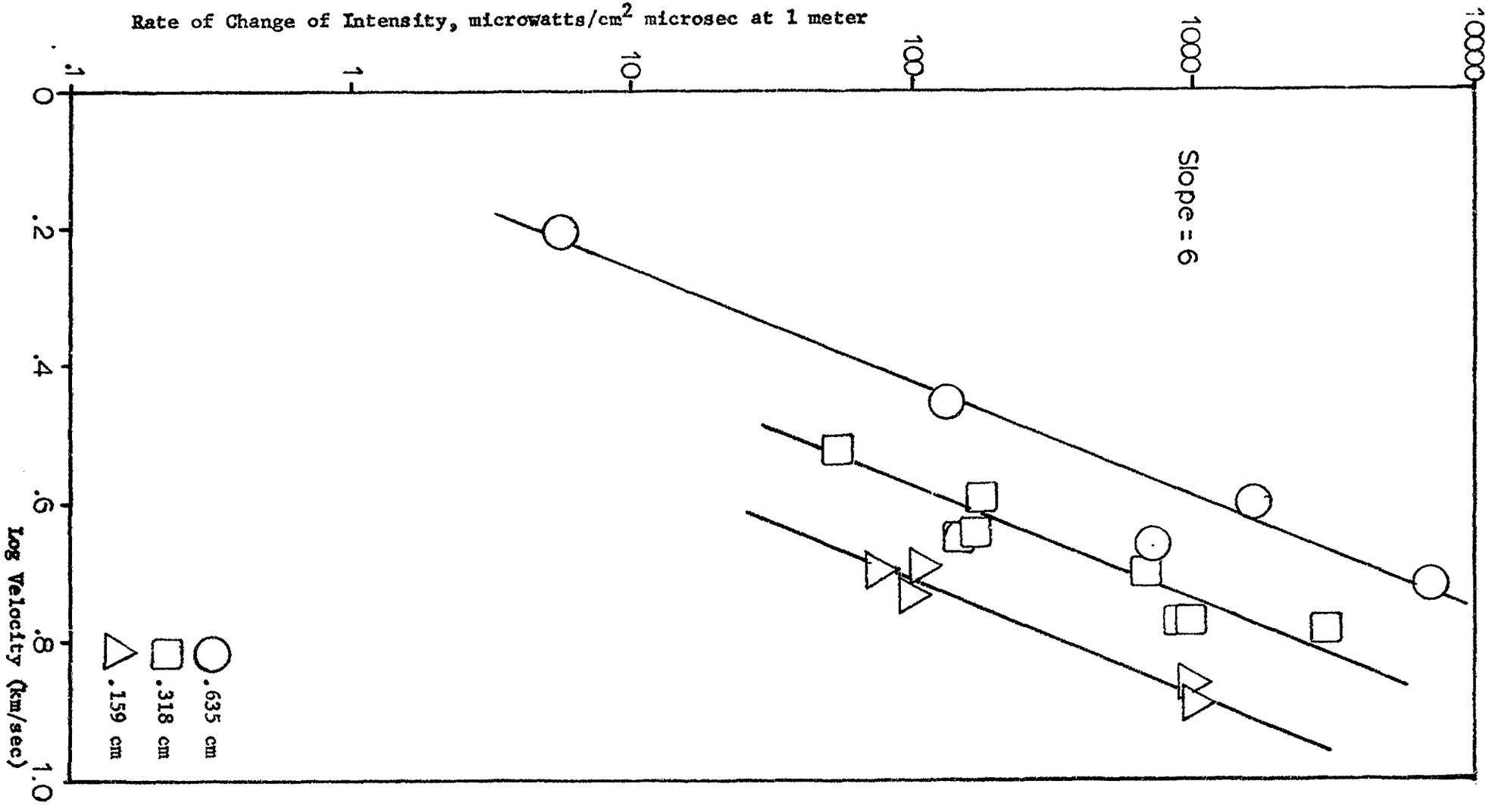

Figure 51. Spike Rate of Change of Intensity for Cu-Cd Impacts, 3610Å

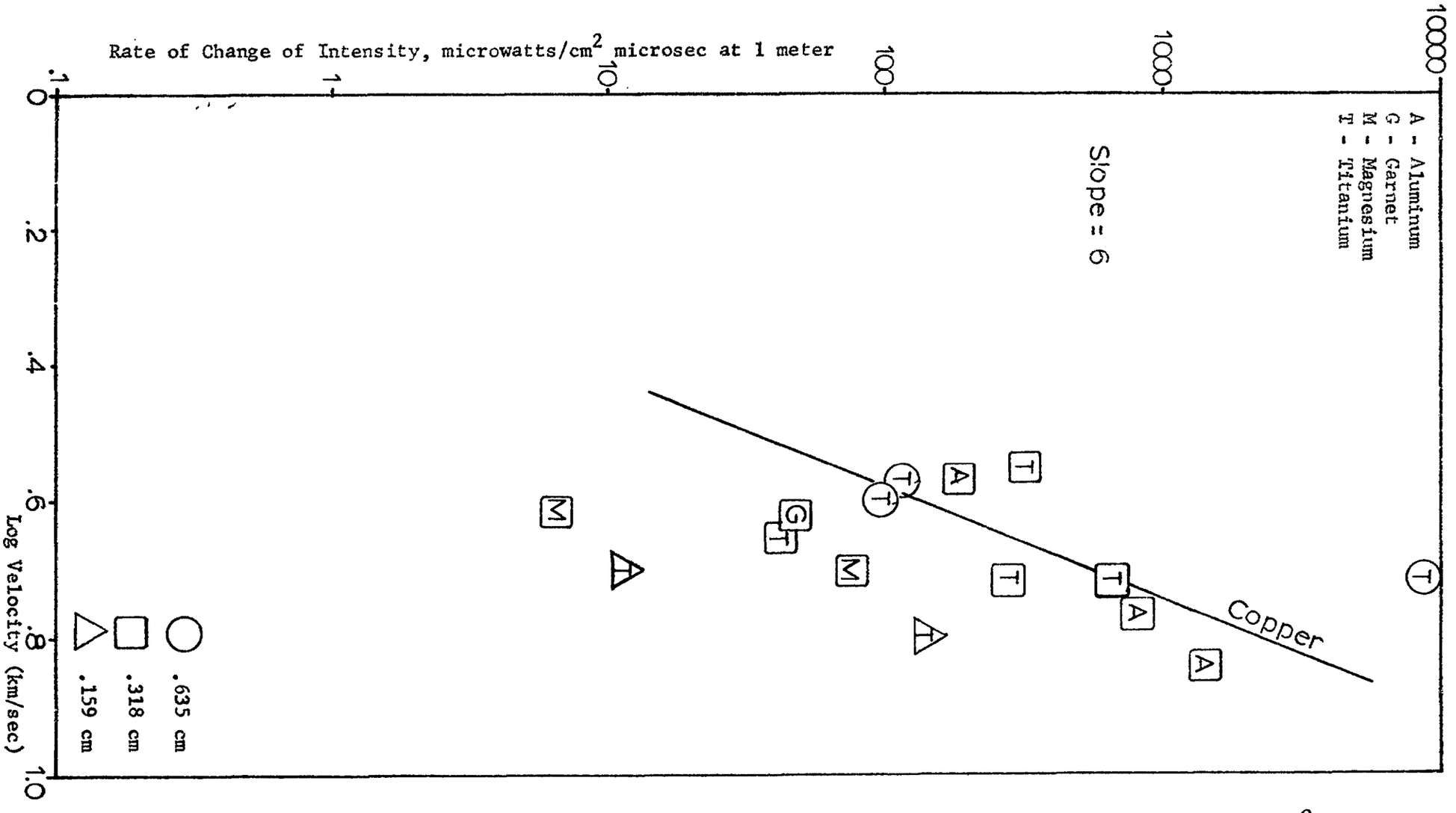

Figure 52. Spike Rate of Change of Intensity for Various Projectile Materials Impacting Cadmium, 3610Å

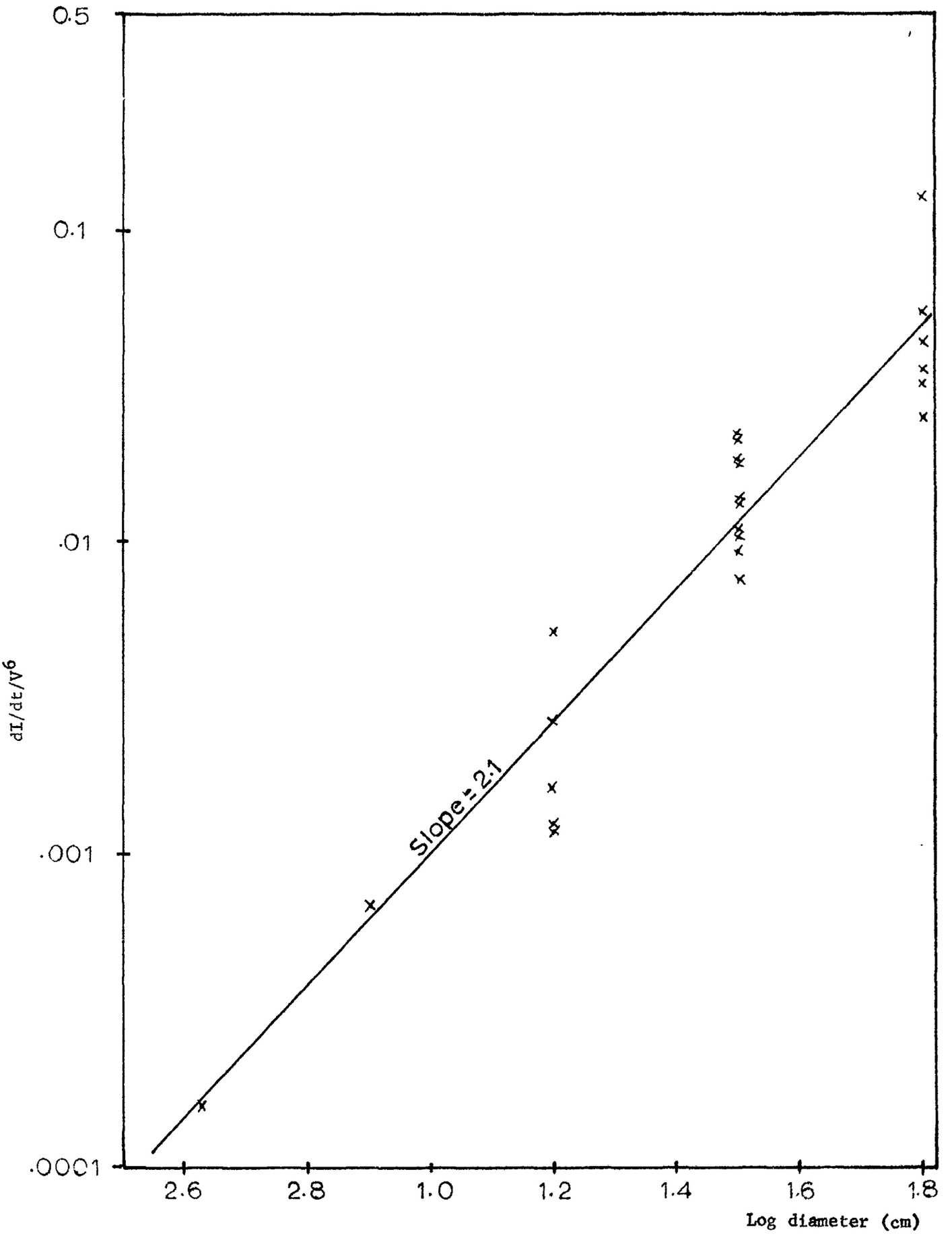

Figure 53. Dependence of dI/dt on Projectile Diameter, 3610Å.

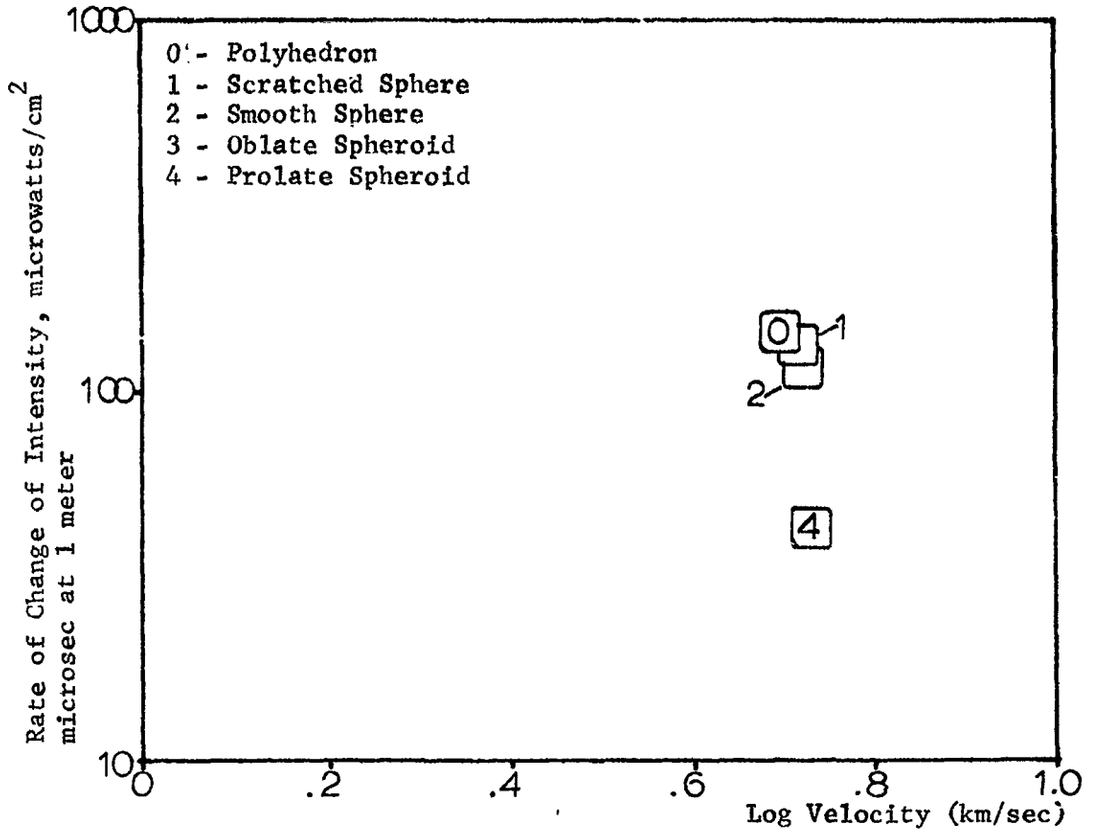

Figure 54. Spike Rate of Change of Intensity for Various Projectile Shape, Polychromator Head-on, 5085Å.

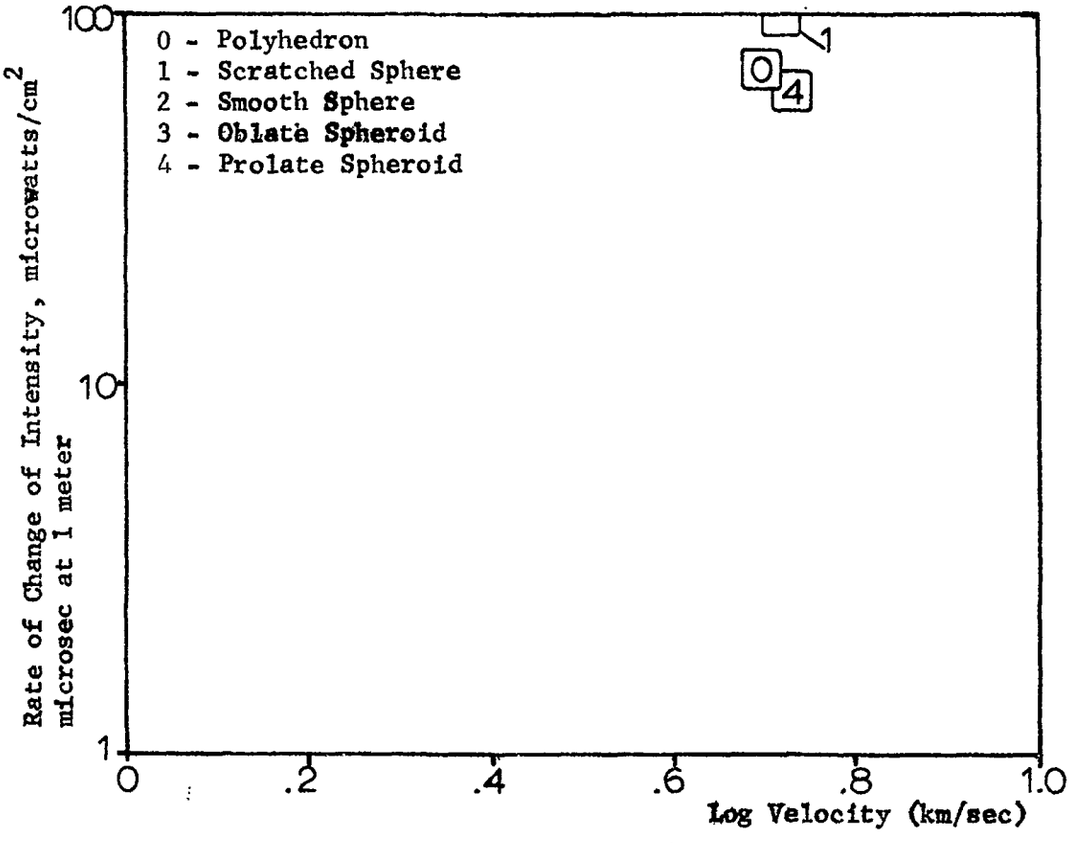

Figure 55. Spike Rate of Change of Intensity for Various o Projectile Shapes, Polychromator Head-on, 3610A